THE UNIVERSITY OF HULL

Energy Conversion and Storage *via* Photoelectrochemical Methods

Being a thesis submitted for the Degree of

In

The University of Hull

By

Amal A Altalhi

2013

Table of Contents

Acknowledgments

Completing my PhD degree is probably the most challenging activity of my first 30 years of my life. The best and worst moments of my doctoral journey have been shared with many people. It has been a great privilege to spend several years in the Department of Chemistry at University of Hull, and its members will always remain dear to me.

My first debt of gratitude must go to my advisor, Dr. Jay D Wadhawan. He patiently provided the vision, encouragement and advice necessary for me to proceed through the doctoral program and complete my dissertation.

I want to thank Prof Steven Kelly for his unflagging encouragement and serving as a role model to me as a junior member of academia. He has been a strong and supportive adviser to me.

I wish to thank my parents, Ahmad Altalhi, Amerah Altalhi, my sisters Hanan and Hend and my brother Khalid. Their love provided my inspiration and was my driving force. I owe them everything and wish I could show them just how much I love and appreciate them. My best friend, Basmah Almehmadi, whose love and encouragement allowed me to finish this journey.

Members of Electrochemistry Laboratory (Yan Zhou, Timothy Johnson and Josh Cooper), also deserve my sincerest thanks, their friendship and assistance has meant more to me than I could ever express.

Abbreviations

CE	Counter Electrode
CPZ	Chlorpromazine
CV	Cyclic Voltammetry
[O] / C_o	Concentration of oxidant
DCP	2,4-Dichlorophenol
DOTAC	Dodecyltrimethylammonium chloride
I_{sc}	Short circuit current
ITO	Indium tin oxide
LLC	Lyotropic Liquid Crystal
n	Number of electrons per mole transferred across an interface
NMP	10-methylphenothiazine
OCV	Open circuit voltage / V
RE	Reference Electrode
[R]	Concentration of reductant
S	Surface area of the electrode
TMPD	*N, N, N′, N′*-tetramethyl-*p*-phenylenediamine
^{t}BuFc	*tert*-butylferrocene
WE	Working Electrode

Roman Symbols

C	Concentration
D	Diffusion Coefficient
E	Potential
F	Faraday's Constant (98485 C mol^{-1})
i	Current
k	Rate Constant
N	Number of Molecules
Q	Charge
R	Gas Constant (8.314 J mol^{-1})
r	Radius
T	Temperature
t	Time

Greek Symbols

α	Symmetry Factor
β	Symmetry Factor
μ	Ionic Mobility
ν	Scan Rate
ω	Rotation Speed of the Electrode

Abstract

Photoelectro analytical chemistry provides an elegant technique by which to explore, amongst others, various industrial and environmental applications. To this end, four areas of photoelectroanalytical chemistry are investigated in order to develop industrially - and environmentally - relevant galvanic and photogalvanic cells, together with exploring the electro-generation of an industrially important molecule and diffusion factors they may affect this generation.

The first study is investigated a long-range charge transfer, using *tert*-butylferrocene (*t*BuFc) as model hydrophobic system. It is found that the apparent one-dimensional diffusion coefficient depends on the *t*BuFc loading. It is suggested that an efficient relay mechanism for electron transfer is through the partitioning of the oxidised form between the two subphases, with inter-pseudophase reaction.

However, the second study investigated the normal lyotropic liquid crystals (in the lamellar or hexagonal phases) as a route to afford a structured, three-dimensional, quasi-biphasic framework within which electron transfer cascades may take place using cyclic voltammetry. It is shown that these can take place through reagent partitioning between the hydrophobic and hydrophilic subphases, and it is illustrated how the structure and its orientation, the nature of the ionic doping of the framework, and the hydrophobicity of the redox analyte may give rise to changes in the observed voltammetric waveshape.

For the case of an artitifical mimic of the first few stages of Photosystem I, it is demonstrated that photo-induced electron transfer is likewise affected by the orientation, and develop a system of photon efficiency of ~0.1%.

Thirdly, a novel attempt at power production was attempted with the construction and optimisation of a photogalvanic cell system. A literature review was conducted and a system proposed utilizing 10-methylphenothiazine (NMP) as a light harvester and zinc as a sacrificial electrode with tetrabutylammonium chloride (TBAP) as a supporting electrolyte and chloroform as a mediator. The study aimed to create a cell that could be produced using industrial run-off or other waste water supplies.

A series of cells was produced with varying concentrations of both zinc and NMP solutions and the power conversions studied by producing a voltage-current plot for each system. A system that exhibited 9.02% conversion efficiency keep, future studies were conducted to show whether the zinc species effected the power conversion or if silver would act in a similar way.

A mechanism was proposed for the power production process and so studies using 2, 4-Dichlorophenol (DCP) rather than chloroform we conducted; it was believed that the dissociation step for DCP was step wise rather than concerted. Lower power production was seen in these cells as predicted by the reaction mechanism. Tris - (4-bromophenyl) - amine (TBA), an alternative light harvester to NMP, was used to see if altering the active chemical agent resulted in efficiency change.

Finally , A photogalvanic cell that employs 2,4-dichlorophenol as a fuel source, an *N*-substituted phenothiazine as light harvester, and sacrificial zinc anode is presented,

and shown to afford a c*a.* 4% light-to-electrical power conversion efficiency in violet light.

Chapter 1- Introduction to Electrical Power Sources

The present rising attention in solar energy conversion mirrors its significance in identifying future sources of energy that will be of low-cost requiring minimal maintenance in an environmentally friendly and sustainable. Moreover, non-renewable sources such as coal, oil, natural gas, *etc;* are limited, whilst demand for these type of sources are rising day by day. Consequently, there is a pressing need to increase the use of renewable energy to fulfil the increasing energy demand.

Nowadays, global warming and speedy decrease in energy sources caused by the large level consumption of fossil fuel are raising concern. Renewable energy resources are attracting a great deal of attention, and photochemical-to-electrical energy conversion is one of the most promising future energy resources.

The EU directive 2009/28/EC introduced in 2009 has that the UK is now committed to finding 15% of its final energy from renewable sources by 2020 which includes a 10% share of renewable energy in the transport sector.[1] With the current renewable energy usage standing at only 11% in 2012 there is clearly still scope for improvements to be made in the next few years.

Along with this, fossil fuels are being consumed at an ever increasing rate and levels of CO_2 greenhouse gases rising; therefore it is arguably more important now than ever before to develop alternative methods to generate energy and to move to renewable energy sources. Many have turned to the use of natural and infinite energy sources such as harvesting wind, tidal and solar energy. An alternative to these

methods, yet still vitally important, is the development and further improvement of batteries or fuel cells which can use resources such as oxygen or CO_2.

This chapter, reviews literature that has been carried out within this area of photoelectrochemistry with emphasis on light – to – electrical energy conversion and storage.

1.1   General Concept

It is widely known that there is increasing pressure to resolve the fuel crises that is currently ongoing in the world with the need of renewable energy is becoming ever more paramount as time goes by, in the scientific community solar energy is an especially hot topic, due to its infinite availability and lack of cost.[1] Figure 1.1 below shows the intensity of solar radiation the earth receives every day.
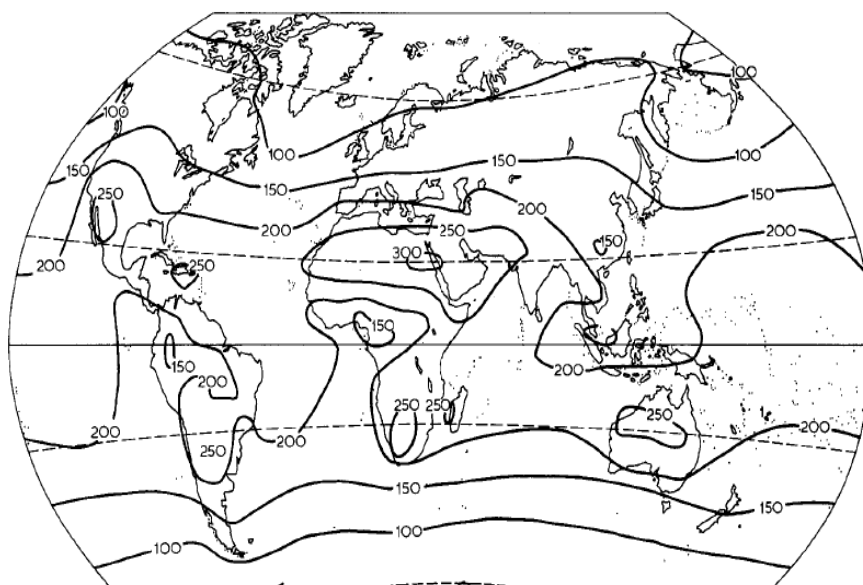
Figure 1.1: The average intensity of solar radiation the Earth receives in 24 hrs. Taken from.[2]

High availability of solar energy in deserts where populations are minimal, long distance between solar availability and populations requires efficient transmission routes (*e.g.* smart grids). Although, the solar energy needs to be stored-this requires integration with galvanic cells.

Currently normal galvanic cells are used to power all our portable devices with many types of these batteries described briefly later; larger batteries, such on redox batteries, are employs for grid-scale storage. Not only is there wide spread research on solar cells as a form of generating electricity for a household or a group of households, there is increasing research into using solar energies in the form of batteries (photogalvanic cells); as portable technology is just as much part of our lifestyle as household technologies, it is photogalvanic cells this thesis concentrates most on.

1.2   Galvanic cells

A galvanic cell is another name for a battery; [3,4] a galvanic cell contains two electrodes, the fuel also known as the "active components", an electrolyte and casing for the battery. The cell works with reactions occurring at each of the electrodes where the chemical energy created is then transferred into electrical energy, *via* a connecting external circuit at the electrodes. Within a galvanic cell the discharge reactions that occur are all spontaneous ($\Delta G < 0$).

There are two main types of battery:

- **Primary batteries**

For a cell to be described as a primary battery, one or more of the electrode reactions must be irreversible. A typical example of a primary battery is the Daniell cell. Another example of a primary battery is Leclanché cell, which was developed by Georges Leclanché in 1868. [5] This cell consist of a carbon rod coated with a thick layer of MnO_2 acting as the cathode (graphite is mixed with the MnO_2 to help improve conductivity) and elemental zinc as the anode.

The electrolyte used in this case is pH-neutral aqueous ammonium chloride (NH_4Cl) and this prevents any reverse reaction, causing the cell reactions to be irreversible and thus the Leclanché is a primary battery. The cell reactions are as follows:

$$Zn(s) \,|NH_4Cl \,(aq) \,|MnO_2(s)$$

Anode: $\qquad\qquad\qquad\qquad Zn \;\rightarrow\; Zn^{2+} + 2e^-$

Cathode: $\qquad 2MnO_2 + H_2O + 2e^- \rightarrow 2MnOOH + 2OH^-$

Electrolyte: $\qquad Zn^{2+} + 2NH_4Cl + 2OH^- \rightarrow Zn(NH_3)_2Cl_2 + 2H_2O$
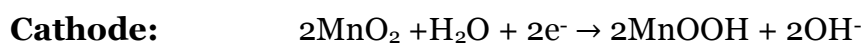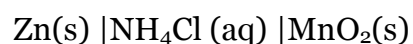
Lechlanché cells are used in applications where current is required intermittently such as door bells. They require little maintenance so can be an attractive option for certain applications.

- **Secondary batteries**

For a cell to be described as a secondary battery, the electrode reactions must be reversible, and hence the battery recharged. Commercially viable secondary batteries are expected to carry out many hundreds and even thousands of charge – discharge cycles. This means that the fully reversible electrode reactions must maintain this reversibility over the required number of cycles. This is no easy task when one considers the number of different side reactions that can occur and ultimately lead to the degradation and malfunction of the battery.

These side reactions include the densification of active material, expansion and detaching of active material, the progressive creation of inactive phases and the corrosion of current-collectors. The deterioration in the performance of the battery is usually exponential so that when the battery degeneration accelerates and the battery quickly becomes inoperable. Despite the potential drawbacks to secondary batteries, there have been some excellent long lasting batteries developed such as the nickel-hydrogen battery which can last over 20,000 cycles.[5]

A typical example of a secondary battery is the lead-acid battery, which was developed in 1859 by Gaston Plante and is one of the oldest examples of a secondary battery.[5] There have been many developments and updates to the lead-acid battery

which today consists of elemental lead as the anode, lead dioxide as the cathode and sulphuric acid as the electrolyte.

Most lead-acid batteries are "flooded" meaning that the sulphuric acid is filled above the top of the plates. As a consequence of this construction vents must be introduced to release the gases produced (namely oxygen and hydrogen from the cathode and anode respectively.

However these released gases also contain trace amounts of sulphuric acid so the cell suffers from corrosion over a period of time. Another problem with this design is that the cell must be kept upright otherwise leakage occurs as the sulphuric acid can escape from the vents. Another consideration which must be taken into account in the application of an automotive battery is the operating temperature. In cold winter conditions the battery may have to operate at low temperatures (down to -20°C) and in warmer climates the engine bay may reach temperatures above 50°C.The cell half reactions for the lead-acid battery are as follows:

$$Pb(s) \,|H_2SO_4 \,(aq)\, |PbO_2(s)$$

Anode: $\quad\quad\quad\quad Pb + (2H^+ + SO_4^{2-}) \leftrightarrows PbSO_4 + 2H^+ + 2e^-$

Cathode: $\quad\quad\quad\quad PbO_2 + (2H^+ + SO_4^{2-}) + 2H^+ + 2e^- \leftrightarrows PbSO_4 + 2H_2O$

Spontaneous cell reaction: $\quad PbO_2 + Pb + 2H_2SO_4 \rightarrow 2PbSO_4 + 2H_2O$
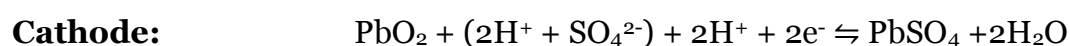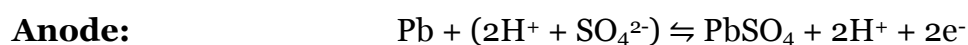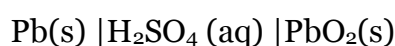
Lead-acid batteries are desirable as they are relatively cheap to make and are used widely in cars and other automobiles to provide a large current which is needed by the starter motor. In most automobiles six cells are connected in series to give an output of 12 V.

1.3   Photogalvanic Cells

Photogalvanic cells have been studied and developed for over 20 years and their efficiency is determined by the ratio of the output power to the input of solar power. They are easily described as a battery where chemical energy is converted into electrical energy, *via* a chemical reaction where light is used to instigate the reaction where the light energy has also been stored within the cell, in contrast to a normal galvanic cell where the reaction within the battery is totally spontaneous. Figure 1.2 shows the basic setup of a photogalvanic cell.

Photogalvanic cells work by creating high energy products where, the product is excited by a photon; the products, full of energy, release this electrochemically in the form of electricity: a concentration change in the two form of a redox couple allows the cell to develop a photovoltage. This is the "Photogalvanic Effect".[3]
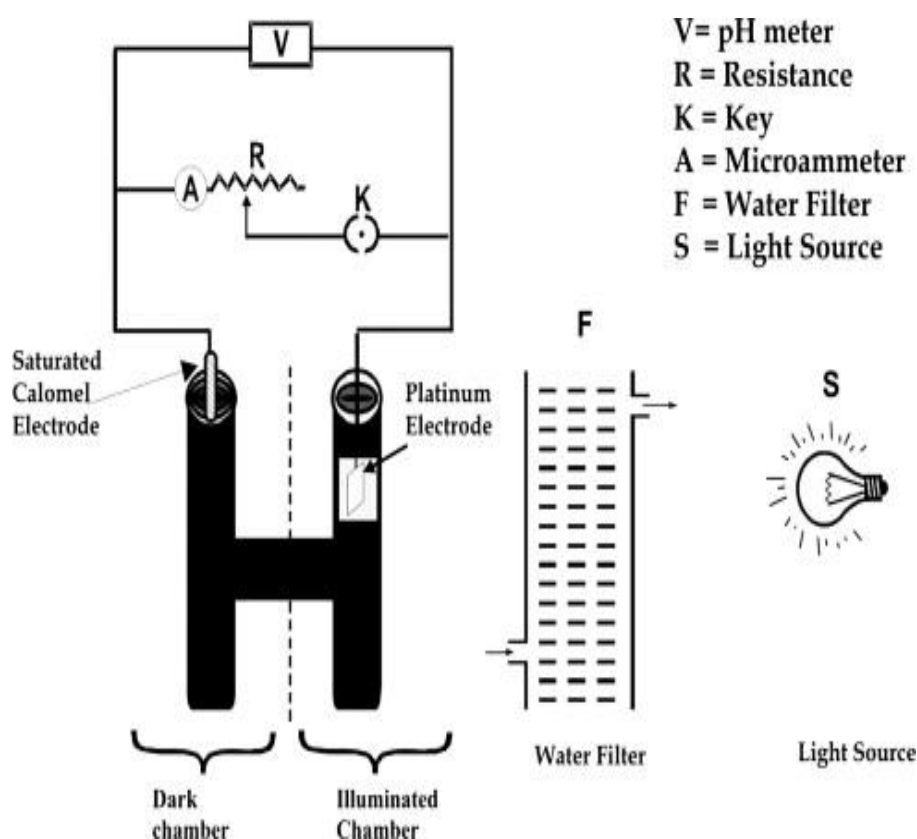
Figure 1.2: An example of a photogalvanic cell. Taken from[3]

So, they work in a very similar way to that of a normal galvanic cell, instead of all the reactions occurring in the cell being spontaneous, in a photogalvanic cell light is needed to instigate the reaction, so ($\Delta G > 0$). Within the cell, the photoelectric (photogalvanic) effect occurs and in most cells this is at the anode.

Photogalvanic cells can be secondary systems if the electrolyte is a redox system, at the start of the process the species in the electrolyte is oxidised releasing an electron that has been photogenerated if the anode is connected to a counter electrode that has been immerged into the electrolyte solution then the electron can travel to the solution and reduce the oxidised species, with this the cell is a secondary system.[5]

1.4   Photogalvanic Effect

The photogalvanic effect also known as the photoelectric effect [6] occurs when the electrode is exposed to radiation and an electron is liberated, the number of electrons emitted does depend on the intensity of radiation that to which the material is exposed. The electron(s) released have kinetic energy and the amount of energy is dependent on the frequency of the radiation.

This effect is a quantum process where all the photons having an amount of energy hf where h is Planck's constant and f is frequency. However this amount of energy does need to be larger than the work function (Φ) of the material for many materials this does occur at ultra-violet or energies that are higher.[3] the maximum amount of kinetic energy is given by Einstein's equation: [6]

$$\mathbf{E_m = hf\text{-}\Phi} \qquad (1.1)$$

The electrons that are liberated can then be transferred from the electrode to the electrolyte, and in an open circuit causes a change in the electrode potential, or in the case of a closed circuit change the current. Only a small change does occur in the region of mV or nA but this change does have a big influence in making the cell more efficient.

This effect enables photogalvanic cells to operate efficiently; for this to occur either of the half cells must exhibit this effect or more preferably both half cells exhibit this effect. The earliest dated observation of the photogalvanic effect was in 1925 where

E.K. Rideal and E.G. Willaims [5] investigated the effect of light on the ferrous, ferric iodide equilibrium.

$$Fe^{3+} + 2I^- \; \underset{\text{Light}}{\overset{\text{Dark}}{\rightleftarrows}} \; Fe^{2+} + I_2$$
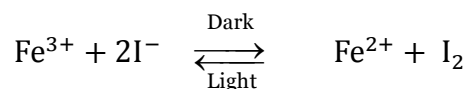
It was noticed that when the ferrous ion and iodine reacted under light electrons were released by the iron and consequently absorbed by the iodine.[5] This effect in contrast to the photovoltaic effect does not need many different materials to take effect.

1.5 Faradaic Process

The Faradaic process is the transfer of electrons between the electrode and redox species in the bulk solution; it is from this process that the current through a cell can flow as this process completes the circuit within the cell, [6] this process is what enables the photogalvanic effect occurs. This Faradaic current (i) can be expressed in term of the flux mol passing through unit area in unit time of redox species to the electrode, j.

$$i = nFAj \qquad (1.2)$$

where n is the number of electrons transferred per mole of redox species, F is Faraday's constant (96485 C mol^{-1}) and A is the electrode area.

1.6   Photovoltaic Effect

This process is similar to that of the photogalvanic effect except the electron generated is not transferred to the solution but is transferred between two different materials; photovoltaic solar cells use this effect as semiconductors within the cells exhibit this effect greatly. This is done as most of the semiconductors have a p-n junction; [7, 8] at this junction the emitted electrons create a flow of current externally without the need of a battery.

1.7   Photochemical Process

Photogalvanic cells work by the principle of photochemistry; [9] this is where light is used to initiate a reaction. The principle is the energy from the light usually from the UV-visible region of the electromagnetic spectrum, to excite the electrons into higher energy levels, leading to the formation of an excited state.

$$A + h\nu \rightarrow A^*$$
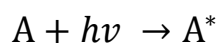
Where A is either an atomic or molecular species in the grand state and A^* is the species A in the excited state, once in this state there are free unpaired electrons that can become very reactive, when the electron is promoted into this state it can occupy one of 2 states and that is either the singlet or triplet state. The singlet state is spin allowed *i.e.* the electron does not change its spin; whereas in the triplet state the electron has changed its spin, which is quantum mechanically forbidden.

The Jablonski diagram (figure 1.3) shows the fluorescence and phosphorescence (light energy released). The electrons that are in the singlet excited state are only in this state for a very short time, (10^{-8} to 10^{-9}s) this is enough time to instigate reactions, the electrons that are in the triplet state can take a lot longer to relax as long as 10 seconds.
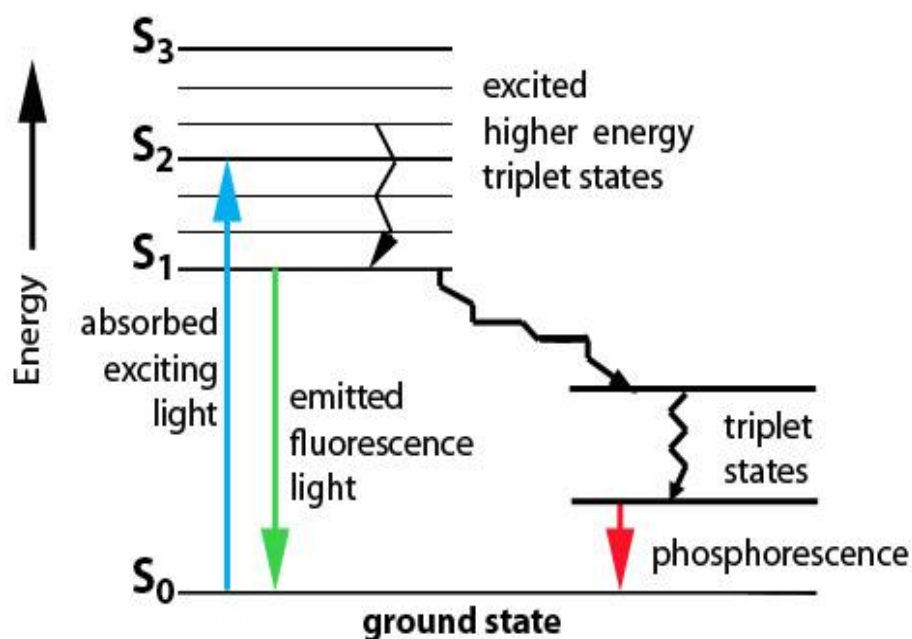
Figure 1.3: Jablonski Diagram. Taken from[9]

The difference between the diagram above and photo-batteries is that the light energy transforms into an electron transfer process which allows for a change in the concerns of the redox species leading to voltage generation potential. The two species react at different electrodes.[12]

$$A^* + X \rightarrow B + Y$$

$$B + e^- \rightleftharpoons A$$

$$Y - e^- \rightleftharpoons X$$
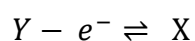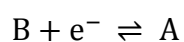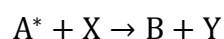
1.8   Photosensitzers

Photosensitizers[13] are molecules that can help initiate photochemical reactions. Such molecules are often employed in medicine for the treatment of cancer. They operate through the photo-excited state, and these can influence reactions that would not normally interact with light, in a similar way to a catalyst. With the photosensitizer molecule once in an excited state can release the corresponding energy as light, heat, electrical *etc*; for this reason it is very useful in medicine in the battle against cancer.

1.9   Reductants in Photogalvanic Cells

Reductants have been investigated to see how they influence output potential in a photogalvanic cell, Gangotri[14] found that that was a minimal improvement in the potential generated using a reductant, it was found that the reductant and its oxidised counterpart act as an electron carrier, but themselves have little influence in the cell as a whole.

A mixture of reductants and using a dye as a photosensitizer has recently been studied by Gangtori again where Dextrose and EDTA were used as reductants and Azur A was used as the photosensitizer[15], it was found that increasing the concentration of the reductants in this case generated an improvement in the potential generated, as did increasing the concentration of the photosensitizer.

1.10   Metals in Photogalvanic Cells

Metals have only recently started being studied with chromium based complexes being at the forefront of the research with Pokhrel.[16,17] looking at the photogalvanic behaviour of: $[Cr_2O_2S_2(1\text{-Pipdtc})_2(H_2O)_2]$ it was found that the complex bridged *via* the oxygen and sulphur atoms there was a substantial increase in the photopotential generated, with this value increasing in aqueous solutions, with a further increase with malachite green present indicating these complexes could become very useful in the study of photogalvanic cells.

1.11   Factors Influencing the Efficiency of a Photogalvanic Cell

There are a number of factors[18] (variables) present in a photogalvanic cell that can affect how efficiently it operates such as:

- pH of the system,

- concentration of any photosensitizers present,

- concentration of any surfactants present,

- concentration of any other molecules present,

- the intensity of the light that is irradiating the system,

- what region of the spectrum interacts with the system and

- cell thickness.

If these different variables are each not optimised, then the cell will not work at maximum efficiency.

1.12 Photon Efficiency

This is defined as the number of electrons produced per photon incident onto the system, and it give by the ratio: [19]

$$\eta_{\varphi} = \frac{i_{lim}/q_0}{\int_{\varepsilon_g}^{\infty} A_{\epsilon}N(\varepsilon)d\varepsilon} \qquad (1.3)$$

where: η_{φ} is the photon efficiency, i_{lim} is the limiting photocurrent, q_0 is the charge on one electron (1.602×10^{-19} C), A_{ε} is the optical absorbance of the cell , ε_g is the threshold at which the photons are absorbed below this photons are not absorbed and $N(\varepsilon)$ is the flux density of photons.[20] Knowing all this enables us to calculate the optimum photon efficiency and thus determine the right intensity of the light that is irradiating the cell.

References for Chapter 1

1. K.M. Gangotri and M.K. Bhimwal, *Solar Energy,* 2010, **84**, 1294

2. M.D. Archer, *J. Appl. Electrochem*, 1974, **5**, 17

3. T. Zawodzinski, S. Minteer and G.Brisard, *Interface*, 2006, **15**, 62

4. K.M. Gangotri and V. Indora, *Solar Energy*, 2010, **84**, 271.

5. Organisation for Economic Co-operation and Development, ICT Applications for the Smart Grid: Opportunities and Policy Implications, OECD Digital Economy Papers, no. 190, OECD Publishing, 2012, DOI: 10.1787/5k9h2q8v9bln-en, accessed 11 September 2012.

6. American Physical Society, Integrating Renewable Electricity on the Grid: A Report by the APS Panel on Public Affairs, American Physical Society, Washington, 2010.

7. Smart Grids European Platform, http://www.smartgrids.eu, accessed 11 September 2012.

8. C. Ponce de Léon, A. Frías-Ferrer, J. Gonález-García, D. A. Szánto and F. C. Walsh, *J. Power Sources*, 2006, 160, 716.

9. D. R. Rolison, J. W. Long, J. C. Lytle, A. E. Fischer, C. P. Rhodes, T. M. McEvoy, M. E. Bourg and A. M. Lubers, *Chem. Soc. Rev.,* 2009, 38, 226.

10. A. K. Pandey, P. C. Deakin, R. D. Jansen-van Vuuren, P. L. Burn and I. D. W. Samuel, *Adv. Mater.,* 2010, 22, 3954.

11. H.-K. Song and G. T. R. Palmore, *Adv. Mater.,* 2006, 18, 1764.

12. J. R. Darwent, P. Douglas, A. Harriman, G. Porter and M.-C. Richoux, *Coord. Chem. Rev.,* 1982, 44, 83.

13. H. L. Tavernier, F. Laine and M. D. Fayer, *J. Phys. Chem. A*, 2001, 105, 8944.

14. M. D. Archer, *Specialist Periodical Reports in Photochemistry*, 1995, volume 6, The Chemical Society, London, p.739.

15. M. D. Archer and M. I. C. Ferreira, *in Photochemical Conversion and Storage of Solar Energy*, ed. J. Connoly, Academic Press, San Diego, 1980, p. 201.

16. W. J. Albery and A. W. Foulds, *J. Photochem.*, 1979, 10, 41.

17. C.-T. Lin and N. Sutin, *J. Phys. Chem.,* 1976, 80, 97.

18. W. J. Albery and M. D. Archer, *Electrochim. Acta*, 1976, 21, 1155.

19. A. K. Jana, *J. Photochem. Photobiol.*, A, 2000, 132, 1.

20. K. R. Genwa and M. Genwa, *Sol. Energy Mater. Sol. Cells*, 2008, 92, 522.

Chapter 2 - Introduction to Electrochemistry

Within this chapter the essential principles of electrochemistry underpinning the theory within subsequent chapters are presented.

2.1   Basics of Electrochemistry and Voltammetry

Electrochemistry[1,2] is a branch of chemistry that studies chemical reactions which take place in a solution at the interface of an electron conductor (a metal or a semiconductor) and an ionic conductor (the electrolyte), and which involve electron transfer between the electrode and the electrolyte or species in solution.

If a chemical reaction is driven by an external applied voltage, as in electrolysis, or if a voltage is created by a chemical reaction as in a battery, it is an electrochemical reaction. In contrast, chemical reactions where electrons are transferred between molecules are called oxidation/reduction (redox) reactions. In general, electrochemistry deals with situations where oxidation and reduction reactions are separated in space or time, connected by an external electric circuit to understand each process.

Voltammetry[3] is a category of electroanalytical methods used in analytical chemistry and various industrial processes. In voltammetry, information about an analyte is obtained by measuring the current as the potential is varied. Voltammetric

experiments investigate the half cell reactivity of an analyte. Most experiments control the potential (in volts) of an electrode in contact with the analyte while measuring the resulting current (in ampere's).

To conduct such an experiment requires at least two electrodes. The working electrode, which makes contact with the analyte, must apply the desired potential in a controlled way and facilitate the transfer of charge to and from the analyte. A second electrode acts as the other half of the cell. This second electrode must have a known potential with which to gauge the potential of the working electrode, furthermore it must balance the charge added or removed by the working electrode. While this is a viable setup, it has a number of shortcomings. Most significantly, it is extremely difficult for an electrode to maintain a constant potential while passing current to counter redox events at the working electrode, since this changes the chemical composition of the reference electrode and thus its potential.

To solve this problem, the role of supplying electrons and referencing potential has been divided between two separate electrodes. The reference electrode is a half cell with a known reduction potential. Its only role is to act as reference in measuring and controlling the working electrodes potential and at no point does it pass any current. The auxiliary or counter electrode passes all the current needed to balance the current observed at the working electrode. To achieve this current, the auxiliary will often swing to extreme potentials at the edges of the solvent window, where it oxidizes or reduces the solvent or supporting electrolyte. These electrodes, the working, reference, and auxiliary make up the three electrode system used in this thesis.

2.2   Electrochemical Cells

Electrochemical cells consist of two half cells separated by a salt bridge, as described below. Within a cell the two components that generate the potential of the cell can be represented by the following cell diagram.

$$\textbf{Pt, H}_2 \,|\, \textbf{H}^+ \,\|\, \textbf{M}^{n+} \,|\, \textbf{M} \qquad\qquad\qquad (2.1)$$

The single lines show a phase boundary between the species, *e.g.* electrode and electrolyte with the double vertical line showing the separation *via* a salt bridge. The electrode couple is shown by:

$$\textbf{E}_{\textbf{cell}} = \textbf{E}_{\textbf{right}} - \textbf{E}_{\textbf{left}} \qquad\qquad\qquad (2.2)$$

Where E_{right} is the potential of the right hand side and E_{left} is that of the left hand side and in this case hydrogen which has a potential, by the definition, of 0 V.[3] As a general rule the half cell that is more negative is the left hand side while the more positive half cell is the right hand side.

2.3   Generation of Electrode Potential

Generally studies are carried out with an electrolyte solution, when a piece of metal is immersed into this solution an electrode potential is generated. Within a metal the band gap is low so metals are conducting, whereas in a dielectric the band gap is large so the material is insulating.

When electrons fill the conduction band they can only fill the band until they reach a certain level known as the Fermi level, this level varies from metal to metal, when two metals are in close proximity electrons are transferred from the metal with the higher Fermi level to the one with the lower Fermi level releasing an electric potential. This done to lower the Fermi level of the first metal and to raise the Fermi level of the second metal until they are both equal stopping the electron transfer occurring.[4]

2.4   How are electrochemical experiments carried out?

In dynamic electrochemistry a potential difference is applied between an electrode and a solution containing an electrolyte, this potential difference results in the solution losing its electro-neutrality close to the electrode surface. Towards the end of the 19th century and the start of the 20th century, three models were generated in an attempt to understand what happens. Originally Helmholtz[5] assumed that counter ions formed a layer on the electrode causing the surface area to become neutral.

Later Gouiy[6] and Chapman[7] found that the ions are subject to random thermal motion, so they cannot immobilize onto the electrode instead the ions are spread around the solution forming a diffuse double layer.

Stern[8] then proposed that in fact both models are correct; it is a combination of the two models that some ions are immobilized on the electrode surface due to attraction forces and some ions form the diffusion double layer, figure 2.1 below shows the Stern model:
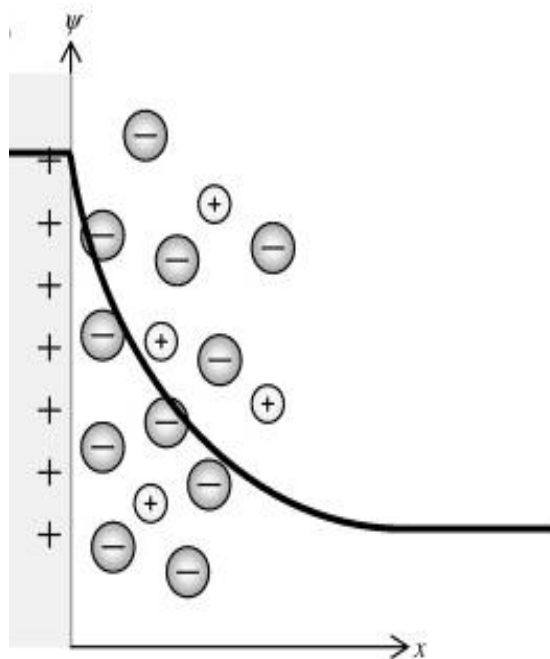
Figure 2.1: Diagram of the stern model.

If the solution used contains electroactive species it can undergo oxidation and reduction *via* the transfer of electrons from the electrode to the electrolyte, this transfer is observed as current and is known as the Faradaic current, and obeys Faraday's Laws on electrolysis. The currents measured will show whether the electrolyte has been oxidised or reduced, if the value is negative then the electrolyte has been reduced, or positive if the electrolyte has been oxidised.

2.5   Mass Transport

In order for the current to be sustained at a given potential there needs to be a constant movement of ions through the solution to the electrode this is known as mass transport. [10] There are three types of mass transport[11, 12]:

- diffusion,

- migration and

- convection.

These all occur simultaneously and each contribute to the total current observed.

2.5.1 Diffusion

Diffusion is the movement of the particles against a concentration gradient, moving from an area of high concentration to an area of low concentration, this is governed by Fick's two laws on diffusion[10, 14]: Fick's first law involves the flux, which is the rate at which the particles move across through the gradient.

$$J_A = D_A \frac{\partial [A]}{\partial x} \qquad (2.3)$$

This is written in terms of diffusion occurring at an electrode surface, where J_A is the flux of the oxidative species, D_A is the diffusion coefficient of the species oxidised, x is the distance from the electrode and [A] is the concentration of the oxidation species. Fick's second law predicts how the diffusion causes the concentration to change with time:

$$\frac{\partial [A]}{\partial x} = D_A \frac{\partial^2 [A]}{\partial x^2} \qquad (2.4)$$

Following this Nernst observed that the area between the electrode and the bulk solution is where the diffusion gradient lies; an example is shown below in figure 2.2:
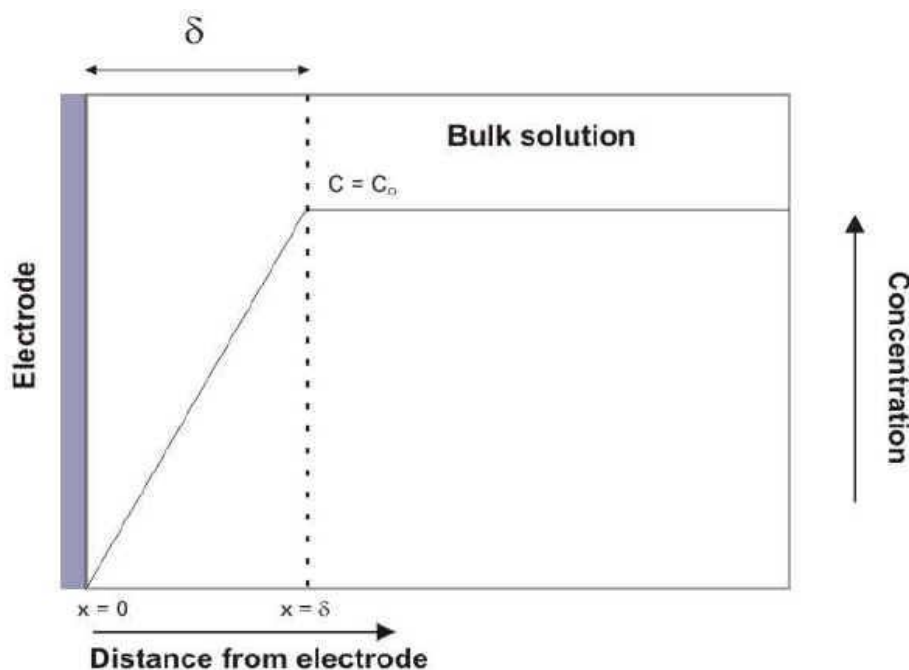
Figure 2.2: Example of Nernst Diffusion layer[15]

Nernst originally estimated the diffusion layer thickness and from this the flux and then the current can be calculated by:

$$i_A = nFAD_A \frac{[A]_{bulk} - [A]_{x=0}}{\delta} \qquad (2.5)$$

Where: n is the number of electrons transferred, F is Faraday's Constant, A is area of electrode, D_A is diffusion Coefficient of species A, [A] is concentrations of species A within the bulk solution and at the electrode surface and δ is the diffusion layer thickness. The current calculated from this equation equates to the diffusion part of the entire current.

2.5.2 Migration

Migration as a form of mass transport can be considered as an electrostatic attraction, caused by the application of voltage to the charged interfaces (electrodes). Due to the electrostatic forces within this charged interface, any charged species present are either repelled or attracted. [16]

Migratory flux within the system can be mathematically illustrated, as in Eq.2.6; however it must be noted that due to the interactions of diffuse layers and ion solvation effects, the migratory flux is difficult to calculate for a real solution.

$$\frac{\partial [O]}{\partial t} = -u[O]\left(\frac{\partial \emptyset}{\partial x}\right) \quad [17] \tag{2.6}$$

To counteract the effect, two practices are commonly seen within electrochemistry. To minimise the effects a large amount of electrolyte is added, effectively shielding the reactants from migratory effects, this addition also serves a useful purpose as a conductor to help in the flow of current through the solution.

Secondly, voltammetric experiments are most commonly carried out in solutions containing a 'background analyte', which is present to negate the effects of migration on the reactants themselves. Background electrolytes are most commonly salts, such as KCl and NaCl.

This has the additional advantage "fixing" the activity coefficients so that dynamic electrochemistry can be investigated in terms of concentrations of redox species.

2.5.3 Convection

The final type of mass transport is convection; this involves transport *via* a mechanical process either naturally or forced[18], natural convection is the result in gravity acting on a change of density around the electrode, whereas forced convection is the result of mechanical stirring for example mixing a solution with the electrode.[18] The mass transport of convection is simply measure by:

$$\mathbf{J_A} = \mathbf{v_A[A]} \tag{2.7}$$

where: v_A is the velocity of the solution upon force and other terms have the same definitions as described previously.

The three forms of mass transport can be collectively combined to form the Nernst-Planck equation:

$$J_A = -D_A \frac{\partial[A]}{\partial x} - \frac{DzE[A]F}{RT}D_A + v_A[A] \tag{2.8}$$

From this it is possible to calculate the total flux required, keeping the current at a constant rate and then keep a constant potential difference being released into the external circuit.

2.6 Ways to Measure Potential Differences and Currents

There are many different techniques that can be used to measure potential difference and currents that are generated through electrochemical processes. Two commonly used techniques are, these are discussed below, chronoamperometry, and cyclic voltammetry. [19]

2.6.1 Chronoamperometry

Chronoamperometry [19-21] works by maintaining the working electrode at a fixed potential *vs*. the reference; normally the voltage at which the species in question will oxidise or reduce, wiliest maintaining the current as a function of time. For simple chemically reversible system, these data provided on the diffusion coefficient of the redox species using the Cottrell equation shown below: [21]

$$i = \frac{nFAD^{\frac{1}{2}}C_0}{(\pi t)^{\frac{1}{2}}} \tag{2.9}$$

where: i = current (A), n = number of electrons transferred during the reaction, F = Faraday's Constant, D = Diffusion coefficient, A = Area of electrode surface, t = time And C_0 = concentration[22].

2.6.2 Cyclic Voltammetry

This is most common form of voltammetry used to study electrochemical processes, it is also one of the simplest techniques to use and understand, with the results obtained giving a lot of information. So this section will be considerably larger to that of the previous techniques. Experiments are carried out by using three electrodes, a working electrode, a counter and a reference electrode.

The purpose of the working electrode is to deliver the electricity to the sample where the electrochemical reactions will take place, whereas the counter or auxiliary electrode is used to carry the current but in no means interfere with the analysis[20], to enable this to happen the electrode needs to have a high surface area.[21] The scans are done at a certain scan rates for example mV s^{-1} however this can vary over nine orders of magnitude (from mVs^{-1} to MVs^{-1}). [21]

The scan is done over a cycle starting at a potential 1, going to potential 2 and back to potential 1, within this process the sample is oxidised and then reduced back to its starting oxidation state if the reaction is reversible or just oxidise if the process is irreversible, this is done over as many scans as desired.

Figure 2.3 below shows a typical cyclic voltammogram that is generated for a reversible:
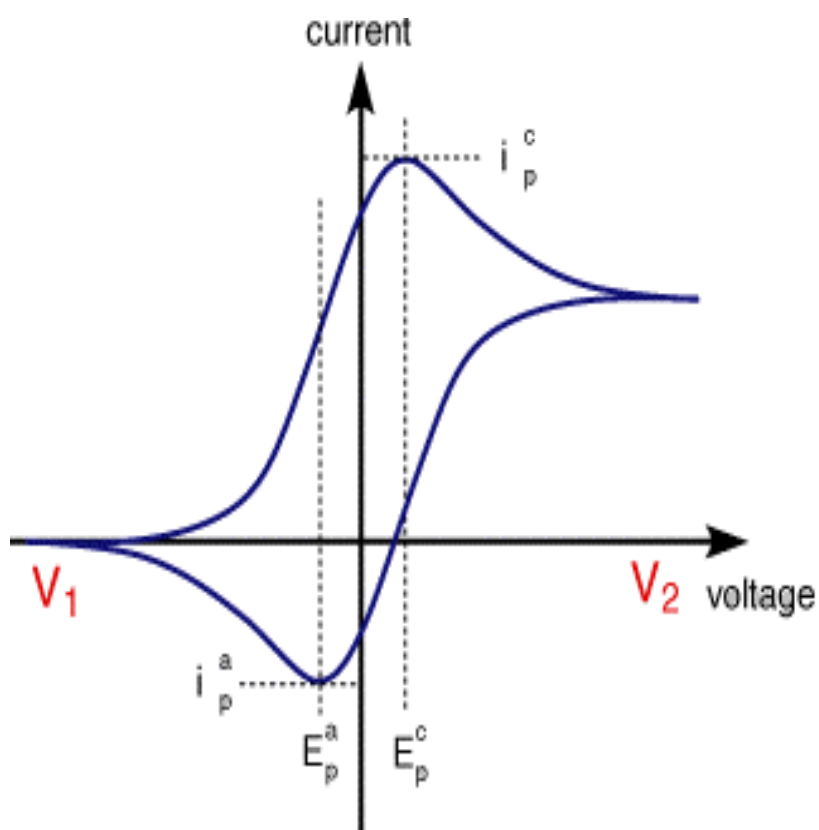
Figure 2.3: A cyclic voltammogram of a reversible chemical process[20]

From the diagram it is clear that when a species is oxidised it gives a prominent peak as well as when it is reduced. When analysing cyclic voltammograms each peak obtained is read separately where the peak current (i_p), peak potential (E_p) and current at which the oxidation or reduction begins (i_o) all these values need to be read and then placed into a table, figure 2.4 below shows where on a voltammogram these values are obtained:
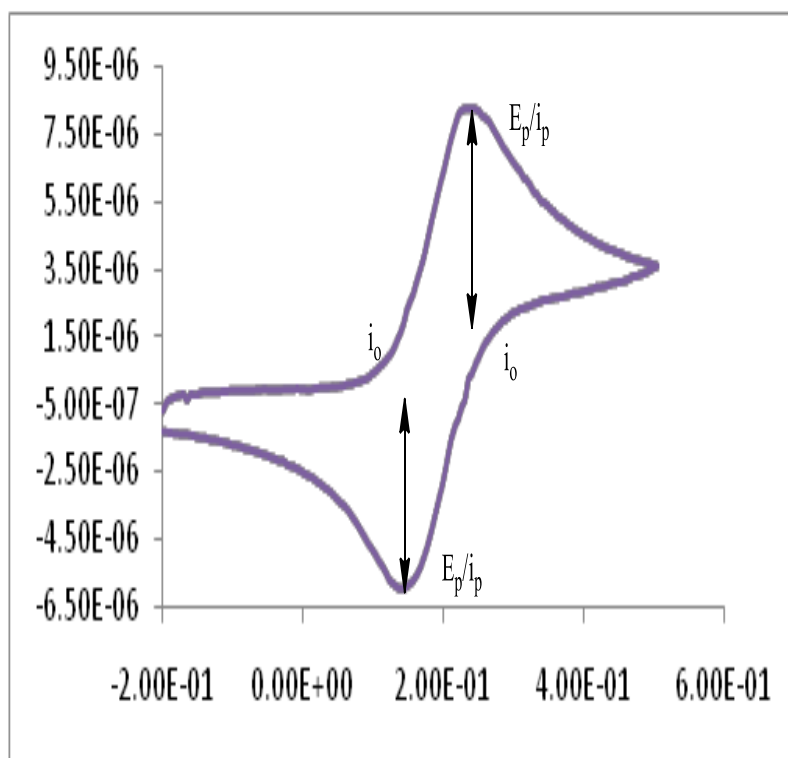
Figure 2.4: Where the values for i_p, E_p and i_o are found.

In the figure above shows a reversible electrochemical reaction and for an irreversible or quasi-reversible reaction (discussed later) the values are obtained in the same way.

2.6.2.1 Reversible Electrochemical Processes

To determine whether the process is reversible or not; the electrode kinetics need to be studied; if the kinetics are faster than the rate of diffusion then the process is reversible, this meaning that the forward and reverse processes are fast enough to maintain equilibrium or "Nernst" conditions[22], which mean it obeys the Nernst equation which is shown below, [23]

$$E = E^0 + \left(\frac{RT}{nF}\right) \ln\left(\frac{a_{ox}}{a_{red}}\right) \qquad (2.10)$$

where: E is the electrode potential at equilibrium, E^o is the standard electrode potential, a: is the activity of the oxidative species and reductive species respectively and F, n, R, T have their usual meanings.

Within equilibrium conditions the activity is unity so this is equal to the concentration of each species at the electrode surface so within a reversible electrochemical reaction the Nernst conditions are defined as:

$$E = E^0 + \left(\frac{RT}{nF}\right) \ln\left(\frac{[A]_{ox}}{[A]_{red}}\right) \qquad (2.11)$$

The reversibility is dependent on the scan rate, when using a faster scan rate the rate of diffusion also increases at the electrode surface as well as the concentration gradient so measurements can become distorted whereas at slower scan rates the electrode kinetics can keep up with the rate of diffusion a lot easier.[23]

When analysing a sample the voltammetry is done over a number of scan rates allowing the diffusion coefficient to be calculated by plotting the peak current (i_p) against the square root of san rate ($v^{1/2}$) which is linear with the slope being used to determine the diffusion coefficient as shown below:

$$Slope = 0.4463 FA \sqrt{\frac{Fn}{RT}} C_{ox} D^{1/2} \qquad (2.12)$$

The electrode kinetics can be seen by plotting the maximum electrode potential (E_p) against the $\log_{10}$ of the scan rate shows how the kinetics change at different scan rates. Within a reversible one- electron electrochemical process the peak separation of the oxidation peak and reduction peak is in the region of 56 m V.[25]

2.6.2.2   Irreversible Electrochemical Processes

Irreversible processes mean the electrode kinetics are slow comparable with the rate of diffusion, so that Nernstian equation is not upheld at the electrode surface.

When this happens the kinetics of the chemical reaction needs to be addressed, the kinetics of these reactions is first order, because of this only the rate constant (k_o) can influence the kinetics, it is found that when a process is irreversible the rate constant is very small; this indicates a lot of energy is needed to drive the oxidation and there is no reverse peak as the reverse reaction does not occur.[26]

When it comes to analysis this is done in the same way as the reversible process, where the peak current, peak potential and starting current are measured but only the oxidation peak is analysed.
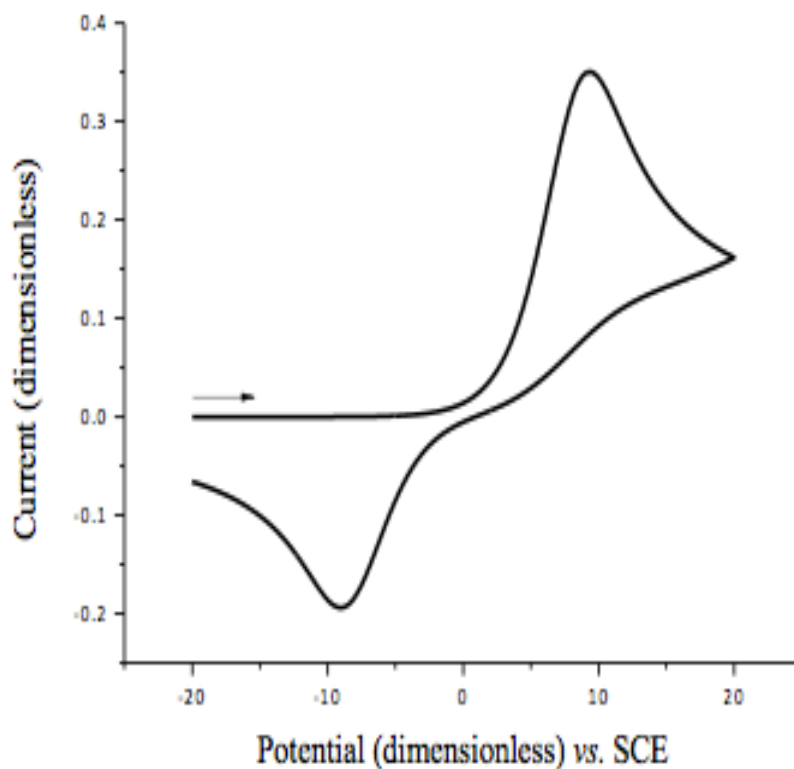
Figure 2.5: Digital simulation of a voltammogram for an electrochemically

irreversible system.

2.6.2.3 Quasi-Reversible Electrochemical Processes

A quasi-reversible process[24] is a process that is neither reversible nor irreversible, when a one electron process is quasi-reversible generally at slower scan rates the peak to peak distance is of about 56 mV however when faster scan rates are used the peak to peak distance can be lot larger an example of a quasi-reversible cyclic voltammogram is shown in figure 2.6 below:
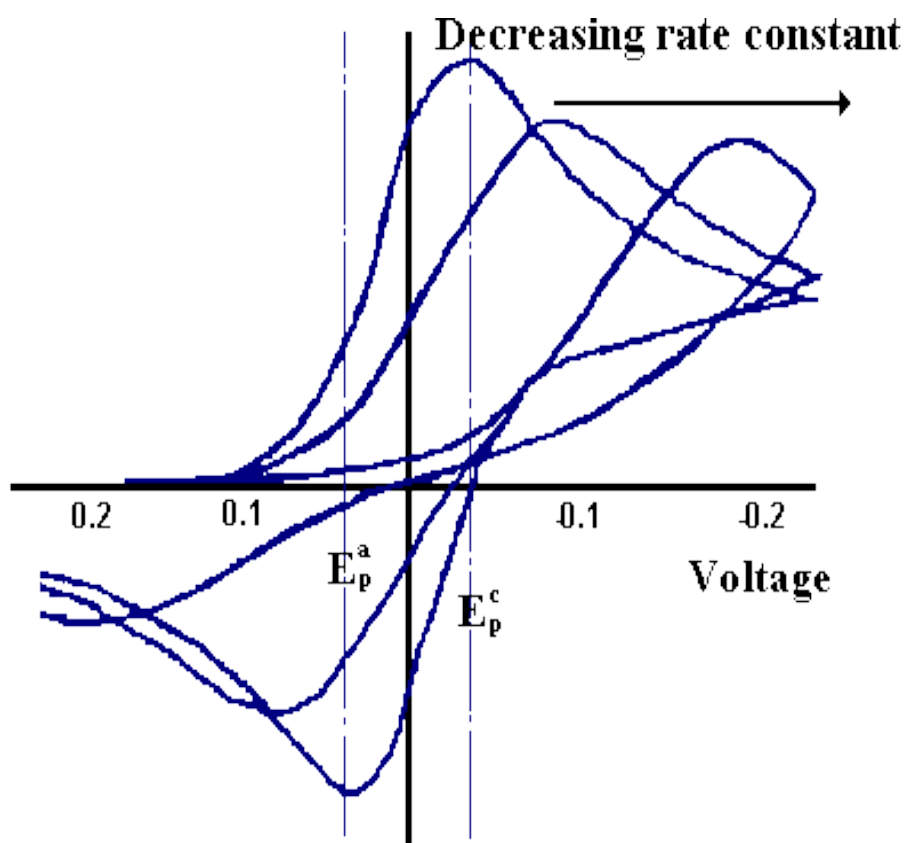
Figure 2.6: Example of a quasi-reversible cyclic voltammogram[24]

The voltammogram with the two vertical lines represents the 56 mV difference, this is at a high rate constant, indicating the electrode kinetics and the kinetics of the reaction are equal and meet the Nernst requirements.

2.7   Research Objectives

Electrochemistry has many reasons for study not just to find out electrical properties of molecules but also to find ways to power peoples ever needing reliance on electricity, understanding electrochemistry enables us to make galvanic cells (batteries) to power portable devices with the way the world is there is the need to try and find ways to use solar power within a battery system (photogalvanic cell); it is this area of electrochemistry on what this thesis focuses on:

Parts of this thesis are studying electron transport in the isotropic micelles cubic representative in I_1 phase and anisotropic representative in H_1 and L_α phases lyotropic liquid crystal (LLC) (chemical nanosystems), to investigate a long range of electron transport between molecules contain with the individual micelles. After that, to use the nanosystems to develop energy storage devices such as batteries and solar cells, to generate a working galvanic cell that can be used in portable devices with the intention to converting the cell into an operable photogalvanic cell in the future. However, the use of birefringent lyotropic liquid crystal frameworks causes the possibility of anisotropic diffusion of redox analytes doped within the phase. We are concerned with effects due to the orientation of the phase relative to the electrode. We probe the flux within these structured liquid nanosystems within merely one dimension.

The others parts are studying and optimising a series of photogalvanic cells in order to achieve the highest power conversion as well as study the mechanism for power production within the cells. They would be desirable to produce electrical power from wastewater.   Then, investigate if we can use environmental pollutants, such as

chlorinated organic (such as chloroform, polyaromatic chlorides, *et hoc genus omne*) to generate electricity using light to "*de-toxify*" those pollutants by removing the chlorine. The long term plan of these studies however, is to use these pollutants as electrochemical remediation power sources for waste water management: Generate electricity from "free energy" and "waste", environmentally friendly and a very little cost to operate.

References for Chapter 2

1. D.R. Crow, *Principles and Applications of Electrochemistry*, 1994, 4, 105

2. P.H. Reiger, *Electrochemistry*, 1994, 4, 60

3. H. von Helmholtz, *Wied Ann*, 1879, 7, 337

4. L.G. Gouy, *J. Phys Chem*, 1910, 9, 457

5. D.L. Chapman, *Phil. Mag*, 1913, 25, 475

6. O. Stern, *Z. Elektrochem*, 1924, 30, 508

7. S.P. Kounaves, *Instrumental Techniques for Analytical Chemistry*, 1997, 1, 709

8. P. Ostapczuk, Z.Kublik, *J. Electroanal. Chem*, 1976, 68, 193

9. A. J. Bard & L. R. Faulkner, *Electrochemical Methods: Fundamentals and Applications*,2001, 2, 156

10. D.B. Hibbert, *Intro to Electrochemistry*, 1993, 157

11. A.D. McNaught, A. Wilkinson, *IUPAC Compendium of Chemical Terminology*, 1997,2

12. C.H. Hamann, A. Hamnett and W. Vielstich, *Electrochemistry*, 1998, 1, 82

13. R.A. Etchenique, E.J. Calvo, *J, Electrochem Commun*, 1991, 1, 167

14. A.C. **Testa**, W. **Reinmuth**, *Anal. Chem*, 1961, 33, 1320

15. D. Gust, T. A. Moore, A. L. Moore, *Acc. Chem. Res.*, 34 (2001) 40.

16. J. Barber, *Chem. Soc. Rev.*, 38 (2009) 185.

17. G. Steinberg-Yfrach, P. A. Liddell, S.-C. Hung, A. L. Moore, D. Gust, T. A. Moore, *Nature*, 385 (1997) 239.

18. R. E. Blankenship, D. M. Tiede, J. Barber, G. W. Brudvig, G. Fleming, M. Ghirardi, M. R. Gunner, W. Junge, D. M. Kramer, A. Melis, T. A. Moore, C. C. Moser, D. G. Nocera, A. J. Nozik, D. R. Ort, W. W. Parson, R. C. Prince, R. T. Sayre, *Science*, 332 (2011) 805.

19. W. Vredenberg, *BioSystems*, 103 (2011) 138.

20. J. Armstrong, W. Armstrong, *New Phytol.*, 126 (1994) 493..

21. J. D. Wadhawan, A. J. Wain, R. G. Compton, *ChemPhysChem*, 4 (2003) 1211.

22. C. R. Bradbury, L. Kuster, D. J. Fermín, *J. Electroanal. Chem.*, 646 (2010) 114.

23. G. P. Kissling, C. Bunzli, D. J. Fermín, *J. Am. Chem. Soc.*, 132 (2010) 16855.

24. C. E. Banks, T. J. Davies, R. G. Evans, G. Hignett, A. J. Wain, N. S. Lawrence, J. D. Wadhawan, F. Marken, R. G. Compton, *Phys. Chem. Chem. Phys.*, 5 (2003) 4053.

25. M.-H. Lee, S.-G. Oh, K.-D. Suh, D.-G. Kim, D. Sohn, *Colloids Surf. A.*, 210 (2002) 49.

26. A. N. Galatanu, I. S. Chronakis, D. F. Anghel, A. Khan, *Langmuir*, 16 (2000) 4922.

Chapter 3 - Experimental

3.1   Instrumentation

The electrochemical measurements were recorded using an Autolab PGSTAT30 potentiostat controlled by a Pentium IV processor computer. In all cases, unless otherwise stated, a three electrode system was employed, with a platinum wire wound into a spiral serving as the counter electrode, and a standard calomel electrode as reference electrode in aqueous systems whereas in non-aqueous systems either a silver/silver chloride or silver wire were utilised as the reference electrode .

 The working electrodes were polished prior to voltammetry being undertaken using decreasing grades of carbuundum paper (400, 1200 2400 grade, Presi, France) followed by polishing on a cloth using 3 μm alumina paste (Presi, France).

3.1.1 Microelectrodes

All microelectrodes were polished prior to use using a fine grade of carborundum paper (2400) and finally alumina paste (0.3 μM). Each microelectrode was electrochemically calibrated prior to use in order to obtain an accurate measurement of the electrode radius. This was achieved using solutions of containing various concentrations of either ferrocyanide or ferrocene depending on the system in use and using the following equation:

$$i = 4nFDCr_0 \qquad\qquad (3.1)$$

The diffusion coefficient, D was taken to be 0.76×10^{-5} cm² s⁻¹ for ferrocyanide [1] in aqueous 0.1 MKCl and 2.3×10^{-5} cm² s⁻¹ for ferrocene in 0.1 M trtra-*n*-butylammonium perchlotate (TBAP) and acetonitrile.[2]

3.1.2 Indium Tin Oxide Electrode

Indium tin oxide (ITO) [3] is one of the most widely used transparent conducting oxides because of its two chief properties, its electrical conductivity and optical transparency, as well as the ease with which it can be deposited as a thin film. As with all transparent conducting films, a compromise must be made between conductivity and transparency, since increasing the thickness and increasing the concentration of charge carriers will increase the material's conductivity, but decrease its transparency.

Thin films of indium tin oxide are most commonly deposited on surfaces by physical vapor deposition. Often used is electron beam evaporation, or a range of sputter deposition techniques. ITO is often used to make transparent conductive coatings for displays such as liquid crystal displays, flat panel displays, plasma displays, touch panels, and electronic ink applications. Thin films of ITO are also used in organic light-emitting diodes, solar cells, antistatic coatings and EMI shieldings. In organic light-emitting diodes, ITO is used as the anode (hole injection layer).[4]

ITO is also used for various optical coatings, most notably infrared-reflecting coatings (hot mirrors) for automotive, and sodium vapor lamp glasses. Other uses include gas sensors, antireflection coatings, electrowetting on dielectrics, and Bragg reflectors for VCSEL lasers. ITO was also used as a sensor coating in the later Kodak DCS cameras, starting with the Kodak DCS 520, as a means of increasing blue channel response.[4] ITO thin film strain gauges can operate at temperatures up to 1400 °C and can be used in harsh environments, *e.g.* gas turbines, jet engines, and rocket engines.[5]

3.1.3 UV-Visible Spectrometry

UV-visible spectrometry was undertaken using an Agilent 8453E UV-visible spectrometry system (Agilent Technologies, Germany), with a clear glass cuvette of path length 1 cm. The spectrometer was controlled using UV-vis chemstation software.

3.2 Reagents

All reagents were prepared using Analytical Grade chemicals, and all aqueous solutions were made up using deionised water from an Elgstat water system with a resistivity of not less than 18 MΩ cm. Any solvents used were of HPLC grade, and used without further purification. All solutions were purget with impurity free nitroben prior to voltammetry, whilst the experiments themselves were conducted under a nitrogen or argon atmosphere.

References for chapter 3

1. G. Kawachi, E. Kimura, Y. Wakui, N. Konishi, H. Yamamoto, Y. Matsukawa and A. Sasano, *IEEE Trans. Electron Devices* 41, 1120 (1994)

2. C. W. Tang and S. A. Vanslyke, *Appl. Phys. Lett.* 51, 913 (1987)

3. Y. Lee, J. Kim, J. N. Jang, I. H. Yang, S. Kwon, M. Hong, D. C. Kim, K. S. Oh, S. J. Yoo, B. J. Lee and W. Jang, *Thin Solid Films* 517, 4019 (2009)

4. T. Ameri, G. Dennler, C. Waldauf, H. Azimi, A. Seemann, K. Forberich, J. Hauch, M. Scharber, K. Hingerl and C. J. Brabec, *Adv. Funct. Mater.* 20, 1592 (2010)

5. J. Jeong and H. Kim, *Sol. Energy Mater. Sol. Cells* 93, 1801 (2009)

Chapter 4 - Concentration-Dependent Diffusion Coefficients of *tert*-Butylferrocene within I_1 phase liquid crystals

4.1   Basic about Liquid Crystals

Liquid crystals (LCs) are a state of matter that has properties between those of a conventional liquid and those of a solid crystal.[1,2] There are many different types of LC phase, which can be distinguished by their different optical properties (such as birefringence). When viewed under a microscope using a polarized light source, different liquid crystal phases will appear to have distinct textures. The contrasting areas in the textures correspond to domains where the LC molecules are oriented in different directions.

Liquid crystals can be divided into thermotropic, lyotropic and metallotropic phases.[1] Thermotropic and lyotropic LCs consist of organic molecules. Thermotropic LCs exhibit a phase transition into the LC phase as temperature is changed. Lyotropic LCs exhibit phase transitions as a function of both temperature and concentration of the LC molecules in a solvent (typically water). Metallotropic LCs are composed of both organic and inorganic molecules; their LC transition depends not only on temperature and concentration, but also on the inorganic-organic composition ratio.

4.1.1 Liquid crystal phases

The various LC phases (called *mesophases*) [1] can be characterized by the type of ordering. One can distinguish positional order (whether molecules are arranged in any sort of ordered lattice) and orientational order (whether molecules are mostly pointing in the same direction), and moreover order can be either short-range (only between molecules close to each other) or long-range (extending to larger, sometimes macroscopic, dimensions).

Most thermotropic the ordering of liquid crystalline phases is extensive on the molecular scale. This order extends up to the entire domain size, which may be on the order of micrometers, but usually does not extend to the macroscopic scale as often occurs in classical crystalline solids. However some techniques, such as the use of boundaries or an applied electric field, can be used to enforce a single ordered domain in a macroscopic liquid crystal sample. The ordering in a liquid crystal might extend along only one dimension, with the material being essentially disordered in the other two directions.

4.1.2 Thermotropic liquid crystals

Thermotropic phases are those that occur in a certain temperature range. If the temperature rise is too high, thermal motion will destroy the delicate cooperative ordering of the LC phase, pushing the material into a conventional isotropic liquid phase. At too low temperature, most LC materials will form a conventional crystal. Many thermotropic LCs exhibit a variety of phases as temperature is changed.

For instance, a particular type of LC molecule (called mesogen) may exhibit various smectic and nematic (and finally isotropic) phases as temperature is increased. An example of a compound displaying thermotropic LC behavior is para-azoxyanisole.[2]

4.1.3   Liquid Crystalline Phases and Composition and Temperature

The simplest liquid crystalline phase that is formed by spherical micelles is the 'cubic', or (I_1 phase) [2]. This is a highly viscous, optically isotropic phase in which the micelles are arranges on a cubic lattice. At higher amphiphile concentrations the micelles fuse to form cylindrical aggregates of indefinite length, and these cylinders are arranged on a long-ranged hexagonal lattice. This lyotropic liquid crystalline phase is known as the 'hexagonal phase', or more specifically the 'normal topology' hexagonal phase and is generally called (H_1 phase).

 At higher concentrations of amphiphile the 'lamellar phase' is formed. This phase is called also (L_α phase). This phase consists of amphiphilic molecules arranged in bilayer sheers separated by layers of water. Each bilayer is a prototype of the arrangement of lipids in cell membranes.

For most amphiphiles that consist of a single hydrocarbon chain, one or more phases having complex architectures are formed at concentrations that are intermediate between those required to form a hexagonal phase and those that lead to the

formation of a lamellar phase. Often this intermediate phase is a bicontinuous cubic phase.

LCs will have an isotropic phase at high temperature. That is that heating will eventually drive them into a conventional liquid phase characterized by random and isotropic molecular ordering (little to no long-range order), and fluid-like flow behaviour. Under other conditions (for instance, lower temperature), an LC might inhabit one or more phases with significant anisotropic orientation structure and short-range orientation order while still having an ability to flow.
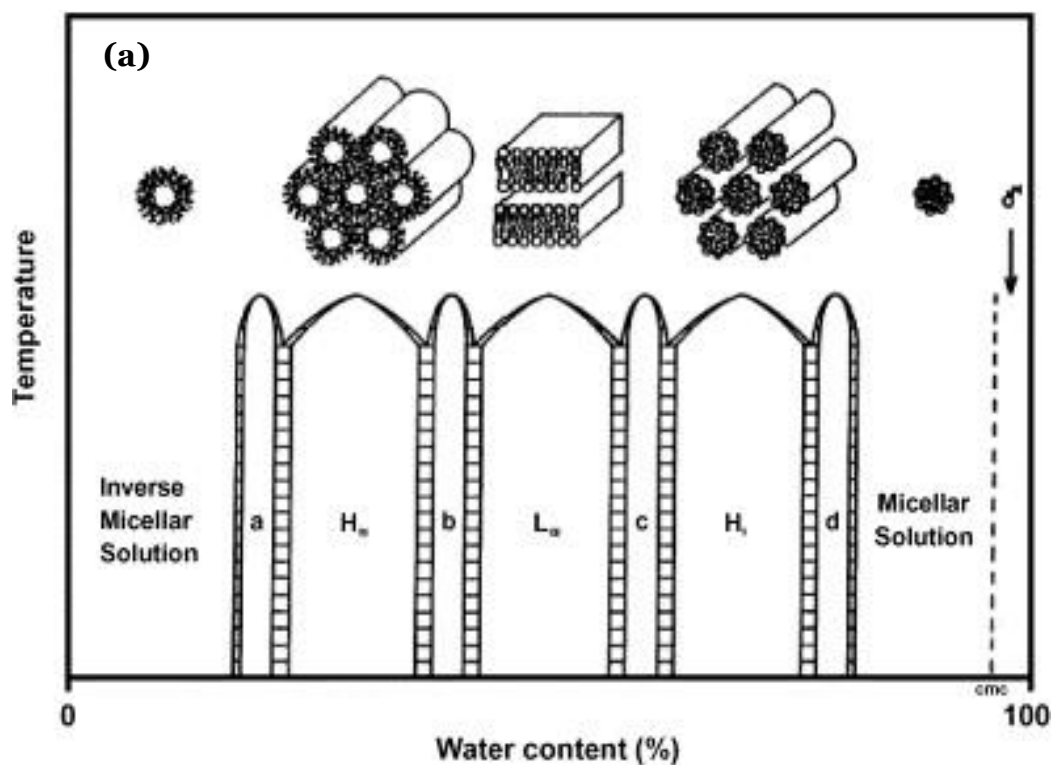
Figure 4.1: (a) Phase diagram of the main liquid crystalline phases. Taken from. [3]
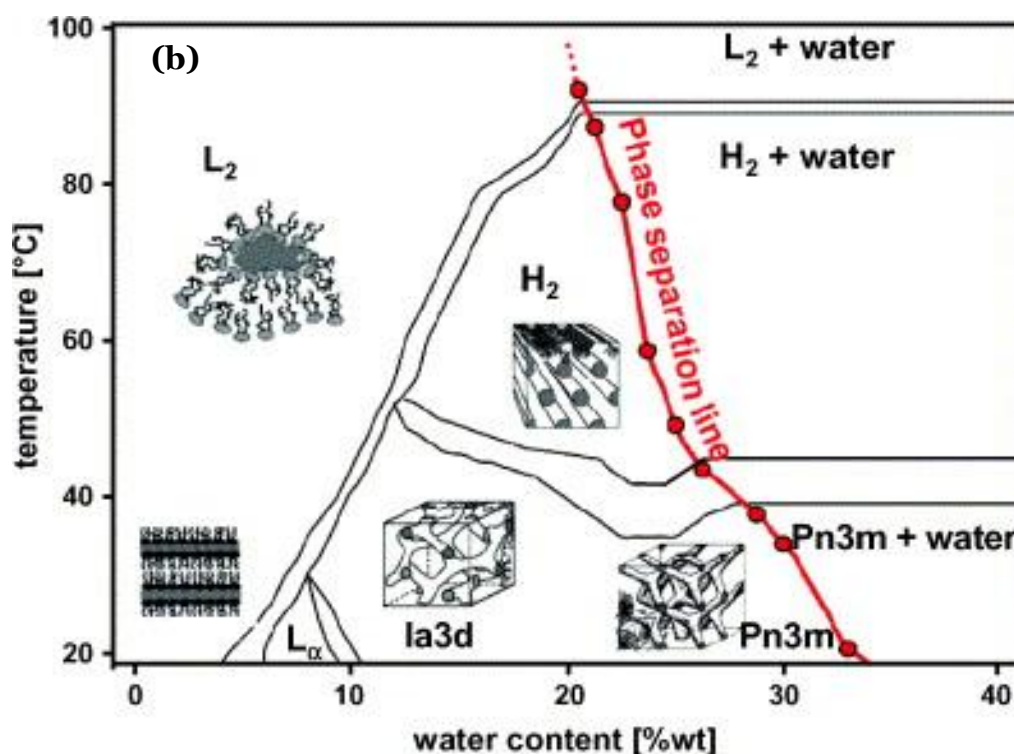
Figure 4.1: (b) Binary monolinolein/water phase diagram as a function of temperature. The phase separation line separates the single-phase and the excess water region; taken from [5]

4.1.4 Cubic Phase (I_1)

There are two distinct aggregate structures that are classes as cubic phases, also known as viscous, isotropic phases [5-7]. One of these consists of small micelles (normal or reversed) and the other one is based on three-dimensional bicontinuous aggregates (see Figure 4.2 and 4.3). In some cases, as the micelle concentration is increased, the micelles arrange into loose lattice patterns which are similar to crystal structures in terms of the arrangement. The first set of structures (small micelles) is labelled *I*, again with 1 or 2 to distinguish between normal and reverse micelles respectively.

As their name suggests the structures are based around one of several cubic lattices, namely, normal cubic lattice, face-centred cubic lattice and body-centred cubic lattice. The bicontinuous classes are labelled V_1 and V_2 again corresponding to normal and reversed structures.

The cubic phases are isotropic and therefore appear black under crossed polarisers. They posses extremely high viscosity and they are distinguished by their position in the phase diagram. The I_1 phases occur at compositions between micellar solutions and hexagonal phases whereas the V phases between the hexagonal and lamellar phases.
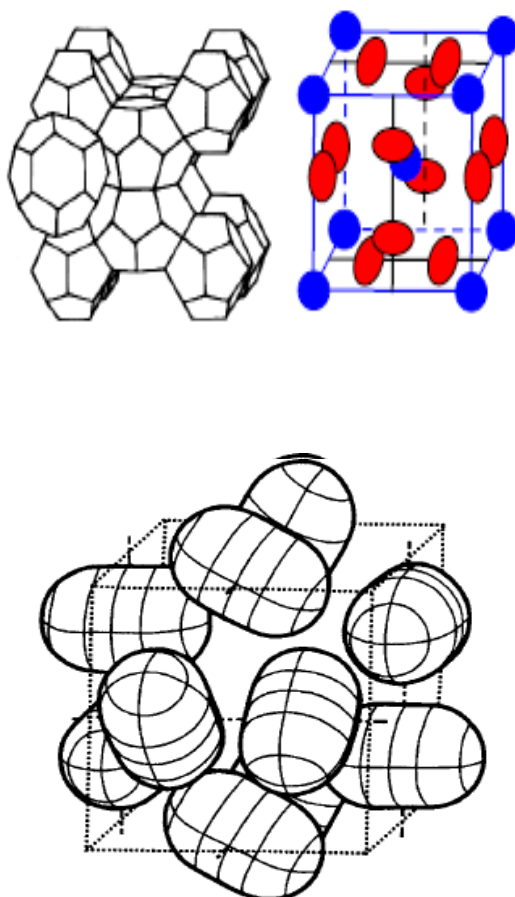
Figure 4.2: I_1 Phase is a highly viscous and optically isotropic phase. Taken from [4]
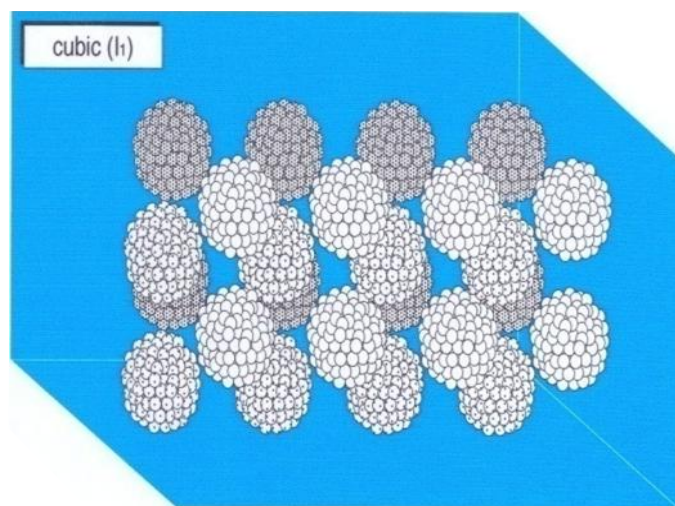
Figure 4.3: The structure of a type I micellar cubic phase showing spherical

micelles disposed on a body-centred cubic lattice. Taken from [4]

4.1.5 Lamellar phases L_α

The most common surfactant mesophase is the lamellar phase (L_α), also known as

the 'neat phase'[8, 9]. Within this phase, the surfactant molecules are arranged into

stacks of ordered bilayers extending over large distances (a micron or more), which

are separated by water layers[10].

The L_α phase is easily recognisable from both its rheological and optical properties.

Within the L_α phase the layers are flat and the alkyl chains are in a liquid-like state so

each parallel layer can slide over each other with ease during shear which accounts

for the low viscosity of the system. It can usually easily be shaken into a container

and at high water concentrations is even pourable. When viewed under crossed

polarisers on a polarising optical microscope, the L_α phase exhibits characteristic

optical textures.

If the sample is non-oriented a mosaic texture with many defects and birefrigence colours results. Shear orientation of the lamellar bilayers parallel to the surface of the microscope slide produces pseudo-isotropic textures such as oily streaks and Maltese crosses [11, 12]. Air bubbles are spherical (if present) due to low viscosity medium they reside in.
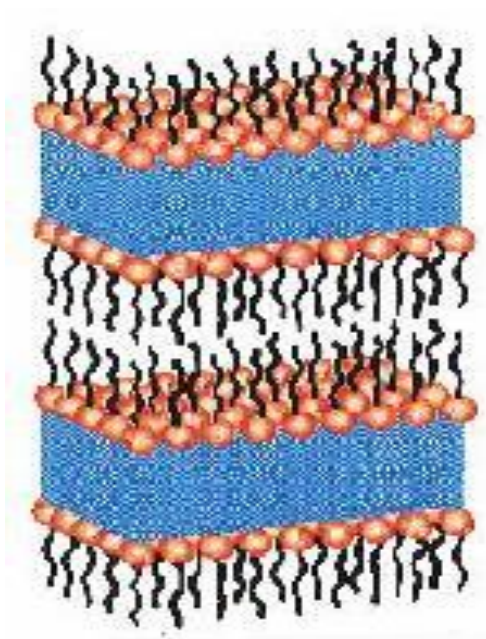
Figure 4.4: The structure of a type L_α micellar the surfactant molecules are arranged into stacks of ordered bilayers extending over large distances. Taken from [13]

4.1.6 Hexagonal Phase (H_1)

There are two types of hexagonal phase, which are the 'normal hexagonal' (H_1) phase, also known as the middle phase from soap industry, and the 'reversed hexagonal' (H_2) phase.[14-17] H_1 is water continuous forming if the surfactant is added to a polar liquid such as water. At low water concentrations, reversed hexagonal phase H_2 can

occur. H_2 is alkyl-chain-continuous forming if the surfactant is added to a non-polar liquid such as oil.

Hexagonal phase is identifiable by unique optical textures observed under polarised light including 'fan like' and so called non-geometric textures. The optical textures are similar for both types of hexagonal phase. The micelle diameter in normal structures is usually between 1.3-2.0 times the all-trans alkyl chain length (l_t) with the inter-micellar separation being in the region of 10-50Å.[15]

4.1.7 Polarising Optical Microscopy

Optical microscopy is an extremely powerful tool when a study on the microstructure of liquid crystal mesophases is initiated.

Polarised optical microscopy exploits optical properties of anisotropy and offers a wealth of information, which is simply not available with any other optical technique[1]. The idea is to identify the mesophases formed by the liquid crystals since most of the mesophases display unique optical textures.[2-4]

- **Polarised Light**

Normal light is an electromagnetic radiation composed of electric (E) and magnetic (B) components vibrating perpendicular to each other and to the direction of propagation. In a microscope, normal un-polarised light from radiant halogen bulb passes through the polariser to transform it to plane polarised light.

The polariser is sited below the specimen stage and the analyser is situated above the objectives and can be moved in and out of the light path as required. When both the analyser and polariser are in the optical path, their permitted vibration directions are positioned at right angles to each other.

In this configuration, the polariser and analyser are crossed, with no light passing through the system under investigation and a dark texture present in the eyepieces[2]. When an anisotropic substance is placed between crossed polarisers, the plane of polarised light is rotate in such a way that some light passes through the analyser and the object appears bright.

- **Birefringence**

Liquid crystals are classified as anisotropic or isotropic. Anisotropic material contains a molecular density which depends on the directions. As a result, light travels with different velocities along different directions in the material leading to different refractive indices. The refractive index is given by:

$$\mathbf{n= v/c}$$

where c is the velocity of the light in vacuum and v is the velocity of the light in that media.

When polarised light passes through an anisotropic phase, it is split into two parallel rays named 'ordinary' and 'extra-ordinary' rays associated with ordinary refractive index (n_o) and extra-ordinary refractive index (n_e). This phenomenon is known as double or birefraction. The birefringence is given by:

$$\Delta n = n_e - n_o$$

Birefringence can be of two types, positive birefringence and negative birefringence. If the characteristic index along the optic axis (n_e) is greater than the characteristic index normal to this axis (n_o) the material is said to be 'optically positive'. In the reverse situation the birefringence is said to be negative.

As the refractive index (n) defines the speed of light in the material, the wavelength (λ) and velocity of the light (v) will be slowed down by (n), the degree of which is dependent on the polarisation. The change in (λ) means changes in the colours observed and that is related to the sample thickness.

On the other hand, isotropic substances have only one refractive index and no restriction on the vibration direction of light passing through them. The isotropic phases under crossed polarisers appear dark (black).

4.2   Aim and Scope

Electron transport within such systems can then take place either through super-exchange phenomena, or *via* carrier hopping, provided counter ion transport is facile[18-21]. Herein, cyclic voltammetry is employed to deduce one-dimensional mutual diffusion coefficients of *t*BuFc (a well-known hydrophobic redox-switchable probe) randomly dispersed within three-dimensions inside the yoctolitre micelle ensembles of the optically isotropic discontinuous cubic phase (I_1) formed at 50 wt. % dodecyltrimethylammonuim chlorides (DOTAC) in brine [17].
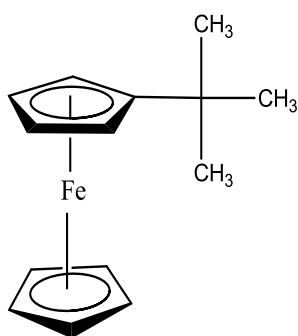
tert-butylferrocene (tBuFc) structure

The long term aims of this studying are:

- To study electron transport in the isotropic micelles cubic representative in I_1 phase and anisotropic representative in H_1 and L_α phases lyotropic liquid crystal (LLC) (chemical nanosystems).

- To investigate a long range of electron transport between molecules contain with the individual micelles.

The battery will consist of using lyotropic liquid crystals as a medium for the electrochemical process to occur, where the redox species is contained within the micelles of the liquid crystal and the electron transfer between the micelles the lamellar and hexagonal phase will each be used to determine whether a certain phase induces a better potential difference. However, this work looks at electron transport with these systems.

Dodecyltrimethylammonuim chloride (DOTAC) structure

4.3   Reagent and Instrumentation

•   All chemical reagents were purchased from Sigma-Aldrich or Strem. Water, of resistivity greater than 18.2 MΩ cm, was obtained from an Elgastat system (Vivendi, UK).

•   All electrochemical experiments were undertaken at 296 ± 0.5 K, using a commercial potentiostat (AUTOLAB, PGSTAT30), utilising a 3.0 mm diameter glassy carbon working electrode, a sodium-saturated calomel reference electrode (SSCE) and a nickel spiral counter electrode. The working electrode was cleaned using carborundum paper of increasingly finer grades and then polished using aqueous 0.3 Ωm alumina slurry.

•   In all experiments, the working electrode was polished and carefully placed in different positions for every change in experimental parameter, so as to encompass any effects due to sample polycrystallinity. Note that since the I_1 phase is isotropic, no consideration was given to how the phase was aligned with the electrode.

4.4   Procedure

•   The I_1 phase was prepared by adding a known mass of ^tBuFc to the solid surfactant and diluting with aqueous 0.1 M NaCl, with the mass ratio of the surfactant to aqueous electrolyte being 1:1 (50 wt. % DOTAC with 50 wt. % aqueous 0.1 M NaCl).

- The mixture was heated in a water bath, with vigorous stirring under nitrogen to 90 $^{\circ}$C to solubilise hydrophobic solutes within the micelles [22] and kept in the molten, isotropic micellar solution for at least two hours , after which, slow cooling to room temperature enabled the formation of the polycrystalline I_1 phase , of density 0.895 g cm^{-3}.

- As this phase is a single thermodynamic phase, all concentrations are reported in terms of moles per unit volume of I_1 phase.

4.5   Results and Discussion

- **Lyotropic Liquid Crystals under polarising microscopy**

All liquid crystals prepared appeared dark (at low *^{t}BuFc* loadings <2.6 mM) when viewed through crossed-polarisers, but exhibited radiance at higher loadings, suggesting hexagonal phase (H_1) formation [23], and we observed that very high loadings (*ca.* 150 mg ^{t}BuFc in 10 g DOTAC/10 g aqueous 0.1 M NaCl) formed two phase systems, where a small amount of the orange oil did not solubilise, even after prolonged periods of keeping the system in the molten state. (Figure 4.5 below)
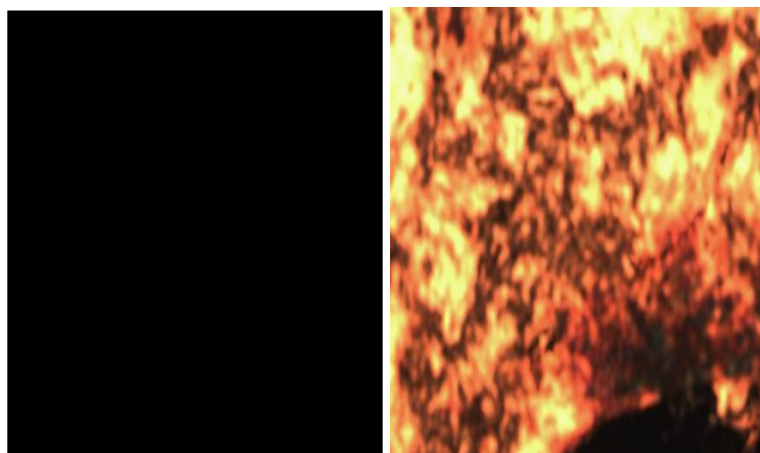
Figure 4.5: All liquid crystals prepared appeared dark (at low ^{t}BuFc when viewed through crossed-polarisers, whereas, they exhibited radiance at higher loadings.

Such loadings correspond to occupancies of greater than one ^{t}BuFc molecule-per-micelle; we propose that saturation of the lyotropic liquid crystal occurs when the complete micellar occupancy is unity [24,25]. This seems reasonable considering the solubilisation of each ^{t}BuFc (of assumed spherical radius [19] 3.9 Å) within the liquid-like hydrophobic micellar core would effect, at most, a micellar swelling [25] (assuming no mixing) of *ca.* 0.8%.

Accordingly, all experiments reported herein were undertaken at fractional loadings less than approximately ½ molecule per micelle (<8 mM) [25-27], and we focus quantitative analysis primarily on low concentration (<2.6 mM) data.

- **Cyclic voltammetry for tBuFc within I₁ phase liquid crystals**

Figure 4.6 illustrates typical cyclic voltammograms observed for the one-electron oxidation of ^{t}BuFc within this I_1 phase. There is a slight loss in signal intensity upon consecutive scans, indicating that the position of the product (^{t}BuFc$^+$) within the micelles is not identical with neutral precursor, as expected.

Similar behaviour was observed when decamethylferrocene or vitamin K_1 were employed as the redox species; in the case of N-methylphenothiazine as the hydrophobic solute, dramatic signal decreases on redox cycling were observed, suggesting that the oxidised form escapes from the micelles [26,27].
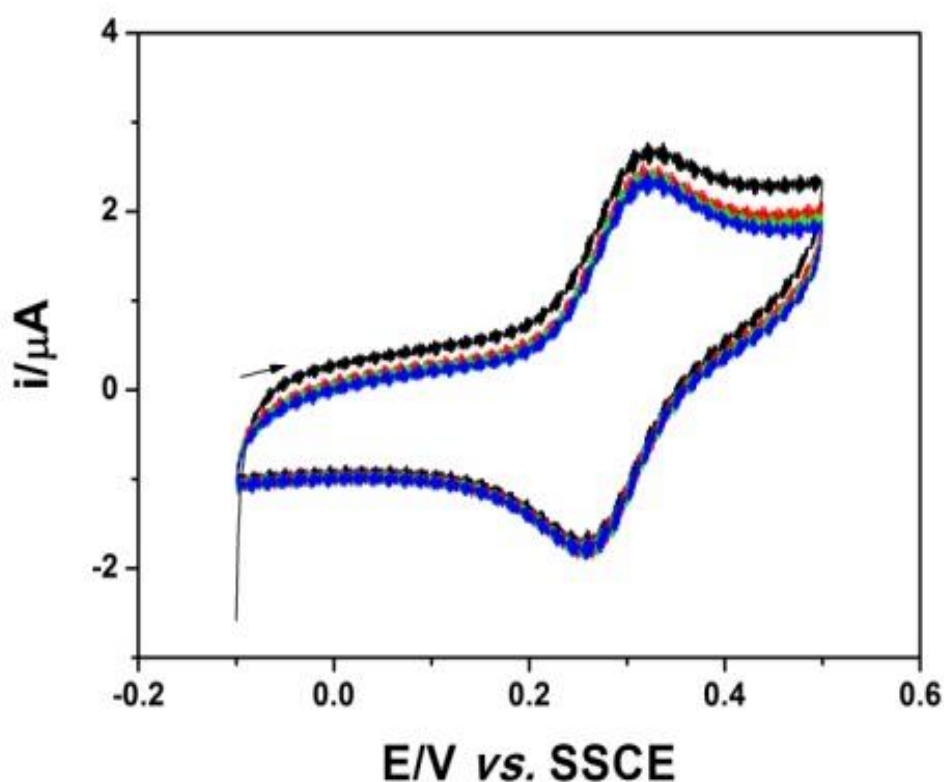
Figure 4.6: Typical cyclic voltammogram (0.1Vs^{-1}) for the oxidation of 7.6 mM ^{t}BuFc within I_1 phase liquid crystals.

Nevertheless, the waves exhibit characteristics of both fast heterogeneous electron transfer kinetics ($E_p^{Ox} - E_{p/2}^{Ox} \sim 70$ mV) across the timescales probed, suggesting fast counter ion movements. (Seen figure 4.7):
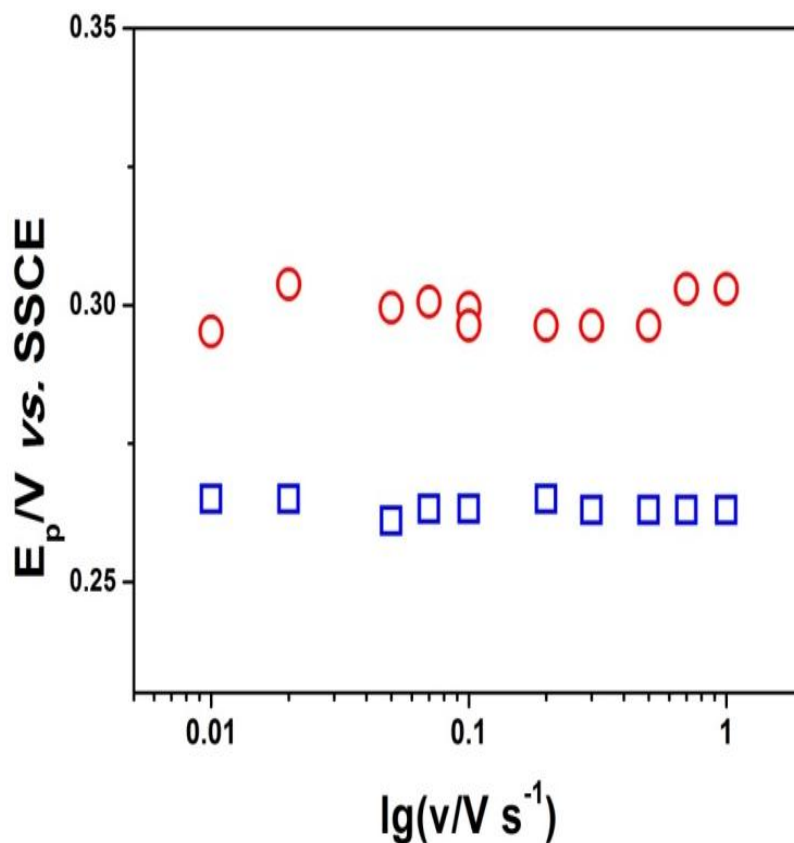
Figure 4.7: The electrode kinetics can be seen by ploting the electrode potential against $\log_{10}$ of scan rate. However, phase separation occurs when approximately each micelle contains one molecule.

- **Access to Diffusion Coefficients**

The voltammetry is done over a number of scan rates allowing the diffusion coefficients to be calculated by plotting peak current against squire root of scan rate, which is liner, figure 4.8:
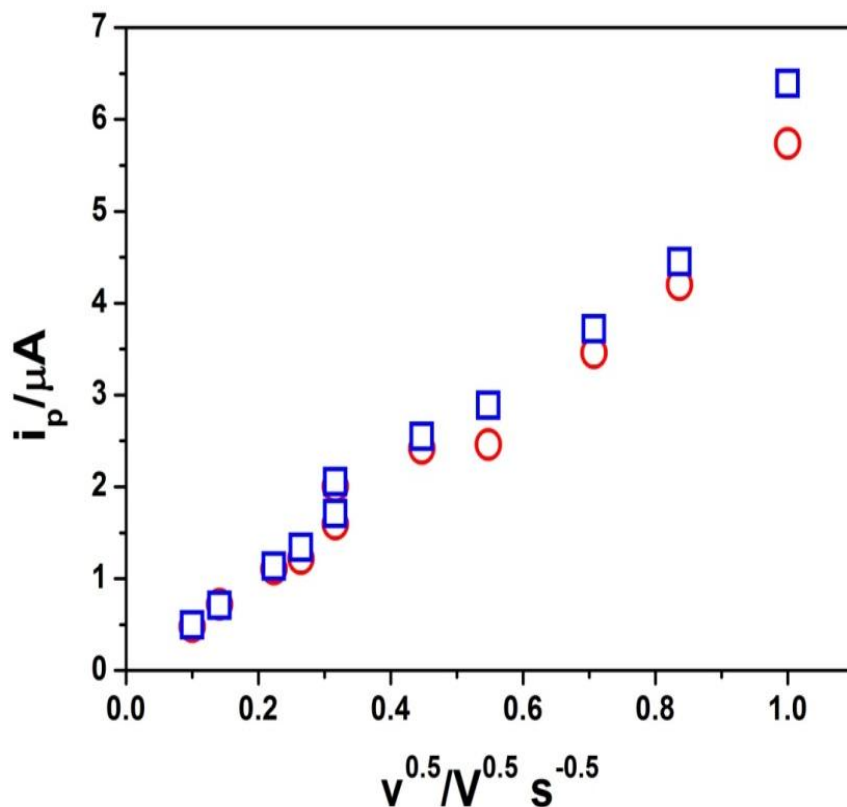
Figure 4.8: peak current against squire root of scan rate.

Use the slope to determine the diffusion coefficients using Randles-Sevíčk expression:

$$i_p = 0.4463 FSc_0 \sqrt{D} \sqrt{\frac{Fv}{RT}} \qquad (4.1)$$

In which the symbols retain their usual meanings, enables the deduction of the apparent diffusion coefficient (D) as a function of the analyte loading. Given that the phase is spatially heterogeneous - the electrode "sees" *both* surfactant and aqueous pseudophases.All analyses employed an effective area (S') given by the ratio of the volume of the micelles to that of a unit cell:

$$S' = \frac{8 \times 35.9}{8.6^3} S = 0.452S$$

(Figure 4.9), Where it is appreciated that the diffusion coefficient is proportional to the loading at low concentrations (<2.6 mM), tailing off to a value reported for the micelle monomer self-diffusion at 8 mM (0.4 molecules-per-micelle). Increasing the concentration further caused a plateau which dropped when the system phase separated.
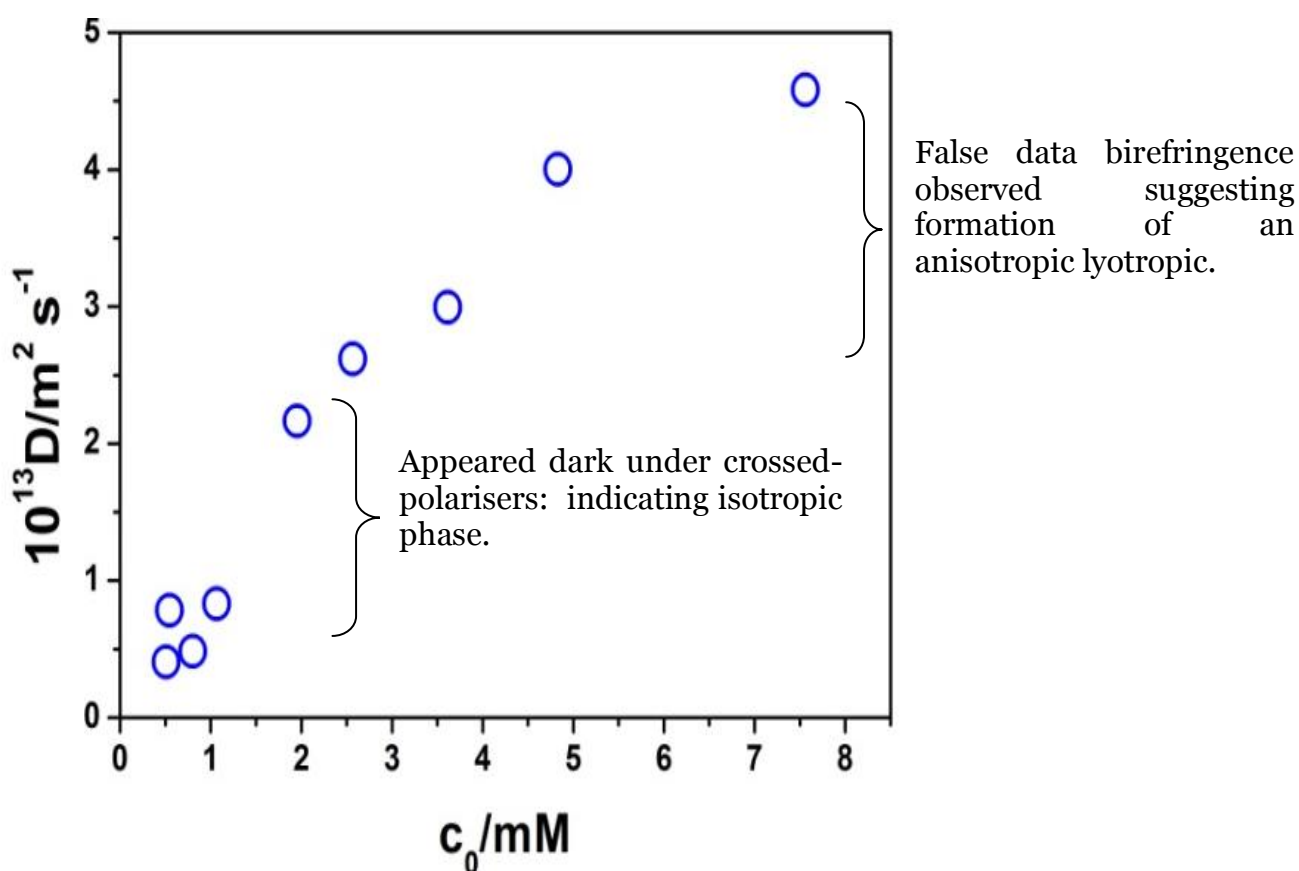
Figure 4.9: Variation of the area-corrected diffusion coefficient with *t*BuFc loading; note that the concentration scale ranges from 0.03-0.4 *t*BuFc molecules-per-micelle.

- **Physical diffusion *vs.* bounded diffusion and Accounting for Occupancy Probability**

Consideration of mass transport of ^{t}BuFc within the system would suggest mechanisms similar to that in solids (exchange, ring, interstitial, interstitialcy, crowdion, vacancy, divalency, relexation, dislocation pipe, grain boundary or surface mechanisms) [28]. However, assuming the electrode/electric field does not perturb the structure of the material, only the exchange/ring routes appear possible as a means of physical translation, through the context of the fragmentation-coagulation mechanism; although this is on-going at all times, it leads to net mass transport only when there is a unoccupied micelle next to an occupied micelle[13].

Furthermore, as for supramolecular systems with irreversibly attached redox functionalities, there is a possibility for carrier hopping as a competing route[29], so that in the kinetic limit that physical displacement rate constant (k_{ex}) is smaller than that for hopping (k_{hop}), percolation behaviour is observed since the process is governed by the exact distribution of redox sites within the system and their interconnectivity. In the opposite limit ($k_{ex} > k_{hop}$, the "mean-field" condition), reorganisation of the molecular distribution is fast, so that there is no "memory-effect".

There is another consideration within the present system which involves the partitioning of the product species from surfactant to aqueous subphases, which would allow for a route for inter-subphase electron transfer [30], and would allow for mean-field conditions to operate, and can be approximated by the notion of "bounded diffusion", corresponding to some physical displacement of otherwise

lattice-anchored molecules. Thus, considering D_p as the diffusion coefficient for physical diffusion, and D_e as the hopping/bounded diffusion coefficient, we may write, assuming correlation factors of unity [29-30]:

$$D = P_0 D_p + (1 - P_0) D_e \qquad (4.2)$$

where P_0 is the probability that a micelle is unoccupied. For very low ("rare event") concentrations (<2.6 mM, corresponding to $P_0 > 0.9$), we observed < 0.5% error in approximating P_0 by the Poisson distribution:

$$P_0 = e^{-\bar{x}}$$

Where $\bar{x}$ is the mean number of ^{t}BuFc molecules-per-micelle[31-34;] assuming an aggregation number of 90, we found

$$\bar{x} = (0.0528 \pm 0.0003) c_0.$$

This formulation, though approximate, enables ensemble properties to be encompassed within the analysis[35]; for ease, since $\bar{x}$ is small, we approximate through linearization of the exponent:

$$P_0 \approx 1 - \bar{x}; \quad (1 - P_0) \approx \bar{x}.$$

Thus, we estimate D_p as $8.6 \pm 2.5 \times 10^{-14}$ m^2 s^{-1} from a plot of $\dfrac{D}{P_0}$ vs. c$_0$ in the limit

$c_0 \to 0$. Pleasingly, this suggests micellar fragmentation-coagulation occurs within

$\sim \dfrac{(2r_m)^2}{6D_p} = 35 \, \mu s$, as anticipated[5], affording, $k_{ex} = 12(2r_m)D_p L = 3 \times 10^6 \, M^{-1} \, s^{-1}$, where

r_m is the spherical micelle radius (2.13 nm) [5] and L is Avogadro's number. Comparison with the rate constant for bounded motion, obtained from a plot of

$$D_e = \left(\dfrac{D - D_p P_0}{1 - P_0} \right) \text{ vs. } c_0 \text{ for } P_0 > 0.9 \text{ affords: } k_{hop} = \dfrac{6D_e}{\left\{ (2r_m)^2 + 3r_m^2 \right\}} = 1 \times 10^9 \, M^{-1} \, s^{-1},$$

implying the predominance of percolation effects at low concentrations (<2.6 mM), as expected. This value is about one order of magnitude larger than ferrocene-self-exchange kinetics in *homogeneous solvents* [9]; such apparent rate enhancement derived from the confinement of redox sites is not unknown [3], but may represent the occurrence of a smaller reorganisation energy, or error in approximating partitioning and inter-subphase electron transfer *via* a bounded diffusion harmonic model.

To unravel whether partitioning of ^{t}BuFc$^+$ occurs between the two pseudophases, we sought to estimate the interaction potential energy (w) between the electron-exchanging redox species (^{t}BuFc and ^{t}BuFc$^+$) *via* D_e, based on a regular solution model [8]:

$$\frac{D_e}{D_e^{ideal}} = 1 - 2\alpha P_0 (1 - P_0) \tag{4.3}$$

where $D_e{}^{ideal}$ may be estimated from the data at low loadings: $D_e^{ideal} = 5.4 \pm 1.6 \times 10^{-12} c_0$

, and the interaction parameter, $\alpha = \dfrac{zw}{RT}$ in which z = 2 (the number of nearest neighbours in the *Pm3n* structure); our data conformed to:

$$\frac{D_e}{D_e^{ideal}} = 1.2 - 4.9 P_0 \left(1 - P_0\right)$$

Pearson's product-moment correlation coefficient of 0.95, suggesting an interaction energy on the order of the thermal energy in the system, $w \sim 3$ kJ mol^{-1}, a positive value indicating that "repulsive" interactions between ^tBuFc and $^tBuFc^+$ pairs occur – ^tBuFc and $^tBuFc^+$ are *incompletely miscible* within the studied system, even at low loadings.

This result is in agreement with our earlier notion [10] that differential partitioning of the two halves of a redox couple between aqueous and surfactant subphases may empower an alternative route for long-range electron transfer. In this manner, the attenuation coefficient for long-range electron transfer, typically [4] *ca.* 1 Å^{-1} for these systems is not prohibitively large.

4.6   Conclusions

Concentration-dependent diffusion coefficients of ^{t}BuFc in the I_1 phase, extracted using voltammetry, appear to occur as a result of the partitioning of the oxidised form (^{t}BuFc) between surfactant and aqueous subphases in a thermally activated process, which we have treated in terms of bounded diffusion: the redox species basculates between water-soluble ^{t}BuFc$^+$ and water-insoluble ^{t}BuFc through inter-subphase electron transfer.

We have treated this as though it is a self-exchange process; strictly, it is not, as the molecular environments of the two forms are not identical – they are in different pseudophases.   Nevertheless, noting the very high viscosity of the I_1 phase, it is remarkable that this process allows charge diffusion to occur faster than in polymeric systems [36] or even redox-active room temperature ionic liquids.[32]

References for Chapter 4

1. For systems developed in the solid state, see H. Hada, K. Takaoka, M. Saikawa and Y. Yonezawa, *Bull. Chem. Soc. Jpn.*, 1981, 54, 1640.

2. Y. Yonezawa, M. Okai, M. Ishino and H. Hada, *Bull. Chem. Soc. Jpn.*, 1983, 56, 2873.

3. M. Sharon, P. Veluchamy, C. Natarajan and D. Kumar, *Electrochim. Acta*, 1991, 36, 1107.

4. S. Licht, in S. Licht, A. J. Bard, M. Stratmann (ed.), *Encyclopædia of Electrochemistry*, 2002, volume 6, Wiley-VCH, Weinheim, p.317.

5. O. S. Ksenzhek and A. G. Volkov, *Plant Energetics*, Academic Press, San Diego, 1998.

6. D. J. Fermın, H. D. Duong, Z. Ding, P. F. Brevet and H. H. Girault, *Electrochem. Commun*, 1999, 1, 29.

7. D. J. Fermın, H. D. Duong, Z. Ding, P. F. Brevet and H. H. Girault, J. *Phys. Chem.,* 1999, 121, 10203.

8. R. Lahtinen, D. J. Fermın, K. Kontturi and H. H. Girault, J. *Electroanal. Chem.,* 2000, 483, 81.

9. H. Jensen, J. J. Kakkassery, H. Nagatani, D. J. Fermın and H. H. Girault, *J. Am. Chem.* Soc., 2000, 122, 10943.

10. D.G. Nichols, *Bioenergetics*, Academic Press, London, 1982.

11. F. So, *Organic Electronics*, CRC Press, San Diego, 2010.

12. F. Marken, J.D. Watkins, A.M. Collins, *Phys. Chem. Chem. Phys.*, 13 (2011) 10036.

13. R.W. Murray, (ed.), *Molecular Design of Electrode Surfaces*, Wiley, New York, 1992.

14. C. Amatore, E. Maisonhaute, B. Schöllhorn, J. Wadhawan, *ChemPhysChem*, 8 (2007) 1321.

15. R.R. Balmbra, J.S. Clunie, J.F. Goodman, *Nature*, 222 (1969) 1159.

16. M.M. Alam, L.K. Shrestha, K. Aramaki, *J. Colloid Interf. Sci.*, 329 (2009) 366.

17. P.D.I. Fletcher, *Mol. Cryst. Liq. Cryst.*, 154 (1988) 323.

18. K. Fontell, K.K. Fox, E. Hansson, *Mol. Cryst. Liq. Cryst.*, 1 (1985) 9.

19. O. Söderman, H. Walderhaug, U. Henriksson, P. Stilbs, *J. Phys. Chem.*, 89 (1985) 3693.

20. M. Törnblom, R. Sitnikov, U. Henriksson, *Liq. Cryst.*, 27 (2000) 943.

21. T. Bull, B. Lindman, *Mol. Cryst. Liq. Cryst.*, 28 (1973) 155.

22. L.B.-Å Johansson, O. Söderman, *J. Phys. Chem.*, 91 (1987) 5275.

23. M. Kahlweit, *Pure Appl. Chem.*, 53 (1981) 2069.

24. A. Malliaris, J. Lang R. Zana, *J. Phys. Chem.*, 90 (1986) 655.

25. J. Burgess, E. Pelizzetti, *Prog. React. Kinetics*, 17 (1992) 1.

26. C. Rodríguez, H. Kunieda, *Langmuir*, 16 (2000) 8263.

27. E. S. Blackmore, G.J.T. Tiddy, *J. Chem. Soc., Faraday Trans. II*, 84 (1988) 1115.

28. T.A. Bleasdale, G.J.T. Tiddy, E. Wyn-Jones, *J. Phys. Chem.*, 95 (1991) 5385.

29. T. Gannett, D.F. Milner, M.J. Weaver, *J. Phys. Chem.*, 89 (1985) 2787, and references cited therein.

30. Z. Zahl, R. van Eldik, M. Matsumoto, T. Swaddle, *Inorg. Chem.*, 42 (2003) 3718.

31. J.E. Halls, N.S. Lawrence, J.D. Wadhawan, *J. Phys. Chem. B*, 115 (2011) 6509.

32. J.R. Manning, *Diffusion Kinetics for Atoms in Crystals*, D. Van Nostrand Co., New Jersey, 1968, p.75*ff*.

33. D.N. Blauch, J.-M. Savéant, *J. Am. Chem. Soc.*, 114 (1992) 3323.

34. B.J. McClelland, *Statistical Thermodynamics*, Chapman and Hall, London, 1973, p.124 *ff*.

35. R. G. Compton, M.E. Laing, A. Ledwith, I.I. Abu-Abdoun, *J. Appl. Electrochem.*, 18 (1988) 431.

36. W. Wang, R. Balasubramanian, R.W. Murray, *J. Phys. Chem. C*, 112 (2008) 18207.

Chapter 5 - Voltammetry within Structured Liquid Nanosystems: Towards the Design of a Flexible, Three-Dimensional Framework for Artificial Photosystems

---

- **Electrochemistry of TMPD and Et_2Fc within the L_α phase and H_1 Phases**

5.1 Theory and Amis

The use of birefringent lyotropic liquid crystal frameworks causes the possibility of anisotropic diffusion of redox analytes doped within the phase. In this work:

- We are concerned with effects due to the orientation of the phase relative to the electrode.

- We probe the flux within these structured liquid nanosystems within merely one dimension.

- We explore the use of normal lyotropic liquid crystal mesophases [1-4] formed at ca. 50 wt. % of surfactant in water as a "backbone" structure for the development of an inexpensive, self-reconstructing, flexible, and self-assembling soft matter-based three-dimensional nanosystem, to a proof-of-concept, in which the surfactant pseudophase is populated with hydrophobic molecules with the aqueous subphase[5,6].

Indeed, the micellar palisade layer allows for charge transfer processes to occur within a medium of attractive dielectric constant ($\varepsilon_s \sim 30$) [7, 8], and the surfactant medium allows for the probing of micellar orientation effects on the charge-transfer process; these are seen to play a major role in both the voltammetry of model compounds, and photochemically-induced electron transfer processes.
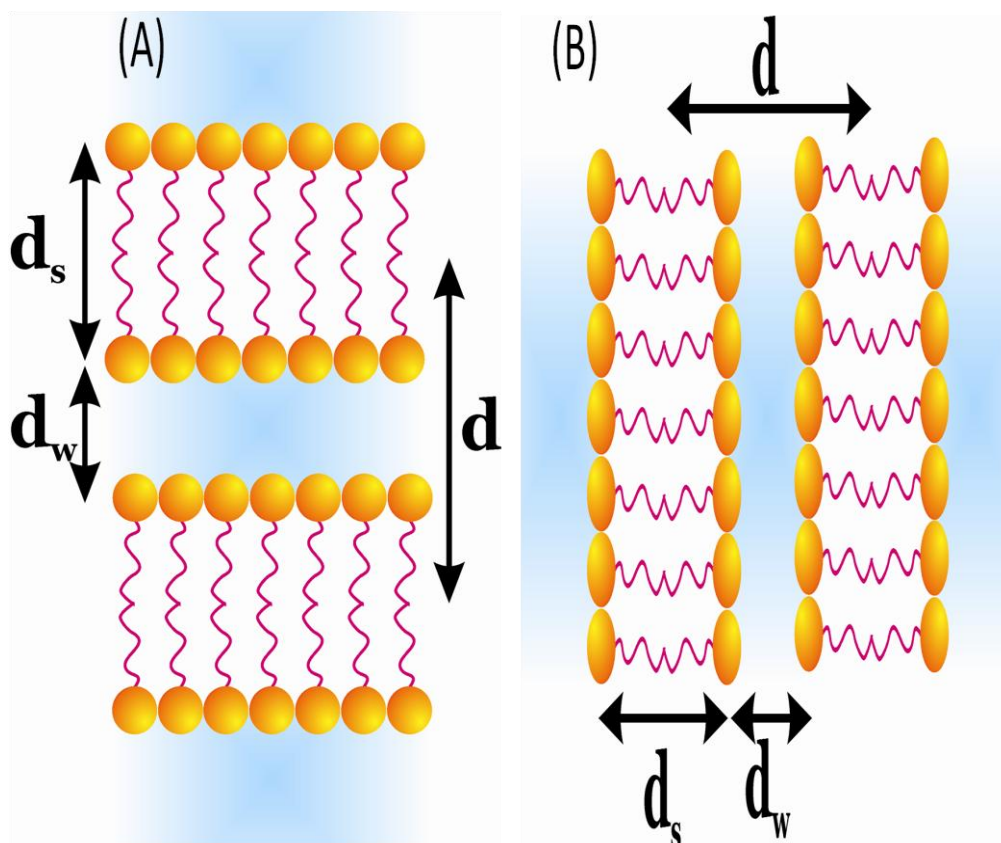
Figure 5.1: Schematic illustration of the L_α phase in two different idealised orientations when the applied magnetic field is in (a) a horizontal position, (b) a vertical position. The thicknesses of the surfactant subphase (d_s), the aqueous pseudophase (d_w) and the fundamental repeat distance (d) are also indicated.

5.2   Relationship between apparent diffusion coefficient to the structure and orientation of the L$_\alpha$ phase

In noting that small-angle X-ray scattering of lamellar phase lyotropic liquid crystals enables the observation of between two and five peaks with Bragg spacings in the ratio

$$1 : \frac{1}{2} : \frac{1}{3} : \frac{1}{4} : \frac{1}{5} : ....etc.$$

The fundamental repeat distance [labelled d in Figure 5.1(a)] is readily determined experimentally. This value corresponds to the sum of the surfactant bilayer thickness (d_s) and that of the water layer (d_w), and allows for the calculation of the surfactant bilayer thickness through the relationship

$$d_s = \frac{d}{\left[1 + \dfrac{\varphi_{\text{water}}}{\varphi_{\text{surfactant}}} \right]}$$

in which φ_i represents the volume fraction of pseudophase i. Assumption of an ideal swelling behaviour (the change in the volume fraction water swells the crystal spacing distance d *without* change in d_s) enables estimation of d_w with surfactant concentration present in the lyotropic liquid crystal.

Thus, for the case of partitioning-diffusion of redox analytes within these structured systems, if the transfer of electroactive species at the pseudophase | pseudophase interface occurs rapidly compared with any electron transfer, then the distribution equilibrium is always maintained and the apparent diffusion coefficient may be expressed as [3,9]

$$D_{ap} = \frac{d^2 D_A D_S}{K_P \left\{ \dfrac{d_w}{K_P} + d_s \right\} \left\{ \dfrac{d_s}{K_P} D_S + d_w D_A \right\}}$$

In which D_A is the diffusion coefficient of the redox analyte within the aqueous subphase, D_S corresponds to that within the surfactant pseudophase, and the partition coefficient,

$$K_P = \frac{c_S}{c_A}$$

 is the ratio of analyte concentration in surfactant (s) to aqueous (a) layers. Note that D_A is not necessarily identical to that observed in bulk solution, owing to the nano-restricted environment of the hydrophilic channels; indeed, Owen and co-workers [11] suggest that D_A could be as much as orders of magnitude lower than in bulk solution.

Note that this expression does not hold when inter-subphase electron transfer is faster than cross-pseudophase material transport [3-10].

Now, considering the orthogonal orientation of the L_α phase [as illustrated in Figure5.1 (b)], where the aqueous and surfactant pseudophases are aligned so that they are parallel to each other and perpendicular to the electrode surface, the differential diffusivity of the partitioned redox probe within the two subphases may allow for the electro-generated product in one subphase (typically the aqueous subphase) to mediate the redox process in the more viscous subphase.

Under the assumption that this can be treated as a self-exchange process, it has been demonstrated [2, 3] that this impacts on the apparent diffusion coefficient through the relationship

$$D_{ap} = \frac{D_A + K_P D_S}{1 + K_P}$$

whereas the following expression describes the convolution of diffusion in both phases without inter-subphase electron transfer [3]:

$$D_{ap} = \left(\frac{\sqrt{D_A} + K_P \sqrt{D_S}}{1 + K_P} \right)^2$$

Thus, the determination of apparent diffusion coefficients may be employed to determine whether the phases orient in the idealised ways illustrated in Figure 5.1.

5.3   Experimental

5.3.1 Chemical reagents

• All chemical reagents were purchased from Sigma-Aldrich or Fisher Scientific in the purest commercially-available grade, and used as received.

• Water, with a resistivity of not less than 18 MΩ cm, was taken from an Elgastat system (Vivendi, Bucks., UK). Oxygen-free nitrogen was obtained from BOC Gases, UK.

5.3.2 Instrumentation

- The field strengths of the magnets employed for sample alignments were undertaken using a home-made Hall probe.

- Optical microscopy was undertaken using an Olympus BX-51 polarising microscope.

- Transmission electron microscopy (TEM) was undertaken using a JEOL 2010 running at 200 kV.

- Electrochemical measurements were undertaken using a commercially-available computer-controlled potentiostat (μAutolab Type III, Eco Chemie, The Netherlands), with the media thermostatted at 294 ± 2 K. The working electrode was a 3.0 mm diameter glassy carbon disc electrode (purchased from BASi, UK) and was cleaned and polished on a napped polishing pad using an aqueous alumina (0.3 μm, Presi, France) slurry.

- The working electrode was introduced carefully into the liquid crystal phase, such that its surface was always horizontal and parallel to the bottom of the flat-bottomed sample container, and placed in different positions for every change in experimental parameter, so as to encompass any effects due to sample polycrystallinity.

- A nickel wire spiral formed the counter electrode, and a saturated silver/silver chloride electrode was employed as the reference electrode.

5.3.3 Formulation of Normal Lyotropic Liquid Crystals

Lyotropic liquid crystals in the lamellar (L_α) or hexagonal (H_1) phases were prepared in flat-bottomed sample containers, employing Brij 30 or Triton X 100 surfactants, respectively.[1-4]

Briefly, surfactant/aqueous electrolyte mixtures in the mass ratio required by the published phase diagrams were homogenised in the presence of the required amount of redox dopant, through heating, under a stream of nitrogen to approximately 320 K, with stirring, so as to form the micellar isotropic phase, for about one hour. The samples were then allowed to cool, slowly to 294 ± 2 K, before further experimentation in the presence of a magnetic field: for both phases studied, the sample was then split into two, with one sample placed into a 3.13 G horizontal magnetic field, or a 1.12 G vertical magnetic field afforded by two permanent ferromagnets. [1, 3]

 For the case of ferrocene-derivate or N,N,N',N'-tetramethyl-$para$-phenylenediamine (TMPD) dopants, various concentrations were employed with 0.1 M aqueous KCl or NaClO$_4$ acting as the ionic dopant; experiments involving gold nanorods employed a set volume of the nanorod solution with water, such that the aqueous component was 0.1 M aqueous KCl; for experiments on the artificial photosystem developed herein,

0.1 M aqueous HCl acted as the ionic dopant, with a known amount of vitamin K_1 (fixed at 112.6 mg) and/or plant pigment (67.5 mg) added.

The density of the liquid crystals was estimated to be *ca.* 1.04 g cm^{-3} (L_α phase using Brij 30) or 1.07 g cm^{-3} (H_1 phase using Triton X 100) at ambient temperatures. As these systems constitute single thermodynamic phases, the concentration of redox-active species are reported in moles per unit volume of the relevant phase.

5.4   Results and Discussion

We first consider the voltammetry of two model one-electron donor systems (one hydrophobic, bis(ethylcyclopentadienyl)iron (Et_2Fc), and a second which partitions easily between aqueous and surfactant subphases, TMPD) within two types of lyotropic liquid crystal phases , with different orientations, to understand which phase is better suited for the development of a three-dimensional biomimetic for Photosystem I.

5.4.1 The L_α phase of Brij 30/H_2O

Brij 30 is a non-ionic surfactant with main component being tetraethylene glycol dodecyl ether.
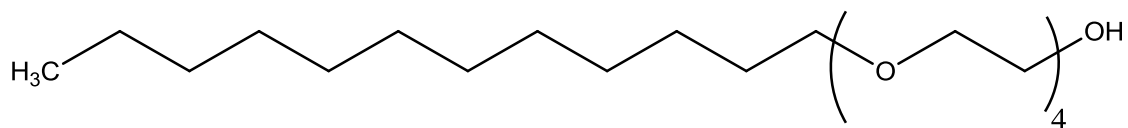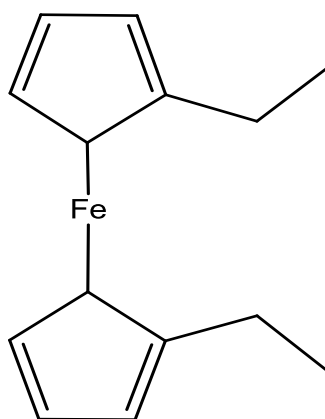
Brij30 structure

The homogeneisation of 55:45 wt.% mixtures of Brij 30 and water yields, at ambient temperatures, the L_α phase consisting of detergent bilayers 37.8 Å thick (with micellar palisade layer of 9.2 Å thick) [12,13] separated by aqueous subphases 23.1 Å in thickness. As the bilayers of this phase are able to slip past each other, the viscosity of the phase is low [13] – the phase pours readily as the container in which it is placed tilts.

Nevertheless, it is optically anistropic, allowing the phase to exhibit birefringence when viewed through crossed polarisers. The presence of electrolyte may alter the phase boundaries governing the specific phase of the liquid crystal, with lyotropic ("salting-out") electrolytes (such as potassium chloride) effecting the decrease in mutual solubility between surfactant and aqueous components.

Indeed, in preliminary experiments, we observed that characteristic L_α textures were observed for Brij 30/0.1 M KCl (aq) in a 40:60 wt. % ratio. Accordingly, this system together with a framework 50:50 wt. % ratio of Brij 30/0.1 M NaClO$_4$ L_α phase was employed in this work. Based on the ideal swelling model (Section 5.2), and ignoring electrolyte effects, we calculate the water thickness to vary from 37.6 -60.3 Å in increasing the water content of the phase.

5.4.1.1   Voltammetry of Et$_2$Fc within the L$_\alpha$ phase

We first consider the voltammetry when the phase was doped with Et$_2$Fc by mixing the relevant species thoroughly at room temperature with heating to form the isotropic micellar phase, and subsequent slow cooling in the presence of an horizontal magnetic field (of strength 3.13 gauss), so that the molecular long axis of Brij 30 (which is the axis of the most negative diagmagnetic susceptibility) aligns perpendicular to the applied magnetic field [14], thereby allowing for the formation of lamellæ stacks parallel to the bottom plane of the container.

bis(ethylcyclopentadienyl)iron (Et$_2$Fc) structure

Figure 5.2   illustrates voltammograms corresponding to the oxidation of 2.5 mM Et$_2$Fc within the L$_\alpha$ phase of Brij 30/H$_2$O doped with 0.1 M KCl(aq) at a glassy carbon disc electrode, scanned at rates in the range $0.01 \leq v/V\ s^{-1} \leq 0.4$.

It is clear that a primary set of oxidation and reduction waves are seen, as anticipated for the chemically reversible one-electron oxidation (and re-reduction) of the ferrocene derivative.
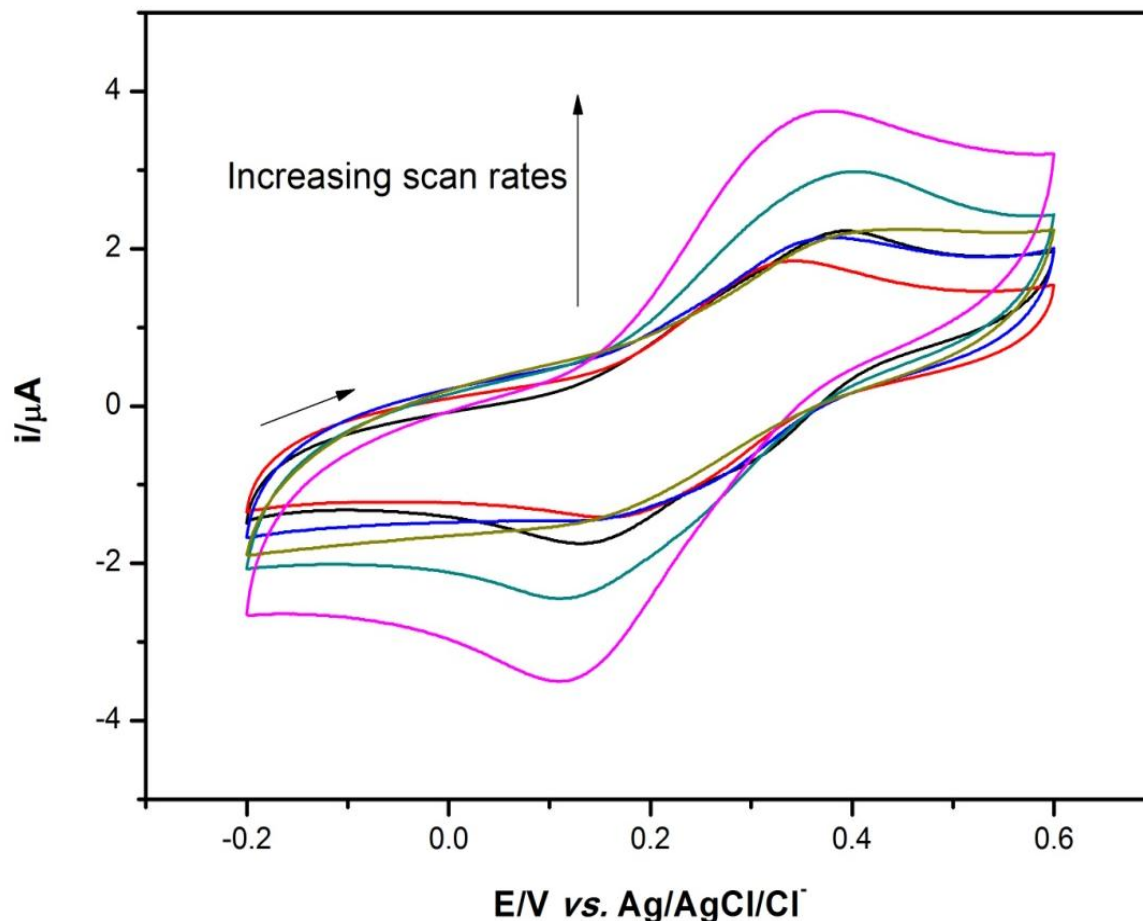
Figure 5.2: Voltammetry of 2.5 mM Et₂Fc in the L_α phase made with Brij 30/0.1 M aqueous KCl (40:60 wt. % ratio). The arrow indicates the direction of the initial potential sweep. **Key:** 0.01 (red), 0.02 (blue), 0.03 (olive), 0.5 (cyan), 0.1 (magenta) V s⁻¹.

However, these waves are broad with large (typically ~100 mV) peak-to-peak separation. Inasmuch as there is no clear trend in peak oxidation potentials with electrochemical timescale, the large peak-to-peak separation observed is not

necessarily attributable to slow heterogeneous electron transfer; conductivity studies of the medium doped with varying amounts of Et_2Fc afforded resistivities (ρ) in the range 0.4 – 0.8 kΩ cm, comparable with dichloromethane solutions containing 0.1 M tetrabutylammonium perchlorate [15], and affording an uncompensated resistance,
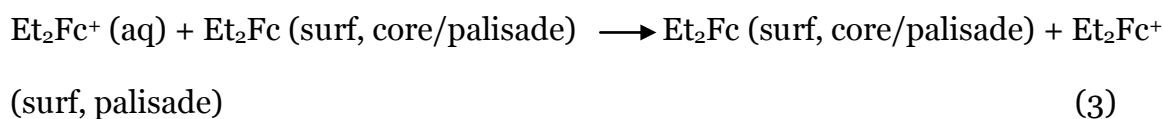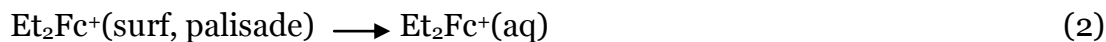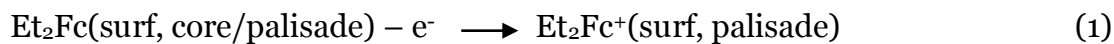
$$R_s = \frac{\rho}{4r_0} \sim 1 \text{ k}\Omega.$$

Moreover, at low scan rates, significant shoulders are observed on each of the waves. Although it is surprising to observe well-defined voltammetry of the extremely hydrophobic Et_2Fc species [16], given that this species is, like most aromatic systems [12,14], a palisade layer resident, this is consistent with work by Murray on the less hydrophobic derivatives ferrocene and 1,1'-dimethylferrocene [14].

We observed the occurrence of diffusional-type behaviour (the peak oxidation currents are directly proportional to the voltage sweep rate, data not shown); we observed an apparent diffusion coefficient of 1.9 x 10^{-8} cm^2 s^{-1}. Given that the superexchange attenutation parameter for alkyl systems is [17] $\sim$1 Å^{-1}, electron transfer between surfactant lamellæ is likely to be kinetically slow – the aqueous pseudophase is simply to wide.

To account for the observation of diffusional behaviour, we suggest that since oxidised ferrocene species are more soluble in aqueous media [16], and in noting the presence of shoulders on the voltammograms, especially at longer experimental timescales, propose, assuming fast reconstruction of the phase after electrode-immersion, electro-generated cation mediation playing a rôle in the charge propagation process, through a quasi-self-exchange process for a species that partitions between the two subphases [13,14]:

The quasi-self-exchange process between the two subphases

$$Et_2Fc(surf, core/palisade) - e^- \longrightarrow Et_2Fc^+(surf, palisade) \tag{1}$$

$$Et_2Fc^+(surf, palisade) \longrightarrow Et_2Fc^+(aq) \tag{2}$$

$$Et_2Fc^+(aq) + Et_2Fc(surf, core/palisade) \longrightarrow Et_2Fc(surf, core/palisade) + Et_2Fc^+$$

$$(surf, palisade) \tag{3}$$

where the symbols (aq) and (surf) refer to the aqueous and surfactant pseudophases, respectively. Note that, strictly, the equilibrium constant (K) for the mediated reaction is not unity – this will actually depend on the difference in formal electrode potential of Et_2Fc^+ within both subphases:

$$(\Delta E^{0'}): K = e^{\frac{F}{RT}\Delta E^{0'}}$$

where F is Faraday's constant, R is the molar gas constant and T is the absolute temperature. Nevertheless, the occurrence of the diffusion-partition and inter-subphase reaction process is manifested in the value of the apparent diffusion coefficient, which can be thought of in terms of a "bounded-diffusion" [12, 13].

5.4.1.2   Voltammetry of TMPD within the L$_\alpha$ phase

In order to examine partition-diffusion behaviour within well-oriented micellar systems, we next examined the voltammetry of TMPD within both types of L$_\alpha$ phase, each oriented in two orthogonal directions.
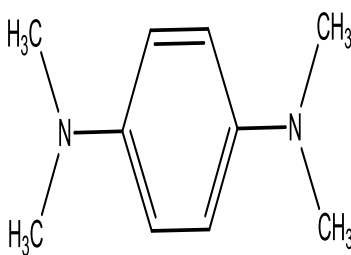
N, N, N′, N′-tetramethyl-p-phenylenediamine (TMPD) structure

Figure 5.3(a, b, e, f) depicts voltammograms corresponding to the one-electron oxidation of TMPD within Brij 30/aqueous electrolyte liquid crystals.

The voltammograms appeared to shift wildly when the concentration of analyte doping changed. At the smaller electrochemical timescales used, these data give rise to peak potentials that were invariant of the voltammetric timescale.
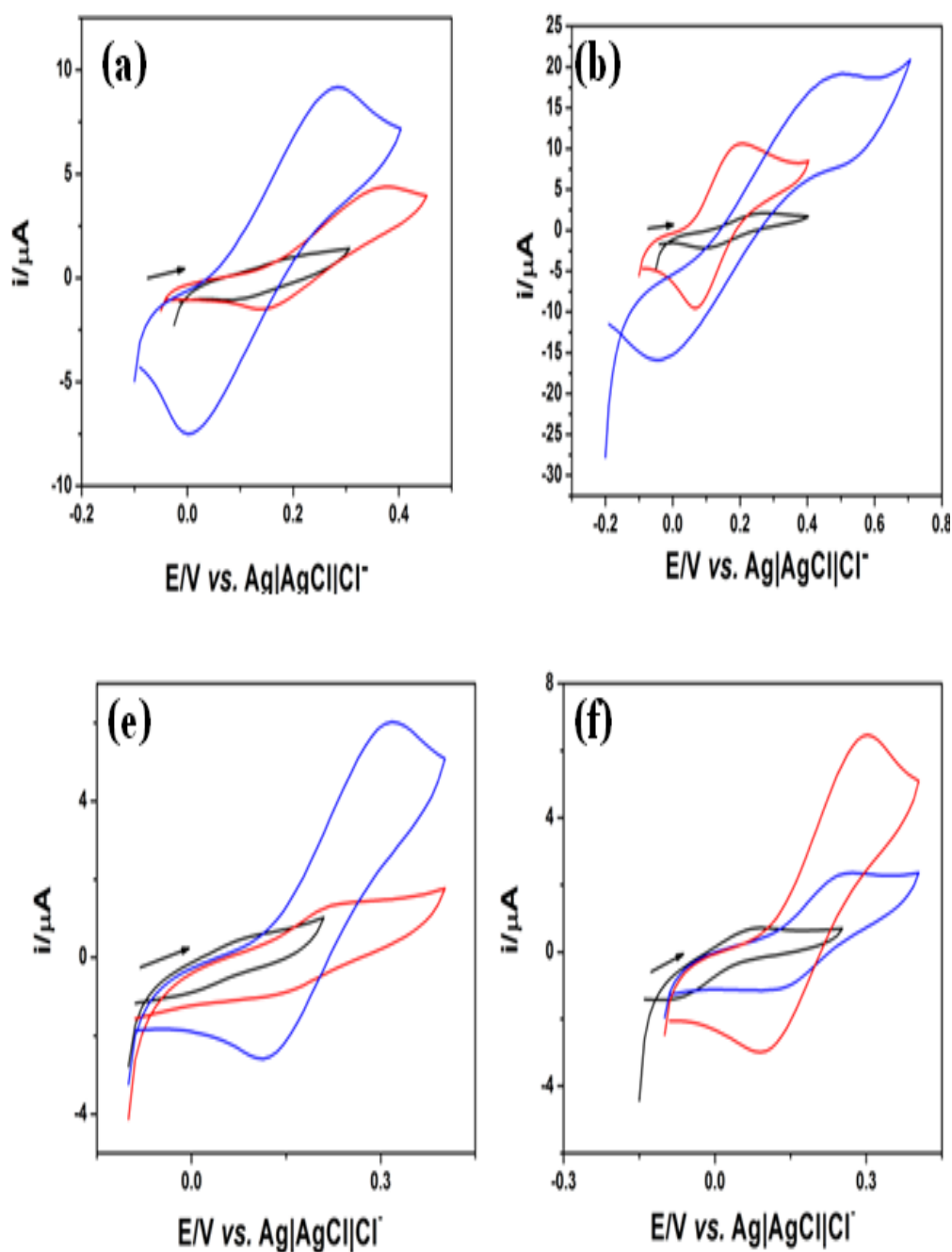
Figure 5.3: Cyclic voltammograms corresponding to the one-electron oxidation of TMPD within the L_α phase formed using Brij 30/0.1 M aqueous KCl (in a 40:60 wt.% ratio), (a and b), or Brij 30/0.1 M aqueous NaClO$_4$ (in a 50:50 wt.% ratio), (e and f). Voltammograms in panels (a), (b), (e), (f) correspond to the first scan obtained (the arrow indicates the direction of the initial potential sweep) at 0.1 V s^{-1} for samples aligned using a horizontal magnetic field (a) and (e), or a vertical magnetic field (b) and (f).

Figure 5.3 (c, g) below, suggesting fast electrode kinetics, note that although under these conditions, a fraction of the TMPD species could exist as the protonated form, it is known that TMPD voltammetry (at least in homogeneous solution) occurs exclusively through the free base form. [18]
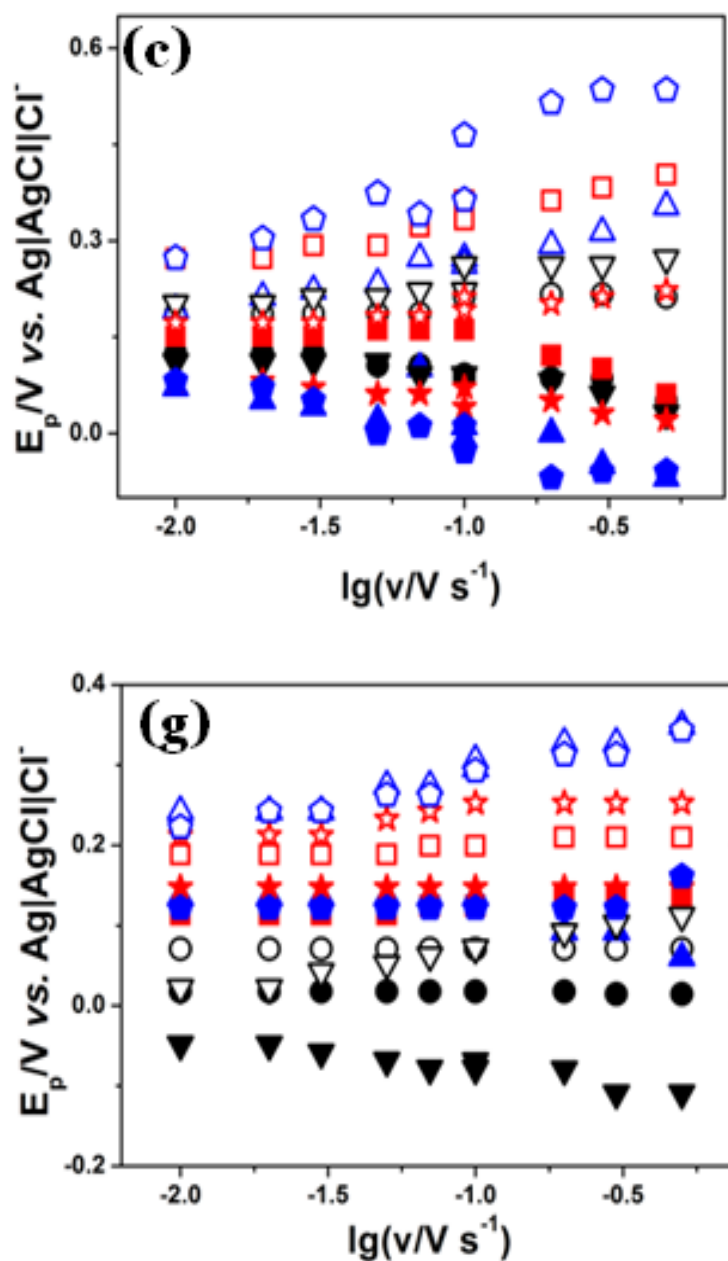
Figure 5.3: Panels (c) and (g) depicts the variation in the peak potentials for the oxidation and re-reductive waves with the electrochemical timescale.

Accordingly, apparent diffusion coefficients were extracted from Randles-Sevčik plots (Figure 5.3 d, h), as outlined in §2.1 only using data that was determined to be commensurate with electrochemical reversibility;
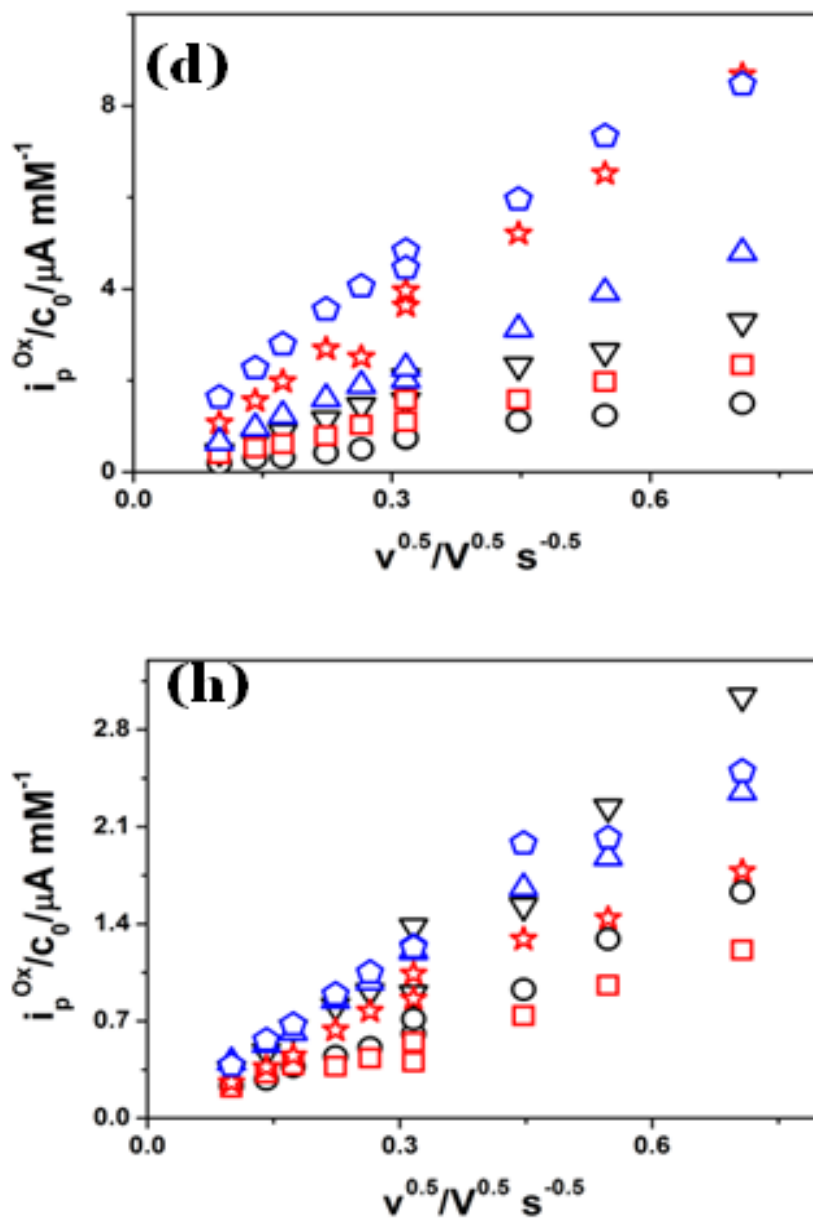
Figure 5.3: panels (d) and (h) are concentration-normalised Randles-Sevčik plots. **Key:** colours indicate concentrations of TMPD within the phase (c_0) with black corresponding to 1.2 mM, red indicating 3.0 mM and blue denoting 5.1 mM.; symbols denote the characteristics pertaining to the peaks in the forward (open symbols) and reverse (filled symbols) waves in the voltammograms, with circles, squares and triangles corresponding to horizontally aligned samples, whilst inverted triangles, stars and pentagons denoting the vertically aligned samples.

These are reported in Table 1:

| [TMPD] mM	10^8 D^h/cm^{2}s^{-1}	10^8 D^v/cm^{2}s^{-1}	D^h/D^v	10^7 $D_S{}^a$/cm^2 s^{-1}	10^7 $D_{ap}{}^{v,SE}$/cm^2 s^{-1}
40:60 Brij30:H$_2$O doped with 0.1M KCl					
1.2	1.4	6.9	0.2	3.4	3.5
3.0	3.6	39	0.1	8.8	9.0
5.1	13	49	0.3	33	33
50:50 Brij30:H$_2$O doped with 0.1M NaClO$_4$					
1.1	1.4	4.3	0.3	3.5	3.7
2.0	0.8	2.0	0.4	2.1	2.2
5.0	3.4	4.0	0.9	8.9	9.1

Table 1: Concentration dependence of the apparent diffusion coefficients for TMPD within the L$_\alpha$ phase of Brij 30/H$_2$O. [a]Calculated value based on a bulk value for D$_A$; [h]magnetic field applied in an horizontal manner; [v]magnetic field applied in a vertical manner; [v,SE]calculated value assuming self-exchange occurs.

where it is clear that in both ratios of Brij 30/aqueous electrolyte employed, the systems tend towards diffusional isotropy, as expected from earlier work [14]. This is especially the case when salting-in ions (ClO_4^-) are present, however this appears to give rise to smaller transport coefficients which are relatively invariant with analyte concentration compared with the salting-out ion (Cl^-) where diffusion coefficients increase with concentration, employing a bulk value for $D_A = 4.4 \times 10^{-6}$ cm^2 s^{-1} and $logK_P = 2$ [14], these trends reflect in the variation of D_S (Table 1).

Notably, the estimated values of D_{ap} either with or without the occurrence of self-exchange process do not match-up with those estimated experimentally for the case when the bilayers are to be aligned perpendicular to the electrode surface. We suggest this may be a result of poor alignment in this direction. Furthermore, we attribute the slower diffusion coefficients for the case when the surfactant and aqueous subphases are better mixed as being due to micelle-bound analyte diffusion with the phase.

5.4.2 The H$_1$ phase of Triton X 100/H$_2$O

In order to determine whether similar effects are observed within a more viscous phase, we next examined the voltammetry of both molecules within the H$_1$ phase made using Triton X 100/aqueous electrolytes.
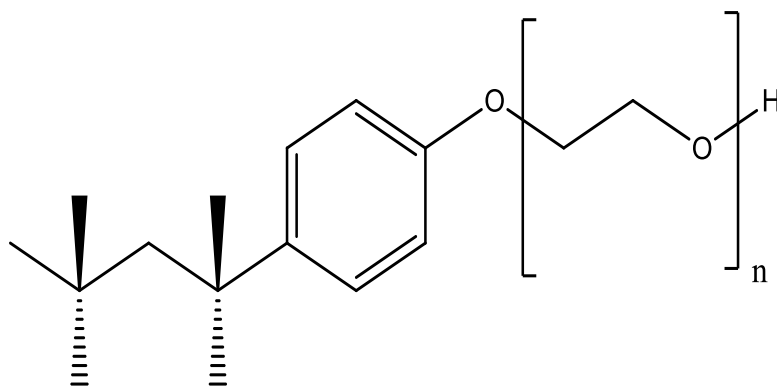
Triton X 100 [(tert-octylphenoxy)-polythoxyethanol] structure

Triton X 100 ((*tert*-octylphenoxy)-polyethoxyethanol) is also a non-ionic surfactant which, at *ca.* 50 wt.% of Triton X 100 in aqueous 0.1 M KCl or 0.1 M NaClO$_4$, self-assembles into the normal hexagonal lyotropic mesophase at ambient temperatures[14].

For the lamellar lyotropic mesophase of the related surfactants nonylphenol decaethylene glycol ether and nonylphenol hexaethylene glycol ether, Johansson and Drakenberg [19] observed that the anisotropy in the diamagnetic susceptibility of the surfactant momomers is such that the lamellar phase is "aligned in the magnetic field with its optical axis parallel to the magnetic field direction" [19], *viz.* the molecular long axis is preferentially aligned parallel to the magnetic field during slow cooling.

This causes the formation of an homeotropic alignment of the H$_1$ phase, in agreement with work by Breyer [20] who noted that such alignment also occurred spontaneously in unaligned H$_1$ phases of Triton X 100 after a few days of storage of the phase in an NMR tube at 277 K, where "rodlike detergent clusters are oriented parallel to the tube axis" [20].

The H_1 phase prepared consists of cylindrical micelles arranged into a hexagonal lattice, as has been demonstrated through X-ray scattering studies [21-25]. For the concentrations employed herein, the lattice parameter (the centre-to-centre distance between micelles),

$$a = \frac{2}{\sqrt{3}} d_{100}$$

where d_{100} is the measured Bragg spacing between {100} planes, has been measured to fall in the range $43.7 - 60.7$ Å [21-25], leading to cylinders of diameter:

$$d_c = \frac{2a}{\sqrt{\frac{2\pi}{3}\left(1 + \left\{\frac{\varphi_{water}}{\varphi_{surfactant}}\right\}\right)}}$$

in the range $42.7 - 59.3$ Å, with micellar palisade layer being calculated to range between $10.4 - 18.7$ Å, employing an estimated hydrocarbon core radius of 11 Å [23], and leading to aqueous subphase thicknesses between $1.0 - 1.4$ Å.

This stiffer phase allows for the ready formulation of two types of aligned lyotropic structure: a *homeotropic* alignment (with respect to the bottom of the sample container) occurs when the magnetic field is horizontal (*viz.* parallel with the bottom of the sample container), with a *homogeneous* alignment when the magnetic field is vertical. In the former structure, the cylindrical micelles are visualised as being perpendicular to the flat bottom of the container; the micelles are arranged so that their long side is parallel to the flat bottom of the container.

Those samples prepared with cooling within the horizontal magnetic field (of strength 3.13 gauss, homeotropic alignment) exhibited properties of a gel that did not flow under inversion of the sample vial, and with resistivity of 0.04 kΩ cm in the direction parallel to the aligned micelles for KCl electrolytes.[14]

In contrast, those samples prepared by cooling within a vertical magnetic field (of slightly weaker strength, 1.12 gauss, homogeneous alignment) were more fluid, and were observed to flow when its container was titled, with resistivity of 0.2 kΩ cm for KCl doped systems.

These resisitivities compare with a value of 0.02 kΩ cm for aqueous 0.1 M KCl. The relatively high conductivity of the homeotropic alignment of the H_1 phase doped with potassium chloride has been noted in earlier work by Owen *et al.* [22] for the case of Brij 56 surfactants, and interpreted through the notion of lower resistive drag within ordered nano-restricted aqueous channels.

5.4.2.1   Voltammetry of Et$_2$Fc within the H$_1$ phase of Triton X 100/H$_2$O

Figure 5.4(a, b) illustrates voltammograms of Et$_2$Fc within the H_1 phase prepared using aqueous 0.1 M KCl, using both alignment methods.

(a)
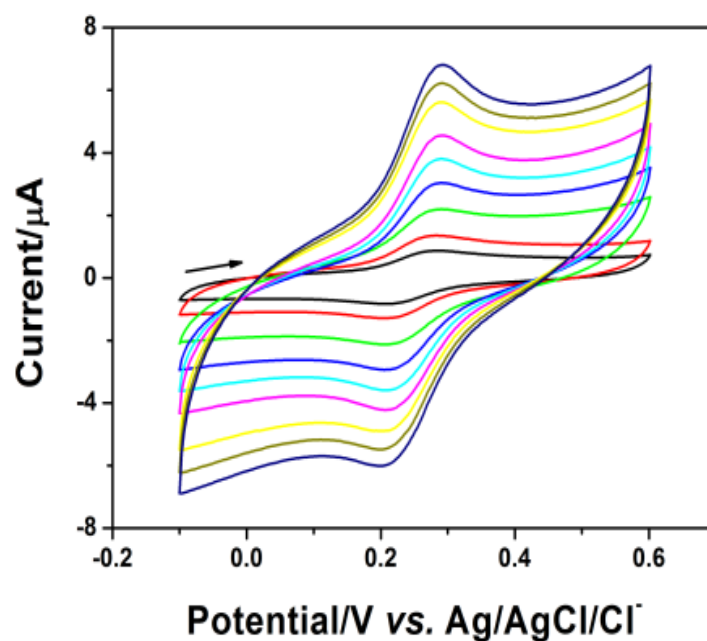
(b)
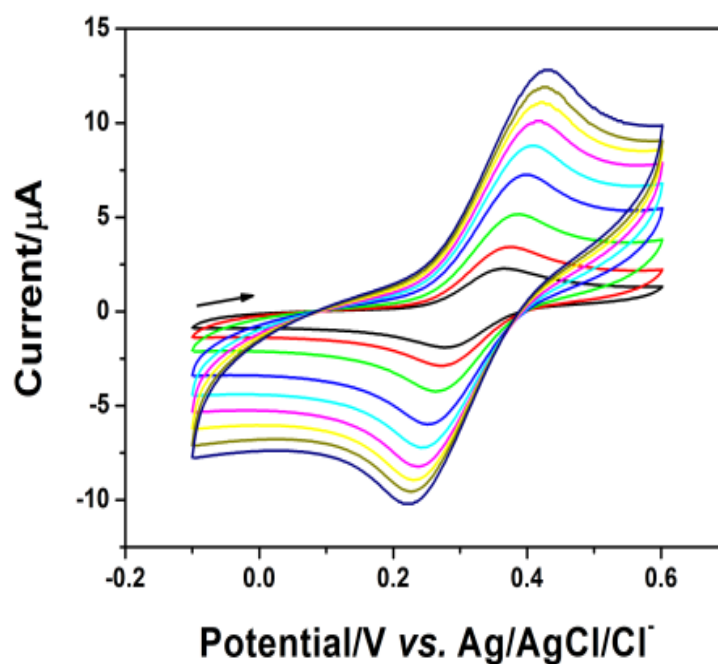
Figure 5.4: Voltammetry of 3.1 mM Et₂Fc within the H₁ phase made with Triton X 100/0.1 M aqueous KCl (50:50 wt. % ratio) in (a) the homoetropic and (b) the homogeneous alignment. The arrows indicate the direction of the initial scan.

Key: 0.025 (black), 0.05 (red), 0.1 (green), 0.2 (blue), 0.3 (cyan), 0.4 (magenta), 0.5 (yellow), 0.6 (dark yellow), 0.7 (ultramarine) V s⁻¹.

These data exhibited features of electrochemical reversibility, except for the homogeneously aligned samples at the smallest timescales probed (*q.v.* Figure 5.4(c)), where it is likely that the deviations from fast electrode kinetics are due to Ohmic losses rather than quasi-reversibility.

For every concentration of Et$_2$Fc employed, diffusion-controlled voltammograms were observed for both types of aligned structure (*q.v.* Figure 5 .4 (d)).

(c)
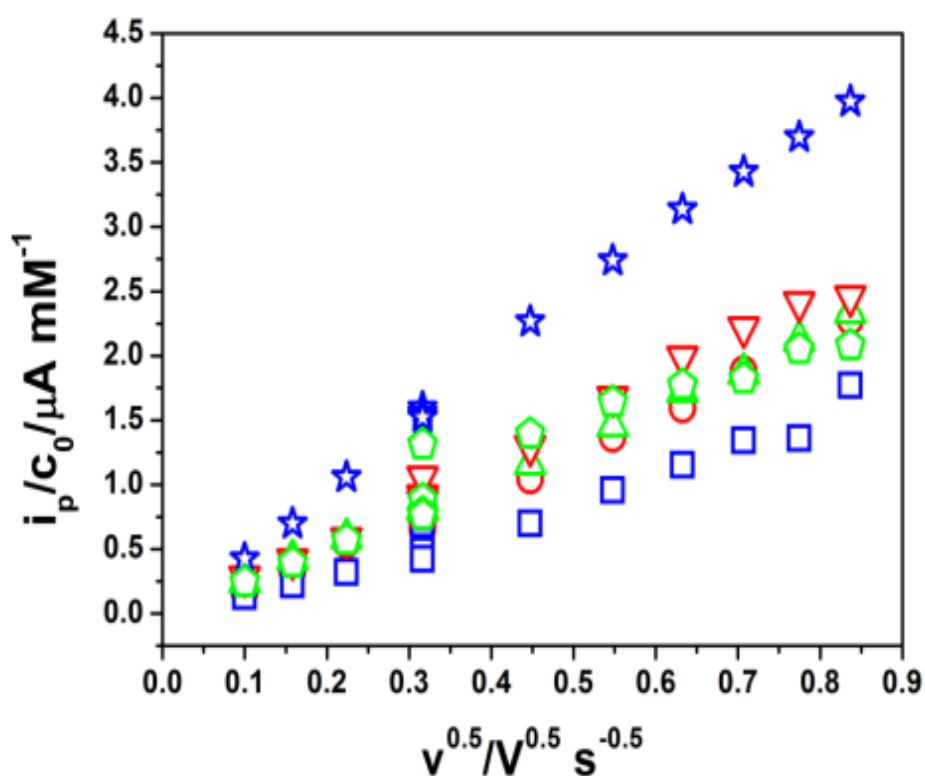
Figure 5.4(c): Plots indicating the variation of the concentration-normalised peak current with scan rate are also given. **Key:** open symbols refer to oxidative processes; c$_0$ = 1.6 (red), 3.2 (blue), 4.5 (green) mM; circles, squares and triangles refer to the homeotropic alignment, with inverted triangles, stars and pentagons referring to the homogeneous alignment.

(d)
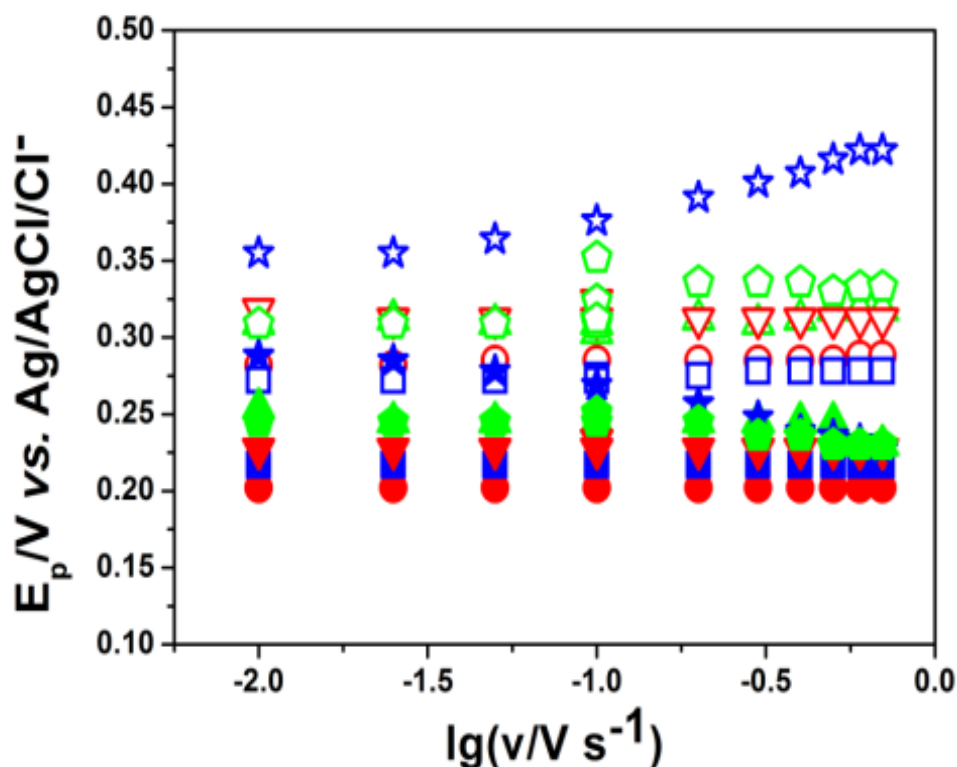
Figure 5.4(d): Plots indicating the variation of the concentration-normalised peak potentials with scan rate are also given. **Key:** open symbols refer to oxidative processes, filled symbols refer to the re-reduction wave; c_o = 1.6 (red), 3.2 (blue), 4.5 (green) mM; circles, squares and triangles refer to the homeotropic alignment, with inverted triangles, stars and pentagons referring to the homogeneous alignment.

Values of the apparent diffusion coefficient are given in (Table 2), where it is seen there is relatively little variation in the apparent diffusion coefficients in either orientation. Moreover, the size of these values matches up with those of TMPD in perchlorate electrolyte-based L_α liquid crystals detailed above. We accordingly suggest that this reflects the transport of micelle-containing analyte within these phases.

[Et$_2$Fc] mM	10^8 D$_{hometropic}$/cm^{2}s^{-1}	10^8 D$_{homogeneous}$ /cm^{2}s^{-1}	D$_{hometropic}$ / D$_{homogeneous}$
1.6	1.8	2.5	0.7
3.1	0.9	6.5	0.1
4.5	2.0	2.0	1.0

Table 2: Apparent homogeneous one-dimensional diffusion coefficients for Et$_2$Fc within the H$_1$ phase of Triton X 100 doped with 0.1 M aqueous KCl.

(a)
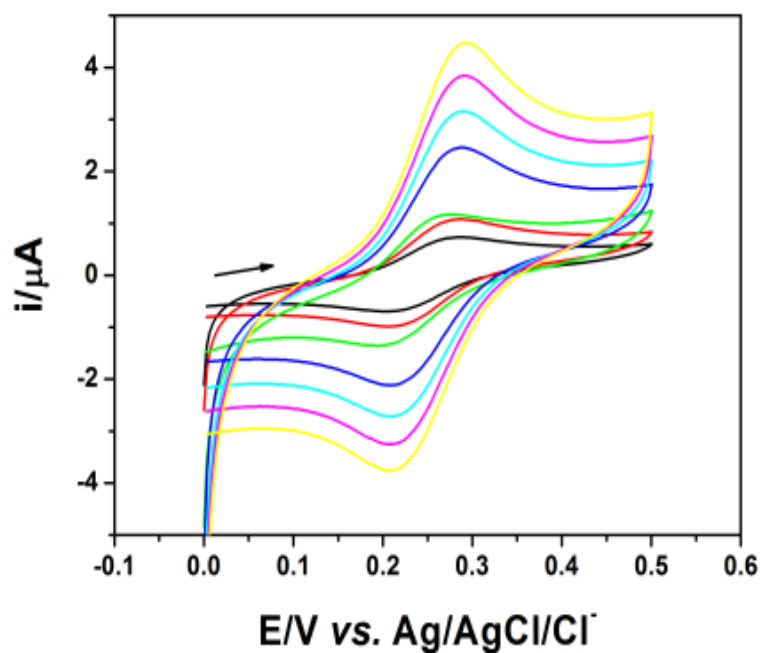
(b)
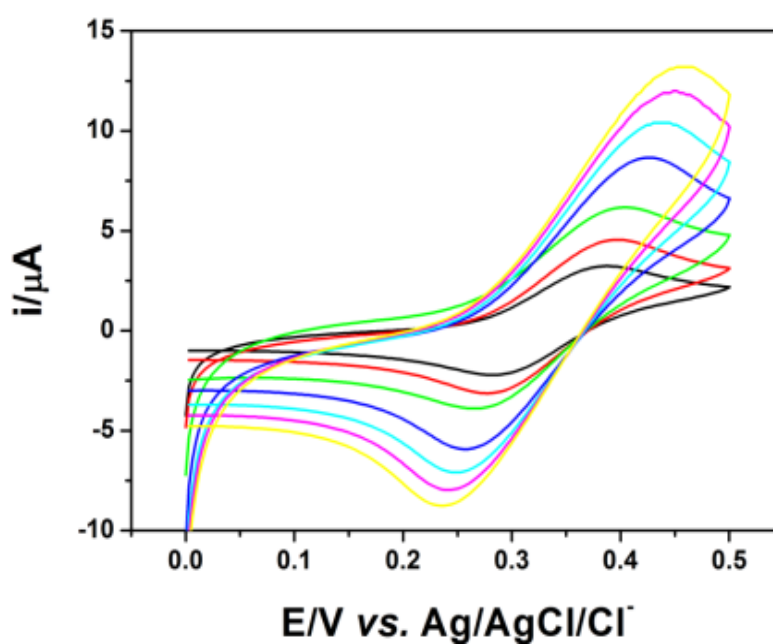
Figure 5.5: Voltammetry of 4.5 mM Et₂Fc within the H₁ phase made with Triton X 100/0.1 M aqueous KCl (50:50 wt. % ratios) doped with 5.0 mL of nanorod solution in (a) the homoetropic and (b) the homogeneous alignment. The arrows indicate the direction of the initial scan. **Key:** 0.025 (black), 0.05 (red), 0.1 (green), 0.2 (blue), 0.3 (cyan), 0.4 (magenta), 0.5 (yellow) V s⁻¹.

Figure 5.5 (a, b) depicts voltammograms of Et_2Fc within the H_1 phase doped with the highest loading of gold nanorod solution. It is clear from these plots and their corresponding analyses based on one-dimensional diffusion (see Table 3), that, in both homeotropic and homogeneous alignments the presence of the nanorods causes, in general, the observation of smaller currents, as anticipated for a blocked electron transfer process [27,28].

Table 3: Apparent homogeneous one-dimensional diffusion coefficients for Et_2Fc within the H_1 phase of Triton X 100 doped with 0.1 M aqueous KCl and a variable amount of Au nanorod solution.

[Et₂Fc]mM	10^8 $D_{hometropic}/cm^2s^{-1}$	10^8 $D_{homogeneous}$ /cm²s⁻¹	$D_{hometropic}$ / $D_{homogeneous}$
4.5[a]	2.0	2.0	1.0
4.4[b]	0.5	0.5	1.0
4.6[c]	0.3	0.2	1.5
4.5[d]	0.3	4.0	0.1

[a]No nanorods present; [b]phase made-up using 1.0 mL of the nanorod solution; [c]phase made-up using 2.0 mL of the nanorod solution; [d]phase made-up using 5.0 mL of the nanorod solution.

For the homeotropically aligned system, the process is electrochemically reversible.

(c)
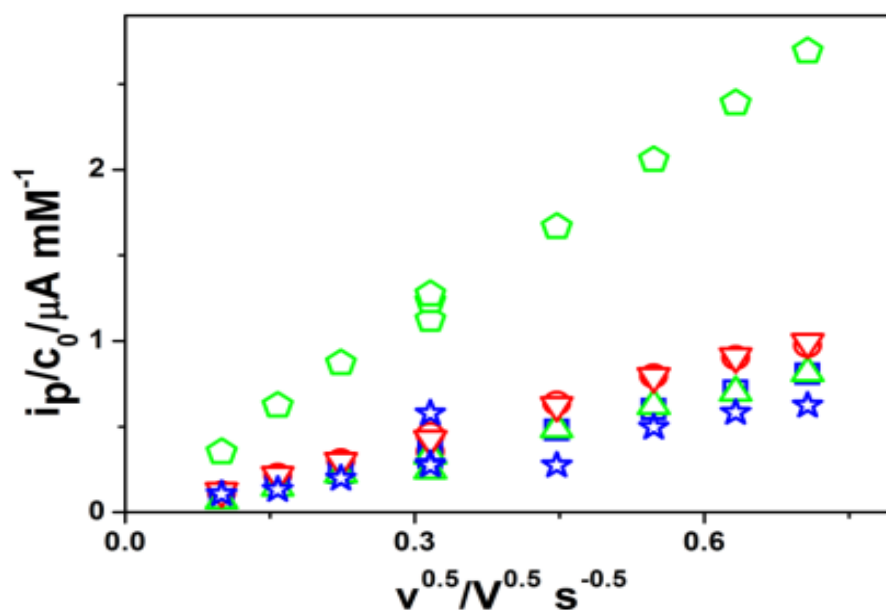
(d)
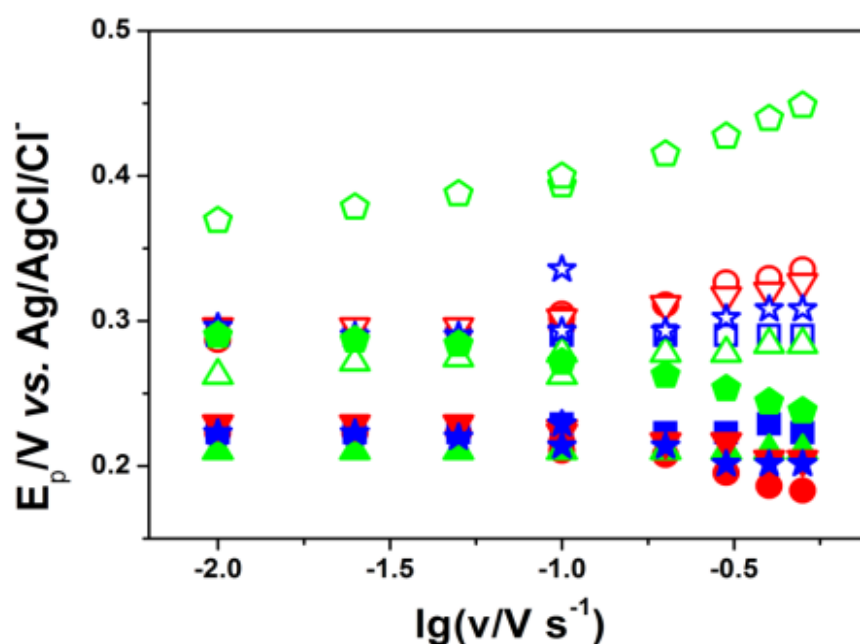
 Figure 5.5: Plots indicating the variation of the concentration-normalised peak current (c) and peak potentials (d) with scan rate are also given. **Key:** open symbols refer to oxidative processes, filled symbols refer to the re-reduction wave; amount of nanorod solution used = 1.0 (red), 2.0 (blue), 5.0 (green) mL; circles, squares and triangles refer to the homeotropic alignment, with inverted triangles, stars and pentagons referring to the homogeneous alignment.

In contrast, the homogeneously-aligned sample shows evidence of blocked electron transfer at low loadings (the peak currents are smaller than for the case of no nanoparticles present), but, paradoxically, gives rise to much larger currents at higher loadings, coupled with the occurrence of significant distortions to the voltammetric waveshape, as anticipated for partially-blocked electrodes [27,28].

We interpret these data through the ability of the nanorods to allowing for some form of mediated electron transfer communication [29, 30] to take place between individual surfactant subphases, through a large triple phase boundary [31, 32]; the system behaves as though it is a gold nanorod "paste" electrode.

The above behaviour for a hydrophobic redox probe differs from our earlier work on a system that undergoes diffusion-partitioning between the two subphases. Accordingly, we revisited these systems.

5.4.2.2 Polarising microscope images of the H_1 phase of Triton X 100/H_2O

To examine this qualitatively, these aqueous KCl based H_1 phases were prepared with the inclusion of a variable amount of CTAB-stabilised gold nanorod solution. The nanorods were characterised through TEM image analysis (see Figure 5.6(d) to have lengths of 33.5 ± 3.3 nm, and widths of 14.1 ± 3.2 nm, yielding an aspect ratio of 2.4, which compares favourably with that anticipated through analysis [29, 30] of the longitudinal plasmon absorption band (which stem from the coherent electronic oscillation along the long nanorod axis), *viz.* aspect ratios in the range 2.5-2.8.

Although these rods are sufficiently large to straddle both aqueous and micellar subphases [24, 26], the incorporation of Au nanoparticles did not produce any visible changes in the optical texture of the H_1 phase when examined under crossed-polarisers [*q.v.* Figure 5.6(c)].

(a)   **(b)**

(c)   **(d)**
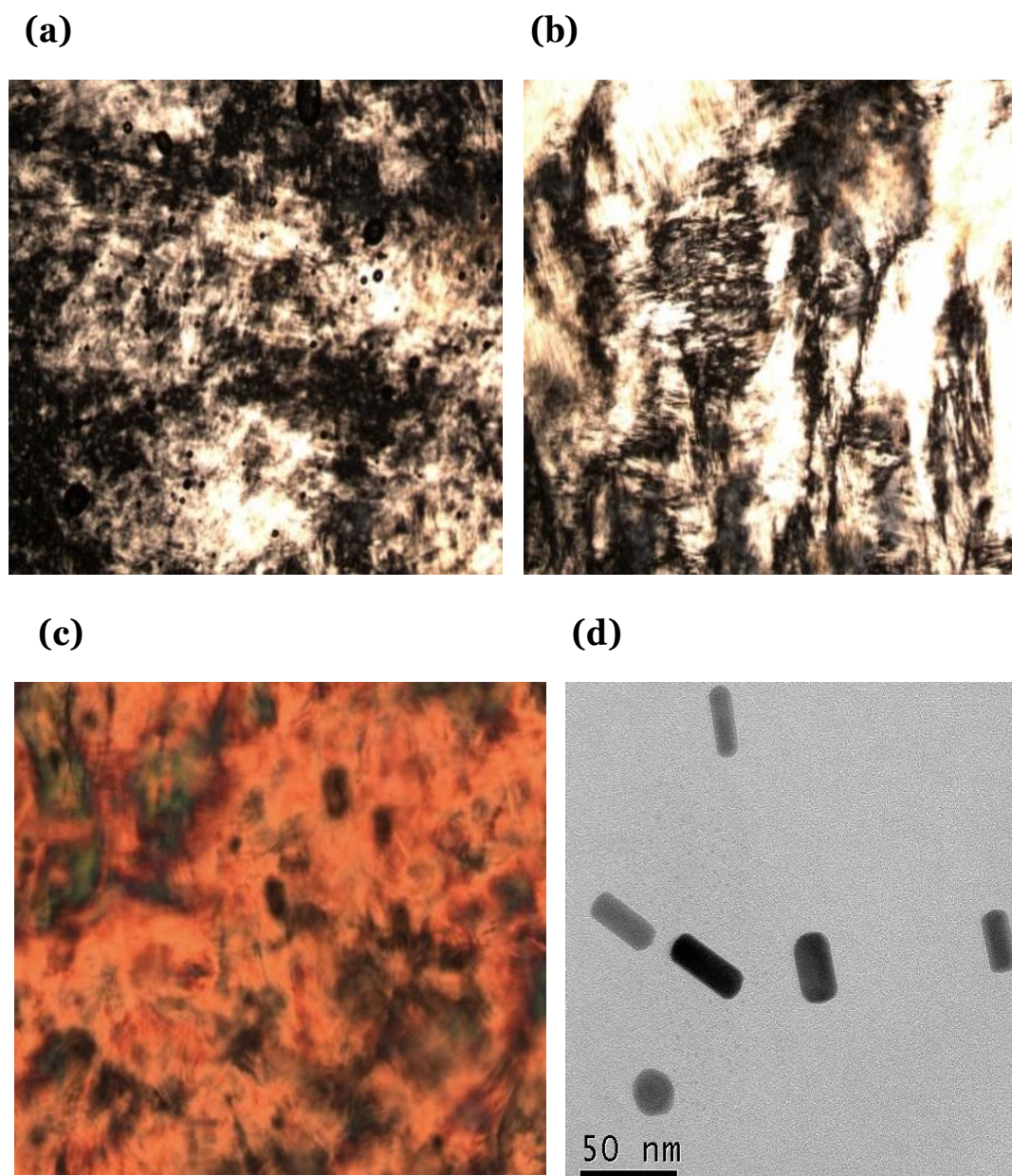
Figure 5.6 Optical polarising microscope images under x10 zoom of the texture of the H_1 phase of Triton X 100/H_2O in the undoped state (a), doped with 0.1 M aqueous KCl (b), and doped with both Et_2Fc and the largest amount of nanorod solution (see text); panel (d) illustrates a TEM image of the nanorods employed.

5.4.2.3   Voltammetry of TMPD within the H₁ phase

Figure 5.7 illustrates voltammograms corresponding to the one-electron oxidation of TMPD within the H₁ phase doped with either KCl or NaClO₄ and oriented either in a homogeneous or a homeotropic manner.
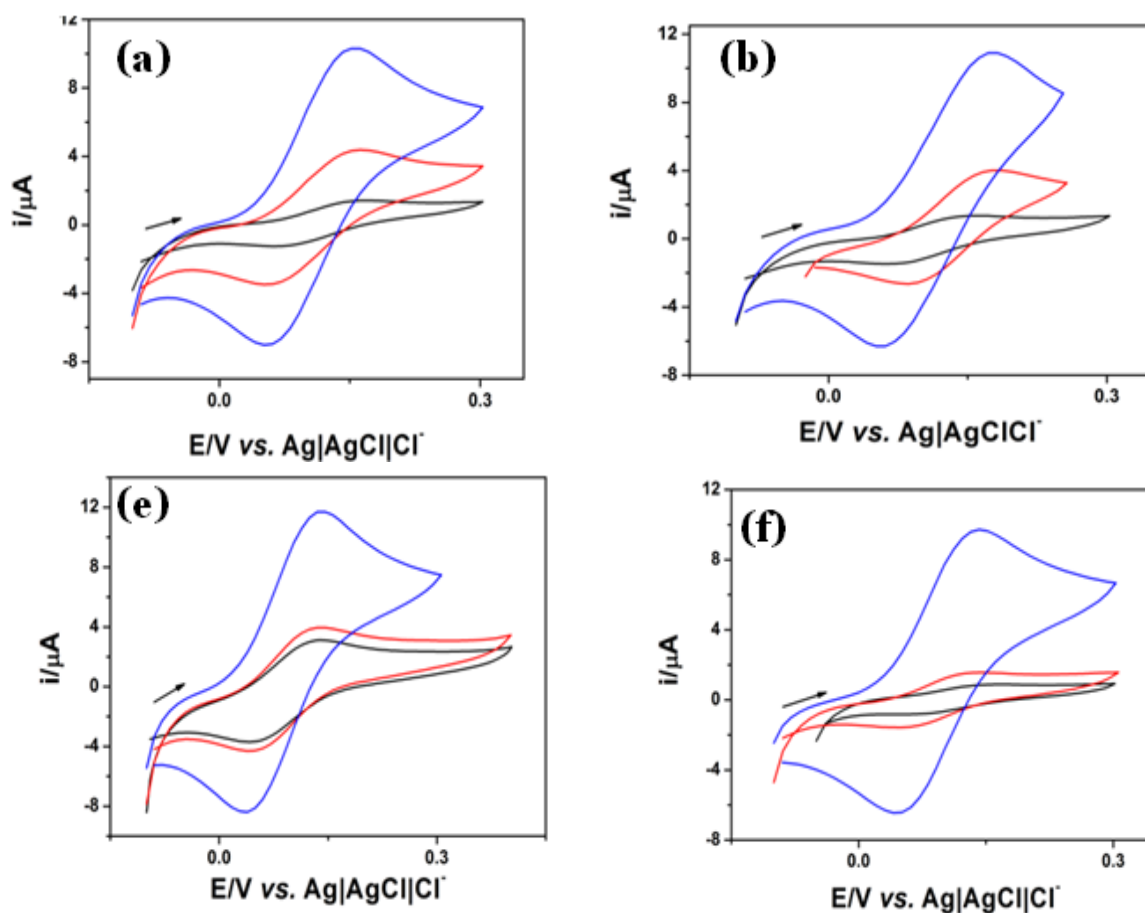
Figure 5.7: Cyclic voltammograms and their analysis (see text) corresponding to the one-electron oxidation of TMPD within the H₁ phase formed using Triton X 100/0.1 M aqueous KCl (in a 50:50 wt.% ratio), (a-d), or Triton X 100/0.1 M aqueous NaClO₄ (in a 50:50 wt.% ratio), (e-h). Voltammograms in panels (a), (b), (e), (f) correspond to the first scan obtained (the arrow indicates the direction of the initial potential sweep) at 0.1 V s⁻¹ for homeotropic samples (a) and (e), or homogeneous samples (b) and (f).

These data have the characteristics of electrochemical reversibility [see Figure 5.7 (c, g)], and, as in earlier work, afford peak currents which exhibit diffusional characteristics [Figure 5.7 (d, h)].

(c)
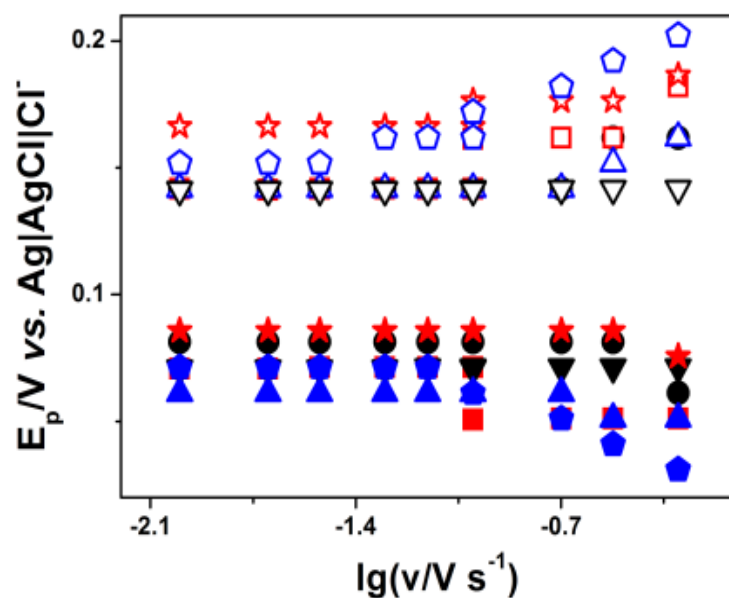
(g)
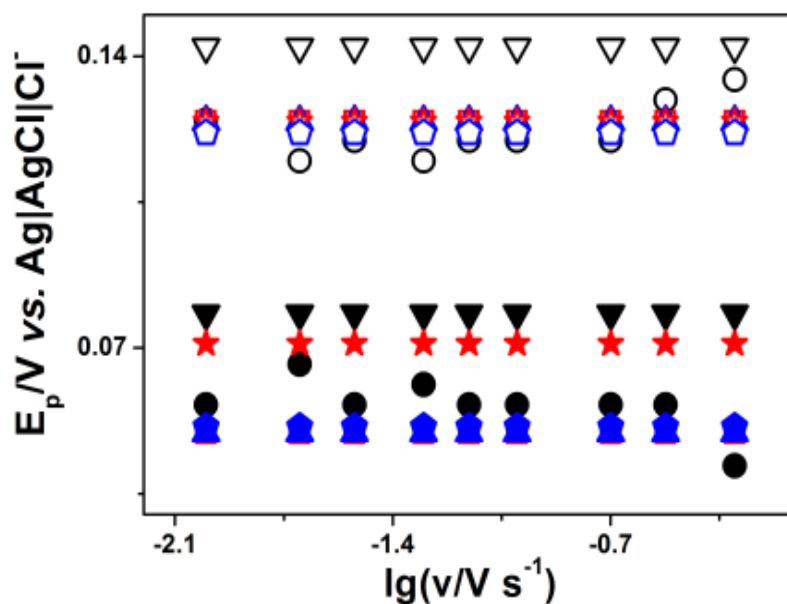
Figure 5.7: A panel (c) and (g) depicts the variation in the peak potentials for the oxidation and re-reductive waves with the electrochemical timescale.

(d)
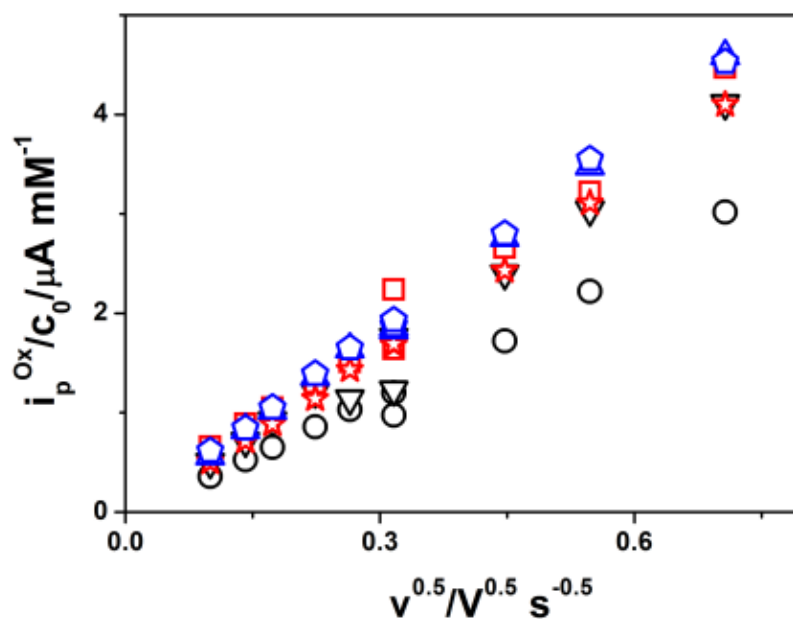
(h)
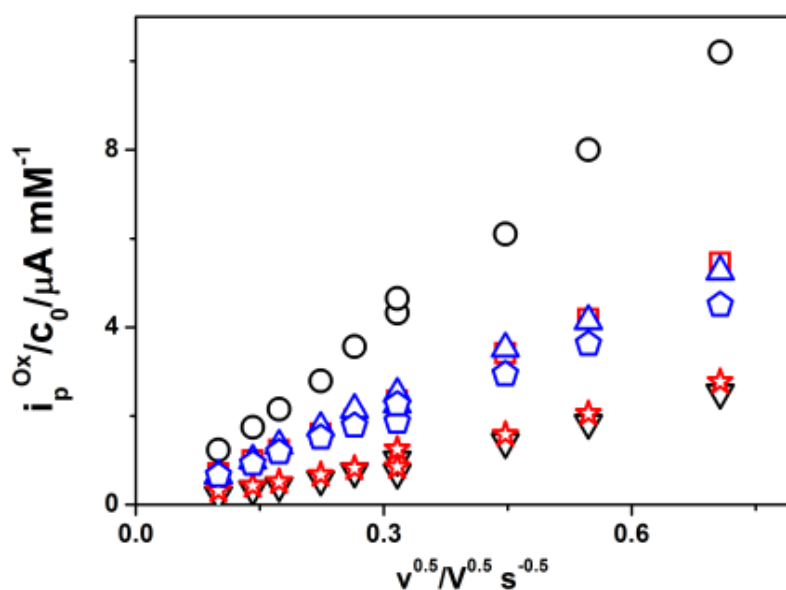
Figure 5.7: panels (d) and (h) are concentration-normalised Randles-Sevčik plots. **Key:** colours indicate concentrations of TMPD within the phase (c_0) with black corresponding to 1.1 mM, red indicating 2.6 mM and blue denoting 5.4 mM; symbols denote the characteristics pertaining to the peaks in the forward (open symbols) and reverse (filled symbols) waves in the voltammograms, with circles, squares and triangles corresponding to homeotropic samples, whilst inverted triangles, stars and pentagons denoting the homogeneous samples.

The diffusion coefficients are concentration dependent (*q.v.* Table 4), with the salting-in electrolyte doping causing a more significant change in the transport characteristic compared with the salting-out electrolyte. Nevertheless, both types of ionic doping causes the system to tend to apparent diffusional isotropy at the highest concentrations of TMPD, in line with expectation from our earlier studies [14]: electron transfer across the subphase | subphase interface is more likely to be significant at the highest loadings employed, thereby allowing the establishment of an electron "pump" through the operation of a "scheme-of-squares" [14].

[TMPD]mM	10^8 $D_{hometropic}$/cm²s⁻¹	10^8 $D_{homogeneous}$ /cm²s⁻¹	$D_{hometropic}$ / $D_{homogeneous}$
50:50 TritonX-100:H_2O doped with 0.1M KCl			
1.1	4.4	8.1	0.5
2.6	10	8.6	1.2
5.4	11	11	1.0
50:50 TritonX-100:H_2O doped with 0.1M NaClO$_4$			
1.0	55	2.9	19
2.1	16	3.6	4.3
5.1	16	12	1.4

Table 4: Concentration dependence of the diffusion coefficients for TMPD within the H$_1$ phase of Triton X 100/H_2O.

5.5   Conclusions

In summary, the occurrence of diffusion of analytes within a micellar framework compared with transport of micelle-containing analytes can be modulated by a number of factors including

(1) The type of ionic doping as well as analyte hydrophobicity

(2) The type of nanostructure formed rather than the particular orientation of the structure, with the H_1 phase acting as a medium that may offer a lower degree of Ohmic loss.

Accordingly, we next seek to address whether this quasi-biphasic and restricted phase may be utilised for the development of a crude artificial mimic of the first few steps of Photosystem I for which the relevant molecules (vitamin K_1 and those constituting plant pigment) are known to be very hydrophobic.

- ## **<u>Electrochemistry and Photoelectrochemistry of Vitamin K$_1$ and Plant Pigment within the H$_1$ Phase (Photosystem II)</u>**

5.6   introduction

Photosynthesis, the process by which solar light energy is harnessed to drive biochemical reactions, is the key to life on Earth [33-36]. Electron transfer cascades play a central rôle within this complex and sophisticated process, not least in allowing the transfer of electrical potential energy from the photoexcited reaction centre to long-term energy storage. In green plants, photosynthesis takes place in chloroplasts (lens-shaped structures 10 μm in diameter) [34, 35], specifically within the thylakoid membrane. The whole process effects the synthesis of hexose sugars from carbon dioxide and water, through a series of "dark" reactions coupled with two light-based processes (in the so-called Z-scheme).

Photosystem II actuates the oxidation of water (to produce oxygen) coupled with, ultimately, the reduction of cytochrome f through a series of proton-coupled electron transfer pathways in bound redox-species [34], which allows for the reduction of the freely-diffusing small blue copper protein plastocyanin. This species acts to regenerate the "special" chlorophyll a-chlorophyll a' dimer of Photosystem I (P700) through reduction of P700$^{+\bullet}$ (in a timescale of $ca.$ 200 μs), which is formed after photoexcitation of P700 and electron transfer to a bound chlorophyll a (A$_0$) in a timescale of $ca.$ 3 ps.

Continuation of the downhill electron transfer series of Photosystem I occurs with $A_0^{-\cdot}$ reducing vitamin K_1 (A_1, phylloquinone) within 40-200 ps, followed by electron transfers to three iron-sulfur proteins and eventually ferridoxin, which allows for the proton-coupled reduction of $NADP^+$.

In seeking to develop artificial mimics of the photosynthetic pathway, it is therefore essential to design supramolecular, three-dimensional ensembles of both photochemically and electrochemically-active systems which are held in a close proximity with good electronic couplings for fast and efficient charge transfer cascades, but, crucially, with channels for proton transfer to occur with the electron transfer [37].

Inasmuch as the engineering of such systems (dyads, triads, *etc.*) is possible [38-41], they are ultimately synthetically-expensive, generally requiring the additional involvement of redox species to allow for proton translocation [42], and do not allow for the ready-probing of the underlying molecular mechanisms [41], so are not facile to optimise in terms of energy conversion efficiencies [43,44].

5.7   Extraction of Plant Pigments

- Plant pigment (a mixture of chlorophylls *a* and *b*) was obtained using fresh spinach leaves (*Spinacia oleracea*) were cut into strips and stirred at room temperature in an aqueous acetone solution (4 : 1 vol./vol. acetone/water) for *ca.* 120 min. [45-48]

- Following filtration, the solvent was removed using a rotary evaporator, and the resulting solid examined *via* UV/visible spectroscopy in methanol. It was estimated from the spectra of several solutions diluted from a 22 mg L^{-1} plant pigment methanolic solution that [48] the solutions contained 15 wt. % chlorophyll (3.4 mg L^{-1} total chlorophyll, present as 2.5 mg L^{-1} of chlorophyll a and 0.9 mg L^{-1} of chlorophyll b, using the relationships:

$$\left[\text{Total Chlorophyll}\right]/\text{mg L}^{-1} = 25.5A_{650} + 4.0A_{665}$$

$$\left[\text{Chlorophyll a}\right]/\text{mg L}^{-1} = 16.5A_{665} - 8.3A_{650}$$

$$\left[\text{Chlorophyll b}\right]/\text{mg L}^{-1} = 33.8A_{650} - 12.5A_{665}$$

where A_i is the observed absorbance at a wavelength of *i* nm. The plant pigment was stored in the dark at 277 K when not in use.

5.8 Voltammetry of VK$_1$ within the H$_1$ phase

Figure 5.8 (a) illustrates voltammograms (at 0.1 V s^{-1}) corresponding to the reduction and re-oxidation of vitamin K$_1$ within the H$_1$ phase doped with 0.1 M aqueous HCl. Vitamin K$_1$ is extremely hydrophobic, so is anticipated to reside within the surfactant subphase.

It is clear from data presented that only a single, albeit broad reduction (and corresponding re-oxidation) wave is observed in both types of aligned structure, with little loss of signal upon repetitive redox cycling, suggesting that there is no loss of product from the surfactant subphase. Following from previous work [48-50], we suggest that these data reflect the two-electron, two-proton transformation of vitamin K$_1$ into the corresponding quinol:

$$\mathbf{VK_1\,(surf)\ +\ 2H^+\,(aq\ or\ surf, palisade)\ +\ 2e^-\ \rightleftharpoons VK_1H_2(surf)} \qquad (4)$$

Furthermore, consistent with earlier reports on the biphasic voltammetry of vitamin K$_1$, is the observation of a large peak-to-peak separation. [48]

The voltammograms demonstrate that the homeotropic alignment gives rise to smaller Faradaic signals, with the Faradaic processes being easier to achieve, at every timescale probed. In both cases, it is evident that zero current passes due to redox processes associated with vitamin K$_1$ reduction/phylloquinol oxidation when the electrode is held at 0.0 V $vs.$ Ag | AgCl | Cl$^-$.

(a)
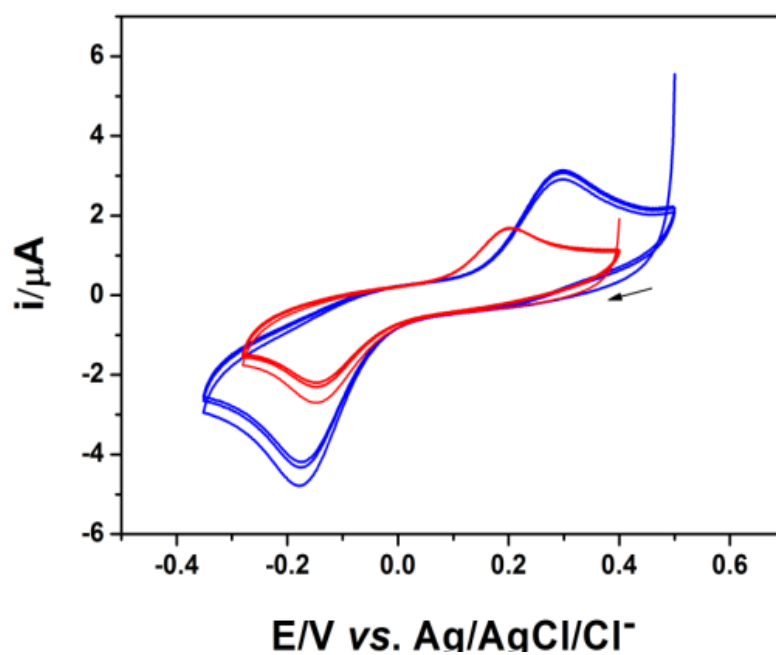
(b)
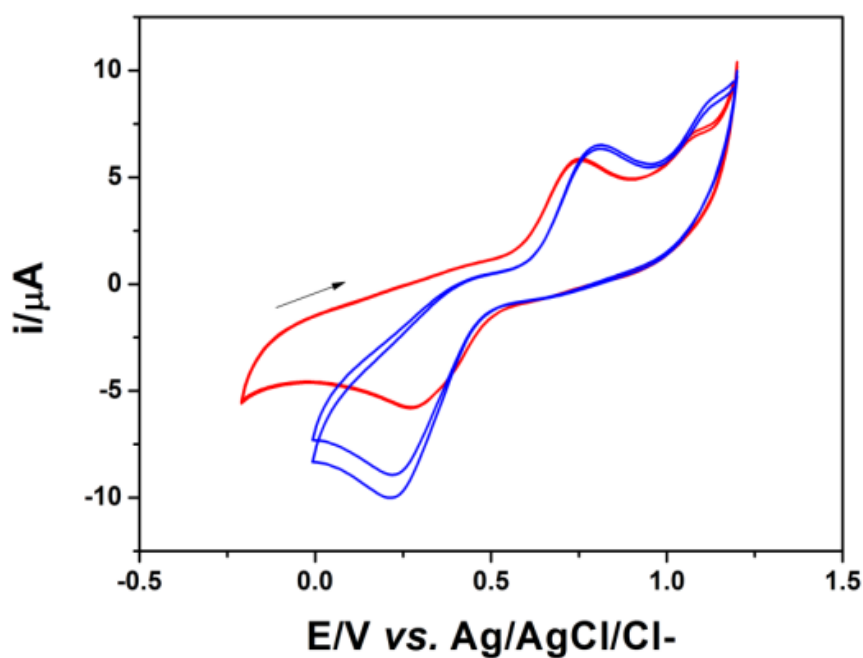
Figure 5.8: Voltammograms (scan rate 0.1 V s⁻¹) corresponding to (a) the reduction of vitamin K₁ and (b) the oxidation of plant pigment, when immobilised within the H₁ phase of Triton X 100/aqueous 0.1 M HCl ,in the homeotropic (red) or homogeneous (blue) alignment. The arrows indicate the direction of the initial potential sweep.

(c)
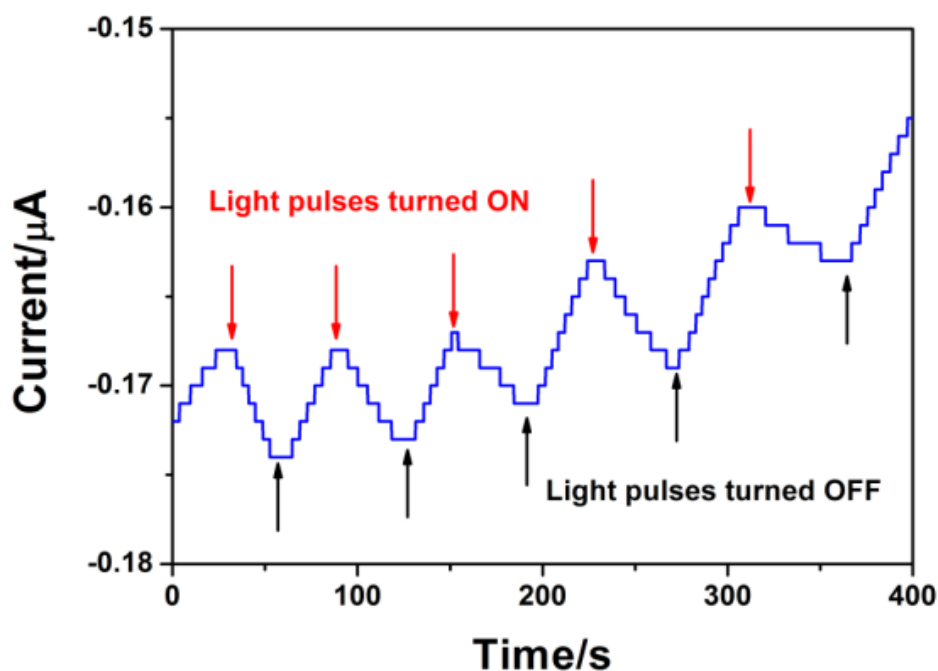
Figure 5.8 Panel (c) illustrates typical photo-reductive currents observed on illumination of the homogeneously-aligned sample with red light, holding the potential of the glassy carbon working electrode at 0.0 V *vs.* Ag | AgCl | Cl⁻.

Similar observations are seen in the voltammetry of plant pigment (a mixture that is *ca.* 80 wt. % chlorophyll a and 20 wt. % chlorophyll b – a species which is thought [51] to be a Förster energy donor to chlorophyll a, and which is identical to chlorophyll a except at the C-7 position where a formyl group replaces the methyl group) within the H_1 phase doped with aqueous 0.1 M HCl, as evidenced in Figure 5.8 b.

In this case, oxidation of the pigment produces the stable cation radical, as reported in earlier work [52-57], with the possibility of engaging in a second oxidation to form the unstable dication [52]. Again, the oxidation is more facile within the homeotropic sample, but the difference is not noticeable. In part this may be due to the fact that

under these acidic conditions, it is the corresponding phæophytin, rather than the metallated species present.

The pH_M of chlorophyll a has been reported [58] as being 3.5 (in 10% water/ethanol at 303 K), with the first dissociation constant for the nitrogen on the porphyrin ring estimated as 1.0 (for chlorophyll a) and 1.1 (for phæophytin a), so that the oxidation process relies on *gegen* ion pairing, which in this case involves chloride ions, rather than formation of O-H covalent bonds through proton incorporation, as in the vitamin K_1 case. As with the phylloquinone dopant, it is unlikely that the plant pigment species exit from the micelles in either oxidised or neutral forms; n-octanol/water partition coefficients are [58] slightly larger for phæophytin a (lgK_P = 2.51) *c.f.* chlorophyll a (lgK_P = 2.44) – this is consistent with little loss in signal on consecutive voltammetric sweeps.

Furthermore, it is noticeable that the Faradaic currents are bigger for the plant pigment compared with vitamin K_1, even though the effective concentration of the former is smaller; we interpret this as being due to both faster heterogeneous electron transfer kinetics (symmetry factor closer to ½) and the larger apparent diffusion coefficient of the chlorophyll species.

This makes sense, even though the size of chlorophyll a is very much more massive than vitamin K_1, since the former is known to aggregate [52-64], and engages in a simple electron transfer process, and so will have contributions to the diffusion coefficient from physical displacement *and* electron hopping [1-4], whereas the vitamin K_1 system requires a proton-coupled-electron transfer process in biphasic media, which may

limit the degree to which the electron hopping pathway may contribute to the diffusion coefficient.

Importantly, the voltammograms illustrate that the reduction of the oxidised form of the plant pigment (likely the cation radical of phæophytin a, Phæo a$^{+\bullet}$) is diffusionally-limited at 0.0 V *vs.* Ag | AgCl | Cl$^-$.

In seeking to develop a crude mimetic of Photosystem I, the H$_1$ phase was prepared with aqueous 0.1 M HCl, vitamin K$_1$ and the plant pigment all acting as dopants, with oxygen rigorously excluded from the sample preparation. Both homogeneous and homeotropic phases were illuminated using red light which was directed onto a glassy carbon electrode surface, with the electrode potentiostatted at 0.0 V *vs.* Ag | AgCl | Cl$^-$.

However, no photocurrents were observed within the homeotropic system. In contrast, the homogeneous case yielded small photo-reductive currents (*q.v.* Figure 5.8 c). We suggest the reason for this difference stems from transport differences, based on the observations made of hydrophobic solutes within these framework materials.

The observation of photo-*reductive* signals is in contrast with the biphasic photoelectrochemistry of chlorophyll a dissolved within vitamin K$_1$ microdroplets previously reported by Wain *et coll.* [17], where the observed photo-*oxidations* were interpreted as being due to the oxidation of the semiquinone form of vitamin K$_1$, owing to the vast excess of vitamin K$_1$ in the liquid state compared with chlorophyll a (1: 10 w/w ratio). We propose the following mechanism [59-64].

Possible reaction mechanism:

$$\text{Phæo a} \xrightarrow{h\nu} \text{Phæo a*} \qquad\qquad (5)$$

$$\text{Phæo a*} + \tfrac{1}{2}VK_1 + H^+ \rightarrow \text{Phæo a}^{\bullet+} + \tfrac{1}{2}VK_1H_2 \qquad (6)$$

$$\text{Phæo a}^{\bullet+} + e^- \rightarrow \text{Phæo a} \qquad\qquad (7)$$

This mechanism is consistent with the photo-induced electron transfer proposed by Wolff and Grätzel [65] between photo-excited chlorophyll and duroquinone within the anionic micelles of an isotropic solution of sodium lauryl sulfate.

Given this unoptimised, proof-of-concept system demonstrates the potential for the H_1 phase in the homogenous alignment for the development of soft-matter-based artificial photosystems, it is instructive to determine the photon efficiency (*viz.* ratio of number of moles of electrons flowing through the electrode per mole of photons incident onto the sample) for this system; using a measured photo flux of 20 μeinstein m^{-2} s^{-1}, and noting the maximum value of the recorded current in Figure 5.8 c is 12 nA, we estimate the incident-photon-to-current efficiency as being on the order of 0.1%. Whilst this value is small within this unoptimised system, we note that it is comparable to other, optimised systems based on a single liquid | liquid interface [66].

5.9   Conclusions

Lyotropic liquid crystals provide an attractive and synthetically-inexpensive, three-dimensional nanostructured framework for electron transport processes. These have been seen to be remarkably affected by the type of ionic electrolyte doping and the hydrophobicity of the redox solute, as well as orientation of the liquid nanosystem, allowing for the development of unusual routes for material transport over distance; a unique route is through the partitioning of species across pseudophases with cross-pseudophase electron transfer.

The incorporation of nanoparticles within such structures can elicit nuances in electrochemically triggered transport processes. For the case of the H_1 phase of Triton X 100/light water doped with plant pigment, vitamin K_1 and aqueous HCl, we have illustrated that it behaves as a crude biomimetic of the first few steps of Photosystem I to a proof-of-concept: photoreduction currents are observed with an incident-photon-to-current-efficiency of *ca*. 0.1%.

References for chapter5

1. J. E. Halls, A. A. Altalhi, F. C. de Abreu, M. O. F. Goulart, J. D. Wadhawan, *Electrochem. Commun.*, 17 (2012) 41.

2. J. E. Halls, N. S. Lawrence, J. D. Wadhawan, *J. Phys. Chem. B*, 115 (2011) 6509, and references cited therein.

3. J. E. Halls, J. D. Wadhawan, *Electroanalysis*, 23 (2011) 997.

4. T. Peiró-Salvador, O. Ces, R. H. Templer, A. M. Seddon, *Biochem.*, 48 (2009) 11149.

5. G. Paillotin, W. Leibl, J. Gapiński, J. Breton, A. Dobek, *Biophys. J.*, 75 (1998) 124.

6. L. A. Evans, M. J. Thomasson, S. M. Kelly, J. Wadhawan, *J. Phys. Chem. C*, 113 (2009) 8901.

7. T. A. Postlethwaite, E. T. Samulski, R. W. Murray, *Langmuir*, 10 (1994) 2064.

8. C. Chen, T. A. Postlethwaite, J. E. Hutchinson, E. T. Samulski, R. W. Murray, *J. Phys. Chem.*, 99 (1995) 8804.

9. J. E. Halls, J. D. Wadhawan, Manuscript in preparation.

10. J. Reiter, T. Uhlírová, J. R. Owen, *J. Electroanal. Chem.*, 646 (2010) 18.

11. S. Eustis, M. A. El-Sayed, *J. Appl. Phys.*, 100 (2006) 044324.

12. W. Zhuang, X. Chen, J. Cai, G. Zhang, H. Qui, *Colloids Surf. A*, 318 (2008) 175.

13. Y.-Y. Luk, C.-H. Jang, L.-L. Cheng, B. A. Israel, N. L. Abbott, *Chem. Mater.*, 17 (2005) 4774.

14. A. S. Poulos, D. Constantin, P. Davidson, M. Impéror, B. Pansu, P. Panine, L. Nicole, C. Sanchez, *Langmuir*, 24 (2008) 6285.

15. C. Lefrou, *Electrochimie sur ultramicroelectrodes : voltammetrie cyclique resolue dans la gamme des nanosecondes – developpement et applicatons*, Ph.D. Thesis, Université Paris VI, 1992.

16. J. D. Wadhawan, R. G. Evans, R. G. Compton, *J. Electroanal. Chem.*, 533 (2002) 71.

17. C. Amatore, E. Maisonhaute, B. Schöllhorn, J. Wadhawan, *Chem.Phys.Chem.,* 8 (2007) 1321.

18. B. A. Kowert, L. Marcoux, A. J. Bard, *J. Am. Chem. Soc.*, 94 (1972) 5538.

19. Å. Johansson, T. Drakenberg, *Mol. Cryst. Liq. Cryst.*, 14 (1971) 23.

20. K. Beyer, *J. Colloid Interface Sci.*, 86 (1982) 73.

21. H. K. Bisoyi, S. Kumar, *Chem. Soc. Rev.*, 40 (2011) 306.

22. P. S. Kumar, S. K. Pal, S. Kumar, V. Lakshminarayanan, *Langmuir*, 23 (2007) 3445.

23. S. V. Ahir, P. G. Petrov, E. M. Terentjev, *Langmuir*, 18 (2002) 9140.

24. M.-H. Lee, S.-G. Oh, K.-D. Suh, D.-G. Kim, D. Sohn, *Colloids Surf. A.*, 210 (2002) 49.

25. A. N. Galatanu, I. S. Chronakis, D. F. Anghel, A. Khan, *Langmuir*, 16 (2000) 4922.

26. D. Constantin, P. Davidson, C. Chanéac, *Langmuir*, 26 (2010) 4586.

27. B. A. Brookes, T. J. Davies, A. C. Fisher, R. G. Evans, S. J. Wilkins, K. Yunus, J. D. Wadhawan, R. G. Compton, *J. Phys. Chem. B*, 107 (2003) 1616.

28. T. J. Davies, B. A. Brookes, A. C. Fisher, K. Yunus, S. J. Wilkins, P. R. Greene, J. D. Wadhawan, R. G. Compton, *J. Phys. Chem. B*, 107 (2003) 6431.

29. C. R. Bradbury, L. Kuster, D. J. Fermín, *J. Electroanal. Chem.*, 646 (2010) 114.

30. G. P. Kissling, C. Bunzli, D. J. Fermín, *J. Am. Chem. Soc.*, 132 (2010) 16855.

31. C. E. Banks, T. J. Davies, R. G. Evans, G. Hignett, A. J. Wain, N. S. Lawrence, J. D. Wadhawan, F. Marken, R. G. Compton, *Phys. Chem. Chem. Phys.*, 5 (2003) 4053.

32. See, for example, D. R. Ort, C. F. Yocum (eds.), *Oxygenic Photosynthesis: the Light Reactions*, Advances in Photosynthesis volume 4, Govindjee (ed.), Kluwer Academic, Dordrecht, 1996.

33. R. E. Blankenship, *Modern Mechanisms of Photosynthesis*, Blackwell Science, Oxford, 2002.

34. J. N. Prebble, *Mitochondria, Chloroplasts and Membranes*, Longman, London, 1981.

35. Govindjee, in M. Yunus, U. Pathre, P. Mohant, *Probing Photosynthesis*, Taylor & Francis, London, 2000, p.9.

36. C. Costentin, M. Robert, J.-M. Savéant, *Phys. Chem. Chem. Phys.*, 12 (2010) 11179.

37. D. G. Johnson, M. P. Niemczyk, D. W. Minsek, G. P. Wiederrecht, W. A. Svec, G. L. Gaines, III, M. R. Wasielewski, *J. Am. Chem. Soc.*, 115 (1993) 5692.

38. D. Gust, T. A. Moore, A. L. Moore, *Acc. Chem. Res.*, 34 (2001) 40.

39. J. Barber, *Chem. Soc. Rev.*, 38 (2009) 185.

40. G. Steinberg-Yfrach, P. A. Liddell, S.-C. Hung, A. L. Moore, D. Gust, T. A. Moore, *Nature*, 385 (1997) 239.

41. R. E. Blankenship, D. M. Tiede, J. Barber, G. W. Brudvig, G. Fleming, M. Ghirardi, M. R. Gunner, W. Junge, D. M. Kramer, A. Melis, T. A. Moore, C. C. Moser, D. G. Nocera, A. J. Nozik, D. R. Ort, W. W. Parson, R. C. Prince, R. T. Sayre, *Science*, 332 (2011) 805.

42. W. Vredenberg, *BioSystems*, 103 (2011) 138.

43. J. Armstrong, W. Armstrong, *New Phytol.*, 126 (1994) 493..

44. J. D. Wadhawan, A. J. Wain, R. G. Compton, *ChemPhysChem*, 4 (2003) 1211.

45. M. Holden, in T. W. Goodwin (ed.), *Chemistry and Biochemistry of Plant Pigments*, 2nd edn., volume 2, Academic Press, London, 1976, p.1.

46. G. Mackinney, *J. Biol. Chem.*, 140 (1941) 315.

47. A. J. Wain, J. D. Wadhawan, R. G. Compton, *ChemPhysChem*, 4 (2003) 974.

48. J.-E. Yang, J.-H. Yoon, M.-S. Won, Y.-B. Shim, *Bull. Korean Chem. Soc.*, 31 (2010) 3133.

49. W. Yao, C. Lau, Y. L. Hui, H. L. Poh, R. D. Webster, *J. Phys. Chem. C*, 115 (2011) 2100.

50. R. van Grondelle, *Biochim. Biophys. Acta*, 811 (1985) 147.

51. T. Saji, A. J. Bard, *J. Am. Chem. Soc.*, 99 (1977) 2235.

52. M. R. Wasielewski, R. K. Smith, A. G. Kostka, *J. Am. Chem. Soc.*, 102 (1980) 6923.

53. E. P. Suponeva, S. Hotchandani, C. Arbour, B. A. Kisselev, *Biologisches. Membran.*, 13 (1996) 229.

54. P. Cosma, F. Longobardi, A. Agostiano, *J. Electroanal. Chem.*, 564 (2004) 35.

55. F. T. Buononsegni, L. Becucci, M. R. Moncelli, R. Guidelli, A. Agostiano, P. Cosma, *J. Electroanal. Chem.*, 550-1 (2003) 229.

56. A. Pandey, S. N. Butta, *J. Phys. Chem. B*, 109 (2005) 9066.

57. A. P. Gerola, T. M. Tsubone, A. Santana, H. P. M. de Oliveira, N. Hioka, W. Caetano, *J. Phys. Chem. B*, 115 (2011) 7364.

58. H. Tributsch, M. Calvin, *Photochem. Photobiol.*, 14 (1971) 95.

59. H. Tributsch, *Photochem. Photobiol.*, 16 (1972) 216.

60. J.-G. Villar, *J. Bioenerg. Biomemb.*, 8 (1976) 173.

61. J.-G. Villar, *J. Bioenerg. Biomemb.*, 8 (1976) 189.

62. J.-G. Villar, *J. Bioenerg. Biomemb.*, 8 (1976) 199.

63. O. S. Ksenzhek, A. G. Volkov, *Plant Energetics*, Academic Press, San Diego, 1998.

64. C. Wolff, M. Grätzel, *Chem. Phys. Lett.*, 52 (1977) 542.

65. D. J. Fermín, H. D. Duong, Z. Ding, P. F. Brevet, H. H. Girault, *Electrochem. Commun.*, 1 (1999) 29.

66. A. R. Brown, L. J. Yellowlees, H. H. Girault, *J. Chem. Soc., Faraday Trans.*, 89 (1993) 207.

Chapter 6 - Self-assembling, Self-reconstructing, *Photo-rechargeable* Biphasic

Batters

There is currently much work being undertaken to develop of electrochemical technologies soon to provide devices that address the Humanity's desire to consume affordable, sustainable, "green", clean and efficient energy systems based on mobile, portable and rechargeable power sources.[1] An entirely new concept redox battery based on a liquid|liquid interface, and which can be charged with solar energy, is developed within this work and realised experimentally; this electrochemical cell is based on electron transfer, rather than ion transfer, is shown to act as a photogalvanic device which, under violet light, is demonstrated to exhibit maximum light-to-electrical power conversion efficiency of *ca*. 9% (fill factor of 16%).

6.1 The theory of this work

We examine the basic theoretical principles underpinning a biphasic battery, with a view to unravel particular insights into the operational viability of such systems, under conditions of open circuit.[2, 3]

6.1.1 Open Circuit Voltage within Photo-rechargeable Biphasic Batteries

Consider the biphasic battery system illustrated in Figure 6.1.
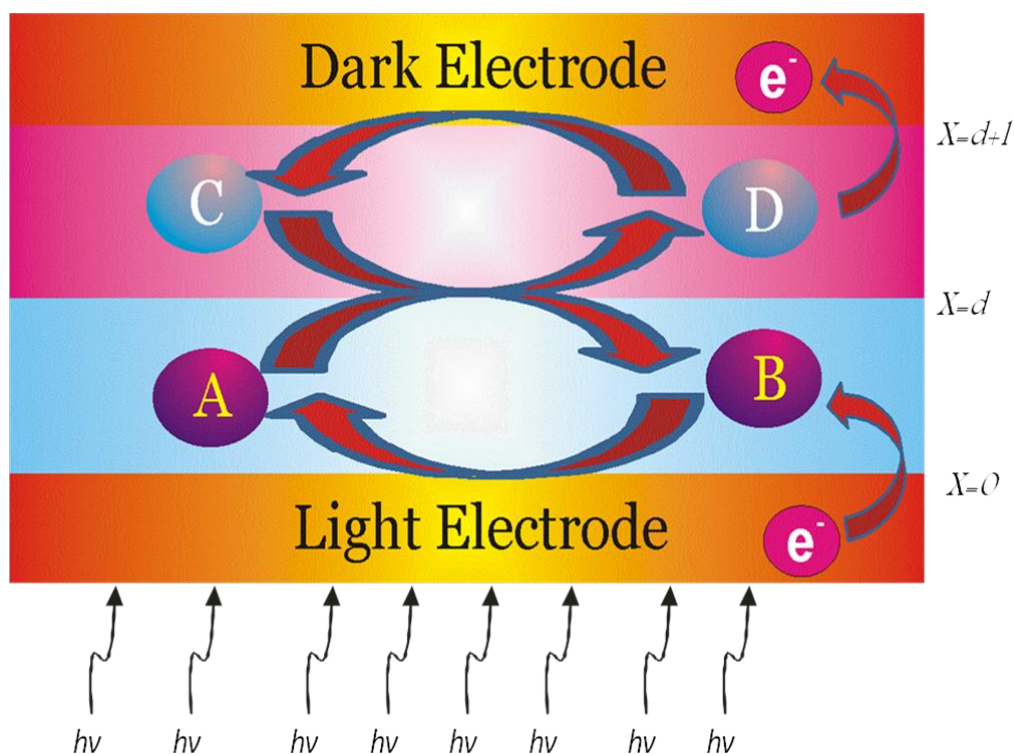
Figure 6.1: Schematic illustration of a biphasic battery in which photo-induced electron transfer occurs only at the interface between two immiscible electrolyte systems. The arrows indicate the heterogeneous electron transfer processes in this stacked system.

It comprises two electrodes parallel to each other, sandwiching a dielectric system comprised of two immiscible liquids (*e.g.* oil and water) that are mutually-saturated. Each of these liquids is loaded with: excess supporting electrolyte, and a redox-active couple.[4]

The liquid | liquid interface is considered to be ideally polarisable, *viz.* there is no exchange of ions between the two phases; it is assumed that only one electron is exchanged between the redox pairs across the biphasic interface. In this model, the denses (α) phase contains photoredox-active species A and its redox partner, B

$$B + e^- \rightleftharpoons A$$
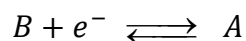
These species are both insoluble within the other liquid phase (β), which contains the electroactive *but photo-inactive* couple C and D

$$C + e^- \rightleftharpoons D$$
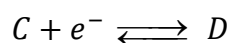
In the following we assume that each of the species A, B , C and D have identical concentrations within the liquid electrolytes at zero time. Thus, at the interface, the equilibrium is established.

$$A + C \underset{k_{off}}{\overset{k_{on}}{\rightleftharpoons}} B + D$$
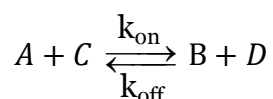
Equality of the electrochemical potentials at the interface enables the deduction of the following Nernst equation which describes the variation of the Galvani potential difference

$$\Delta_\alpha^\beta \varnothing = \varnothing^\beta - \varnothing^\alpha$$

with species activity (a_i) for these bimolecular heterogeneous electron transfer reactions:

$$\Delta_\alpha^\beta \emptyset = \Delta_\alpha^\beta \emptyset^\circ + \frac{RT}{F} In \left(\frac{a_B^\alpha a_D^\beta}{a_A^\alpha a_C^\beta} \right)$$

where the driving force for the redox reaction through the interface (the standard interfacial redox potential) is

$$\Delta_\alpha^\beta \emptyset^\circ = E_{A/B}^{0,\propto} - E_{D/C}^{0,\beta}$$

Note that both of these standard electrode potentials are referenced to the same scale. For reversible energy conversion, it is necessary for this reaction to occur unidirectionally under discharge. We, accordingly, consider the case when the formal electrode potentials of the A/B and D/C redox couples are such that $A + C \rightarrow B + D$ is an endoergic process (k_{on} takes a value of zero), and $B + D \rightarrow A + C$ is spontaneous (k_{off} takes a finite, non-zero value), *viz.* $\Delta E^{0'} = E_{A/B}^{0'} - E_{D/C}^{0'} > 0$.

Thus, in the dark, the biphasic battery system will discharge at a rate dependent on the bimolecular electron transfer kinetics, with generation of A and C at the interface. With time, these concentrations will impact on the ratio of B: A and C: D at the surfaces of the two electrodes located in the different phases, causing the cell electromotive force (emf) to diminish. If we are able to charge-up the cell, [5] *viz.* reverse the spontaneous interfacial reaction, and then we may increase this open circuit voltage. Indeed, although no power is produced when the cell voltage is at the

cell emf, insights into how the latter may be maximised may assist in the engineering of cells with sufficiently large potential differences under conditions of maximum power output.

Let us now consider the case when the cell is charged through photochemically-induced electron transfer at the interface. If the interface is illuminated (or if one of the electrodes is transparent or semi-transparent such that the interface may be illuminated), then the photoredox active species contained within the system, species A, may be photo-excited to form an electronically energetic state (A*).[6]

The concentration of this excited state then will vary on the intensity of the light source, depth of illumination and the rate constant for the exoergic reaction:

$$A^* + \ C \ \rightarrow B + D$$
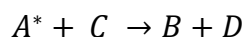
In noting that the concentrations of the various species are non-uniform, the former may be quantitatively deduced through the following differential equation relating the intensity of the transmitted light (I) to the individual species concentrations (c),

$$\frac{\partial I}{\partial x} = -\epsilon(x)c(x)I$$

where: $\epsilon(x)$ is the extinction coefficient at a fixed wavelength, x is the depth of the illumination probed.

This is the case that has been treated by previous workers, albeit under the constraints of analytical approximation and exclusively for homogenous electron transfer.[7, 8] In view of the fact that this pathway may not represent the correct chemistry for any developed system, and to simplify our analysis.

We assume here that the photoinduced interfacial electron transfer is: $A + C \rightarrow B + D$ *viz.* the electron transfer is treated as an optical charge transfer process. Such processes are well-established within the literature,[9] such as the electron transfer reaction occurring between *N*-methylphenothiazine and tetrachlorobenzoquionone within an intimate complex of the two species.[10]

This assumption still allows for this photo-induced electron transfer process to be described through the framework of the Marcus theory (*vide infra*).[5]

Thus, assuming that diffusion-only mass transport applies (the cell thickness is geometrically restricted, and both phases are assumed to be fully electrochemically-supported), the biphasic battery emf may be deduced through the solution of Fick's second law for each species (where we additionally assume that the cell is adequately described using one spatial dimension):

$$\frac{\partial c_A}{\partial t} = D_A \frac{\partial^2 c_A}{\partial x^2} \; ; \; \frac{\partial c_B}{\partial t} = D_B \frac{\partial^2 c_B}{\partial x^2} \; ; \; \frac{\partial c_C}{\partial t} = D_C \frac{\partial^2 c_C}{\partial x^2} \; ; \; \frac{\partial c_D}{\partial t} = D_D \frac{\partial^2 c_D}{\partial x^2}$$

subject to the following pertinent boundary conditions, where all symbols retain their usual meanings Note that, for completeness, the electrode kinetics are given through a Butler-Volmer formalism, with transfer coefficient of ½.[11]

$t \leq 0 \quad 0 \leq x < d \quad c_A = A_o; \; c_B = B_o; \; c_c = c_D = 0$

$x = d \quad c_A = A_o; \; c_B = B_o; \; c_c = C_O; c_D = D_o$

$d < x \leq (d+l) \quad c_A = c_B = 0; \; c_c = C_O; c_D = D_o$

$t > 0 \quad x = 0 \quad -D_B \left(\frac{\partial c_B}{\partial x}\right)_{x=0} = D_A \left(\frac{\partial c_A}{\partial x}\right)_{x=0} = -\frac{i_L}{FS} = -k_{S_2} \, e^{-\left(\frac{1}{2}\right)\zeta\{(c_B)_{x=0} - (c_A)_{x=0} \, e^{\zeta}\}}$

$x = d+l \quad D_D \left(\frac{\partial c_D}{\partial x}\right)_{x=d+l} = -D_C \left(\frac{\partial c_c}{\partial x}\right)_{x=d+l} = -\frac{i_D}{FS} = -k_{S_2} \, e^{-\left(\frac{1}{2}\right)\zeta\{(c_C)_{x=d+l} - (c_D)_{x=d+l} \, e^{\zeta_2}\}}$

Where $i_L = -i_D = 0 \; and \; \zeta = \frac{F}{RT}(E_L - E^{O'}_{A/B}); \zeta_2 = \frac{F}{RT}(E_D - E^{O'}_{D/C}; \text{so that } \zeta_{oc} = \zeta = \zeta_2$

$x = d \quad D_A \left(\frac{\partial c_A}{\partial x}\right)_{x=d} = D_c \left(\frac{\partial c_c}{\partial x}\right)_{x=d} = k_{on}c_A c_C - k_{off}c_B c_D$

For open circuit conditions, the ratio of the redox partners at each electrode allows the determination of the individual electrode potentials through a Nernst formulation, *viz.* $\frac{c_B}{c_A} = e^{\zeta}; \frac{c_{BC}}{c_D} = e^{\zeta_2}$, in order to obtain a degree of generality for the solution of the transport equations, the above were recast into adimensional variables for: time, $\theta = \frac{t}{\tau}$ in while τ is the length of the experimental observation; space, $y = \frac{x}{\sqrt{D_A \tau}}$ and with concentrations normalised with respect to the sum of the initial conditions of species A and B, *viz.* (A$_o$ + B$_o$).

We additionally assume that the diffusion coefficients of species B and A are identical; *mutatis mutandis* for species D and C. The effect of this is to simplify the problem to merely calculating the concentrations pertaining to species A and C.

Thus, numerical simulation in these reduced variables was undertaken using the Backward Implicit finite difference method, with a grid split such that $d = l = \frac{1}{2}\sqrt{D_A \tau}$ (half of the diffusion length developed through reaction at the liquid | liquid interface in each phase.

Based on an Einstein-Smoluchowski view, and under the assumption of very dilute solutions – the value of all initial concentrations was set to 1.0 mM), with explicit application of the boundary condition at *x=d* at t = 0 to initiate the depletion and formation of species.

In this way, the simulation was able to be run over both phases through a back-to-back grid approach, with each phase being treated separately, except at the interface. Convergent results were obtained using 2×10^4 spatial nodes with 10^5 temporal steps in simulations requiring approximately three minutes of computing time.

6.1.2 How does the cell emf vary with the rate constant for the biphasic photo-induced electron transfer?
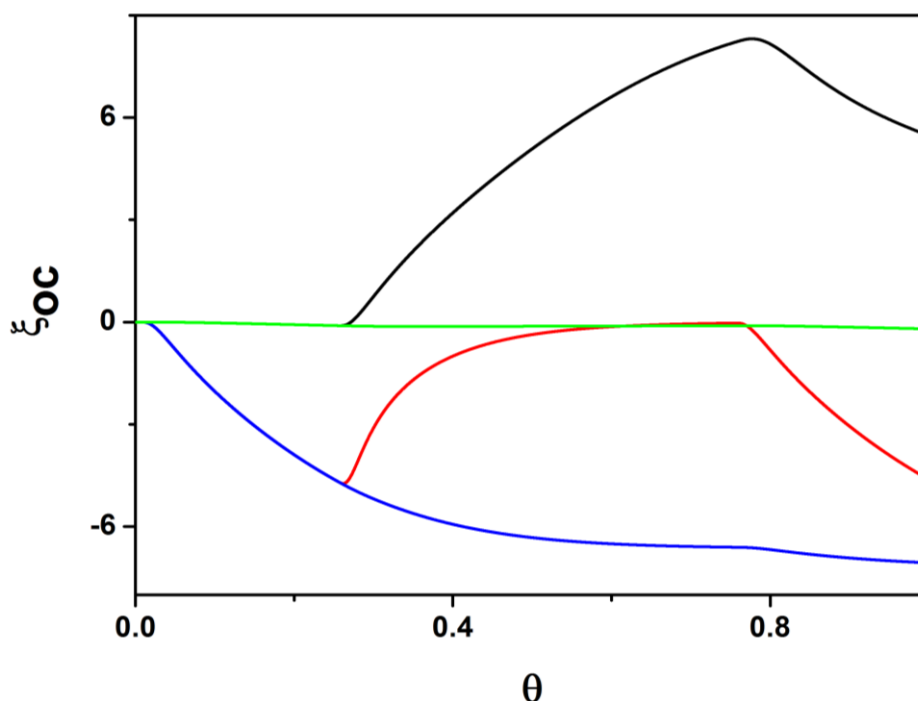
Figure 6.2 : Variation in the cell emf with time in the presence $(0.25 \leq \theta \leq 0.75)$ and absence $(\theta < 0.25$ and $\theta > 0.75)$ of light to drive the electron transfer between species A and C. Initial concentrations of all species was set at 1.0 mM, with the real time set at 1000 s. (a). **Key:** *Black: $k_{on}=10^4 k_{off}=10^{-3}$ m^4 mol^{-1} s^{-1}, Red: $k_{on}=k_{off}=10^{-3}$ m^4 mol^{-1} s^{-1}, Blue: $k_{on}=10^{-4}k_{off}=10^{-7}$ m^4 mol^{-1} s^{-1}, Green: $k_{on}=k_{off}=10^{-7}$ m^4 mol^{-1} s^{-1}* **Note: $D_A=D_B=D_C=D_D=10^{-5}$ cm^2 s^{-1}.**

Figure 6.2 illustrates the results of the simulations, run with open circuit discharge $(k_{on} = 0)$ for the first and last 25% of the dimensionless time, with the middle 50% being for the case when k_{on} takes a non-zero value. Various workers, [12] have explored electron transfer kinetics at both polarised and nonpolarised liquid | liquid

interfaces. In all cases they observe a Marcus-type variation of the electron transfer rate constant with driving force, with a maximum value for the bimolecular rate constant being reported[13] as $\sim 10^2$ cm M^{-1} s^{-1} = 10^{-3} m^4 mol^{-1} s^{-1}. Taking this value, then, as the maximum value for either k_{on} or k_{off}, and considering only pragmatic limiting scenarios, we note from Figure 6.2 that, when the transport rate for all species is identical, maximum photovoltages occur when the ratio of the two bimolecular rate constants, $\frac{k_{on}}{k_{off}}$ is greatest (*viz.* fast charge, slow discharge), as expected; maximising the ratio $\frac{k_{off}}{k_{on}}$ is *not* useful – the cell stays in discharge mode – it is not able to be charged sufficiently rapidly with light energy, irrespective of the light intensity. In this case, ξ_{oc} is always negative, a situation which we will ascribe to being in *dimensionless reverse polarity mode.*

This is not necessarily the same as *true* reverse polarity of the cell[14], since

$$\xi_{oc} = \frac{F}{RT}(E_L - E_{D)-}\frac{F}{RT}\Delta E^{\circ\prime}$$

Interestingly, if the system is fast in both charge and discharge, the cell rapidly moves in to dimensionless reverse polarity under open circuit discharge, with the cell emf reaching a quasi-photostationary- state upon illumination, with both electrodes taking, more or less, the same dimensionless potential. This scenario translates as the case when the measured cell voltage *equals* the difference between the formal redox potentials of the involved redox couples.

Conversely, slow charge and discharge kinetics result in the cell essentially retaining its initial potential – there is little perturbation of the concentrations of the species under open circuit conditions, so that the maximum voltage that can be produced by this cell in real terms is $\Delta E^{\circ\prime}$.

It thus follows that, for the cell to operate successfully in both discharge and charge modes either k_{on} needs to be very much bigger than k_{off}, or, if these rate constants are similar in size, $\Delta E^{o\prime}$ needs to be as large and positive as possible; the discharge kinetics should ideally fall within the Marcus inverted region. These conclusions are valid for the case when diffusion rates in both phases are identical. What happens if this is not the case? Intuitively, we expect the observation of *smaller* cell voltages – the rate of communication of the occurrence of the interfacial reaction to the electrodes is reduced.[15]

In summary, then, the simulations illustrate that the maximum value of the open circuit voltage occurs when: $\Delta E^{o\prime}$ is biggest, and ζ_{oc} is largest. Whilst these conditions may seem intuitive, in considering (ζ_{oc} is largest), it is important to recognise the rôle played by the kinetics of the electron transfer event at the liquid | liquid interface: in general this follows a Marcus-type relationship, in that as the driving force for electron transfer increases, the rate constant increases to a maximum, and then decreases with further increase in $-\Delta G^o$ - the so-called inverted region.

It thus follows that for maximum cell emf under illumination (and noting that this may impact on the maximum power produced), the redox couples in the phases α and β should be selected such that they exist within the Marcus-inverted region,

since then the spontaneous discharge process takes place as pathologically slowly as possible. However, there is an additional potential mechanism for a biphasic battery to operate which we now address: what if there is no interfacial Faradaic reaction, but, rather, there is a photo-induced redox reaction in one phase, causing a photovoltage to be developed at the electrode located therein, with the potential of the other electrode controlled by a non-photo-active redox couple within the other phase? An example of this situation is the case when the photo-induced electron transfer is reaction with the solvent comprising the pertinent phase.

Then the process is kinetically pseudo-first order:

$$A \xrightarrow{\text{hv}} B$$
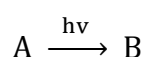
so that the process is still:

$$A + C \underset{\text{Light}}{\overset{\text{Dark}}{\rightleftarrows}} B + D$$
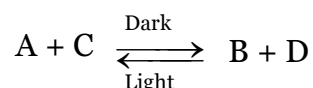
and, under the conditions given for the previous system, the transport equation for species A now becomes:

$$\frac{\partial c_A}{\partial t} = D_A \frac{\partial^2 c_A}{\partial x^2} - k_f c_A + k_b c_B$$

with the boundary conditions identical, except at $x = d$, which is now replaced by a Neumann (no-flux) condition:

$$D_A \left(\frac{\partial c_A}{\partial x}\right)_{x=d} = D_c \left(\frac{\partial c_c}{\partial x}\right)_{x=d} = 0$$

In the above, k_f is maximially ten times the Smoluchowski diffusion-limited bimolecular rate constant, and so takes a maximum value of $\sim 10^{11}$ s^{-1}. However, k_b refers to the back-reaction between the reduced form of the solvent and the oxidised form of species A. Strictly; this is not a pseudo-first-order reaction.

Nevertheless, if species B is stable, and the counter ion is unstable (because reduction has occurred dissociatively, either in concert with the electron transfer, or due to fast stepwise kinetics[9]), we recognise that this system can then be made to store light energy – k_b takes the limiting value of zero, and the system behaves as a photo-battery. The full theoretical analysis of this type of cell will be given in a future work.[16]

6.1.3 Photovoltaic Cell Conversion Efficiency

The conversion efficiency of a solar cell [17] is the percentage of the solar energy shining on a PV device that is converted into electrical energy, or electricity. Improving this conversion efficiency is a key goal of research and helps make solar-to-electrical technologies cost-competitive with more traditional sources of energy.

6.1.4 Factors Affecting Conversion Efficiency

Much of the energy from sunlight reaching a solar cell is lost before it can be converted into electricity. But certain characteristics of solar cell materials also limit the efficiency of the device to convert the sunlight it receives.

6.1.4.1 Wavelength of Light

Light is composed of photons or packets of energy that range in wavelength. When light strikes the surface of a solar cell, some photons are reflected and do not enter the cell. [18] Other photons pass through the material. Of these, some are absorbed but only have enough energy to generate heat, and some have enough energy to separate electrons from their atomic bonds to produce charge carriers negative electrons and positive holes.

Bandga[19-22] is the minimum amount of energy needed to free an electron from its bond, and this energy differs among semiconductor materials. The primary reason photovoltaic cells are not 100% efficient is because they cannot respond to the entire spectrum of sunlight. Photons with energy less than the bandgap of the metal are not absorbed, which wastes as much as 25% of incoming energy.

The energy content of photons above the bandgap is wasted surplus re-emitted as heat or light and accounts for an additional loss of about 30%. Thus, the inefficient interactions of sunlight with cell material waste about 55% of the original energy.

6.1.4.2   Recombination

Charge carriers which are electrons and holes in a semiconductor-based solar cell may inadvertently recombine before they make it into the electrical circuit and contribute to the cell's current. [23, 24] Direct recombination, in which light-generated electrons and holes randomly encounter each other and recombine, is a major problem for some materials. Other materials experience indirect recombination, in which electrons or holes encounter an impurity, defect in the crystal structure, or interface or surface that makes it easier for them to recombine.

6.1.4.3   Natural Resistance

The natural resistance to electron flow in a cell decreases cell efficiency. These losses predominantly occur in three places: [25] in the bulk of the primary solar material, in the thin top layer typical of many devices, or at the interface between the cell and the electrical contacts leading to an external circuit.

6.1.4.4   Temperature

Solar cells work best at low temperatures, as determined by their material properties. All cell materials lose efficiency as the operating temperature rises. Much of the light energy shining on cells becomes heat, so it is good to either match the cell material to the operation temperature or continually cool the cell.[26]

6.1.4.5   Reflection

The efficiency of a cell can be increased by minimizing the amount of light reflected away from the cell's surface. For example, untreated silicon reflects more than 30% of incident light. Various antireflection technologies help optimize light absorption. Most commonly, a special coating is applied to the top layer of the cell.[27] A single antireflective layer will effectively reduce reflection only at one wavelength. Better results, over a wider range of wavelengths, are possible with multiple antireflective layers.

Another way to reduce reflection is to texture the top surface of the cell, which causes reflected light to strike a second surface before it can escape, thus increasing the probability of absorption. If the front surface is textured into pyramid shapes for antireflection, all incident light is bent so that it strikes the polished but otherwise untreated back surface of the cell at an angle. This texturing causes light to be reflected back and forth within the cell until it is completely absorbed.

6.1.4.6   Electrical Resistance

Larger electrical contacts can minimize electrical resistance, but covering a cell with large, opaque metallic contacts would block too much incident light. Therefore, a trade off must be made between loss due to resistance and loss due to shading effects. Typically, top-surface contacts are designed as grids, with many thin, conductive fingers spread over the surface of the cell.

However, it is difficult to produce a grid that maintains good electrical contact with a cell while also resisting deterioration caused by changes in temperature or humidity.[28, 29] Generally, the back-surface contact of a cell is simpler, often being just a layer of metal. Other designs for electrical contacts include placing everything on the back surface of the device, or, as in some thin films, depositing a thin layer of a transparent conducting oxide across the entire cell.

6.1.4.7   Determining Conversion Efficiency

Researchers measure the performance of a photovoltaic (PV) device to calculate the power the cell will produce. Current-voltage (I-V) relationships, which measure the electrical characteristics of PV devices, are depicted by I-V curves. These I-V curves are obtained by exposing the cell to a constant level of light while maintaining a constant cell temperature, varying the resistance of the load, and measuring the current that is produced.[30]

On an I-V plot, the vertical axis refers to current, and the horizontal axis refers to voltage. The actual I-V curve typically passes through two significant points:
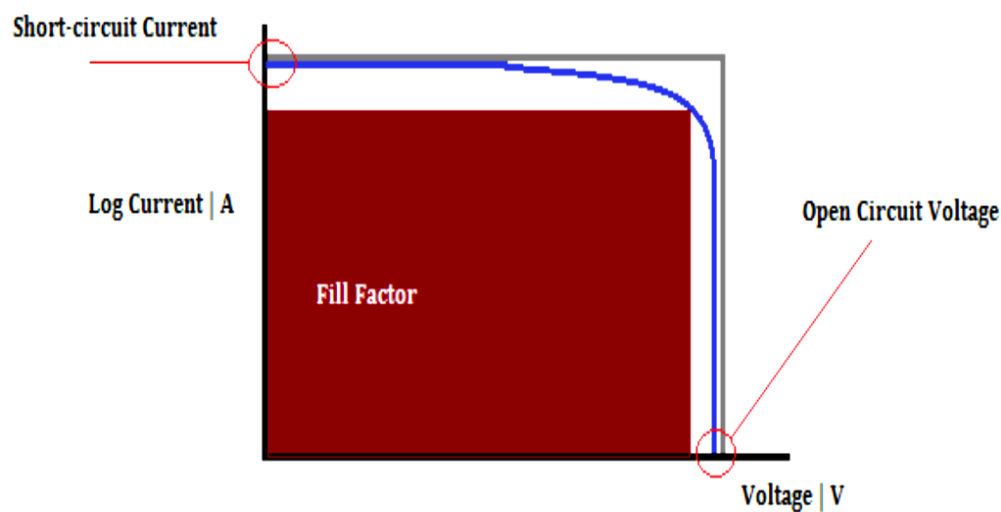
The short-circuit current (I_{sc}) is the current produced when the positive and negative terminals of the cell are short-circuited and the voltage between the terminals is zero, which corresponds to a load resistance of zero, and the open-circuit voltage (V_{oc}) is the voltage across the positive and negative terminals under open-circuit conditions when the current is zero, which corresponds to a load resistance of infinity.

The cell may be operated over a range of voltages and currents. By varying the load resistance from zero (a short circuit) to infinity (an open circuit), researchers can determine the highest efficiency as the point at which the cell delivers maximum power, power is the product of voltage times current.

Therefore, on the I-V curve, the maximum-power point (P_m) occurs where the product of current times voltage is a maximum.[31] No power is produced at the short-circuit current with no voltage or at open-circuit voltage with no current. So maximum power generated is expected to be somewhere between these two points. Maximum power is generated at only one place on the power curve, at about the

"knee" of the curve. This point represents the maximum efficiency of the solar device at converting sunlight into electricity.

6.1.5 Efficiency of Power Cells.

Figure 6.3: A voltage-current graph showing the open circuit voltage (V_{OC}) and the short circuit current (Isc). The grey line represents the ideal situation where as the blue indicated the non-ideal situation.

The efficiency of batteries and solar cells can be measured using a voltage current graph, figure 6.3. This graph is created by measuring the voltage and current produced by a cell when different resistors are placed across the cell.

This graph gives us some important information about the system under investigation. The open circuit voltage (V_{OC}) [32, 33] is the voltage recorded when no current flows. This can be thought of as the maximum current produced by the cell. In contrast the short-circuit current (I_{SC}) is the current produced by the cell when no

voltage is passed. In an ideal system the grey line in the same figure would be seen, however in real systems the blue line, or one much less square, is observed.[34]

$$P = iV$$

where P is power (W), i is current (A) and V is voltage (V)

The voltage current graph also gives us the fill factor. The fill factor is linked to the maximum power that the cell can produce and can be thought of as the largest (in terms of area) rectangle to fit under the curve.

The fill factor reflects the "squareness" of the plot, the higher this value the closer to the idea the system (the quality of the devices). The plot also allows power to be of the cell to be calculated using the equation above, knowing the power produced at different currents we are able to obtain the maximum power produced by the cell. This can be used in:

$$Fiill\ Factor = \frac{P_{max}}{I_{sc}V_{oc}} \times 100$$

To calculate the fill factor, We also use the max power to calculate the maximum power conversion of the cell, to do this the power density must be calculated, these can be seen in:

$$Max.P.D = \frac{P_{max}}{Electrode\ Area}$$

$$\% \, Power \, Conversion = \frac{Max.P.D}{Light \, Intensity} \times 100$$

The equations for max power density (W m²) were Light intensity (W m²) and Electrode area (m²).

The power conversion percentage gives us the ability to compare cells of different types and compositions. It is this factor that is of most interest too research. If a large power conversion can be produced with high efficiency then the cell may be commercially viable. It is important to note that it is not always the most important feature.

Power efficiency is important however if the maximum power output of a cell is very low then the devise might have very little use. It is also important to understand that even a high efficiency cell may be prohibitively expensive to make. Therefore a series of factors should be considered when comparing the overall efficiency of a solar cell system.[35]

6.1.6 Liquid|Liquid interfaces.

When two immiscible liquids are placed in the same vessel a liquid|liquid interface will be produced. In electrochemical systems one photoactive agent may be soluble in one solvent, say chloroform, but not soluble in a aqueous phase. It is therefore important to understand how species can react in these types of systems and how

electrons are transferred across the interface. After all if electrons cannot be transferred no current will flow and so no electrochemistry can be practised.

The liquid|liquid interface is important not only in standard photogalvanic cells but the research into this was first looked into in the field of biology. Robinson showed how plants during photosynthesis need to have electron transfer over cell membranes[36].

The idea was later expanded in great depth by looking at the effect of photo-induced electron transfer. Girault showed a novel way to produce a photocurrent using a cell with a water|1, 2-dichloroethane interface in a dye-sensitized system, his system is shown in Figure 6.4. [31]
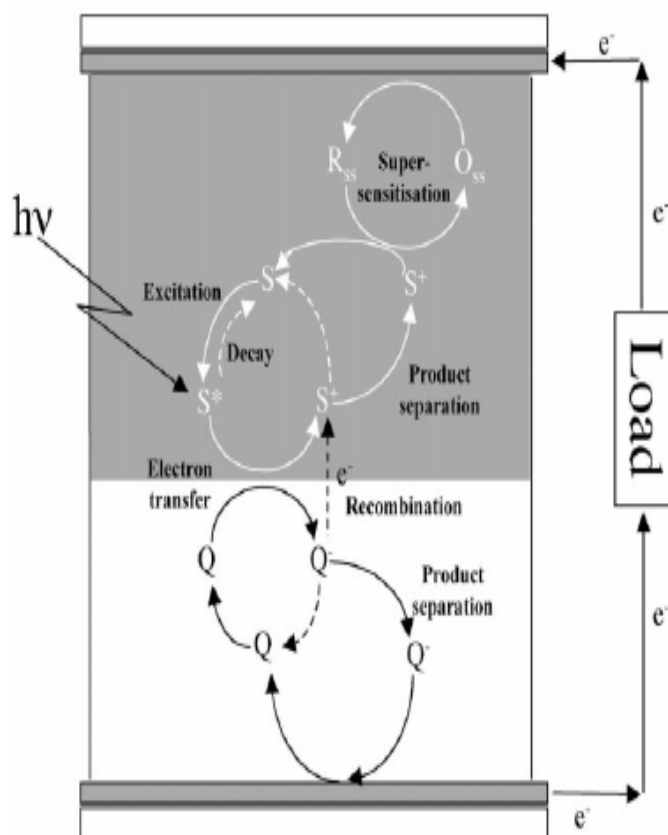
Figure 6.4: The schematic representation shown in [37]

Although the overall efficiency was low this technique proved highly practical due to its simplicity. Girault showed how the Gibbs energy for an electron transfer can be shown by Equation below [38]. He concluded that the electron transfer rate was due to two factors, $G^{o'}$ and W_r.

That being either changes in the electron transfer energy or the work term for the reagents which could be linked to the concentration at the interface. It was later Girault who explained in full the kinetics of a dye-sensitised electron transfer across an interface for both a first and second order electron transfer. [38]

$$\Delta G_{act} = \frac{\left(\lambda + \Delta G^{o'} + W_p + W_r \right)^2}{4\lambda}$$

where ΔG_{actt} is is the activation energy, λ is the reorganisation energy, $G^{o'}$ is the Gibbs energy for electron transfer and W_p and W_r are work terms for products and reagents.[39]

6.2   Aims and scopes

The aim of this work was to study and optimise a series of photogalvanic cells in order to achieve the highest power conversion as well as study the mechanism for power production within the cell. Photogalvanics and photochemistry in general are well studied; however there is still room for huge improvements and investigation within the subject. This study will try to produce a novel system and show how cells can be created using water waste.

6.3   Experimental

- All chemicals were supplied by Sigma Aldrich or Across at the highest commercially available purity. All solutions were degassed in argon or nitrogen prior to testing.

6.4   Procedure

- 10-methylphenothiazine (NMP) and Tetrabutylammonium chloride (TBAP) were weighed out a 100ml solution was then made in 50:50 Chloroform and Acetonitrile. $ZnCl_2$ was also weighed out and made to 100ml in KCl in water (0.1M). The two solutions were then degassed for five minutes in Argon.[36]

- An indium tin oxide (ITO) cell was then half filled with the NMP solution and the Aqueous $ZnCl_2$ solution was then added on top of the organic layer.

- A long wave UV lamp was then focused on the cell. The cell was irradiated with 350nm light.

- A zinc rod was then placed into the aqueous phase and connected to a voltmeter, ammeter and resistor array. A flow of argon gas was also placed over the cell.

- The cell was then tested using a series of fixed resistors as well as a variable resistor. The voltage and current were then recorded after the readings become steady.

6.5   System under investigation

With the above knowledge it was decided that a two phase, liquid|liquid photogalvanic cell should be constructed and tested. The photoactive agent 10-methylphenothiazine was suggested for study and so several experiments were planned using this Thionine like chemical. This was suggested as its likeness to Thionine as well as it never being studied for photocells before.

Tetrabutylammonium chloride (TBAP) is used will be used as a supporting electrolyte, this type of electrochemical spices is used to reduce undesirable currents within the system. Chloroform was proposed as a mediator as it would act as an artificial pollutant. Suggested for study and so several experiments were planned using this phenothiazine derivative like chemical. This was suggested as its likeness to Thionine as well as it never being studied for photocells before.

Tetrabutylammonium chloride (TBAP) is used will be used as a supporting electrolyte, this type of electrochemical spices is used to reduce undesirable currents within the system. Chloroform was proposed as a mediator as it would act as an artificial pollutant.
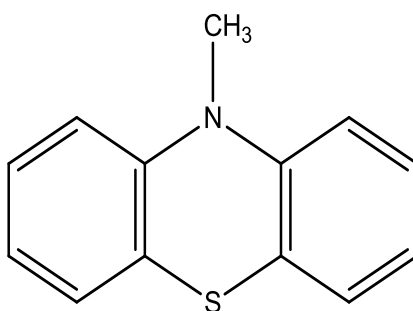
The structure of the photoactive agent 10-methylphenothiazine

6.6   Results and Discussion

Schematic Cell (A): *ITO/100Mm NMP & TBAP in 50:50 $CHCl_3$ CH_3CN/1mM $ZnCl_2$ in aq. KCl/Zn*

In the production of the above cell several key factors should be explained and considered. The two phase NMP reaction shows great promise. The factors of this cell shown below in table 6.1:

100mM NMP/ 1mM ZnCl$_2$	
Max Power	103.556 μW
Fill Factor	15.995 %
Elect. Area	0.785398 Cm^2
Max P Dens	157.3164 μW/Cm^2
Light Intensity	1.74E^{+03} μW/Cm^2
Power Conversion	9.02 %

**Table 6.1:** shows the main factors of cell (A)

Six recordings were made of this cell and using a Dixon Q test[40, 41] one way for data collected in these types of experiment to be statistically checked is with a Dixon Q test. This is used to calculate outliers within data. The Q value is defined as:

$$Q = \frac{\text{Gap}}{\text{Range}}$$

The gap is the absolute value between the suspected outlier and its closest numerical neighbour within the data set. The range is simply the range value of the data set or the largest value minus the smallest.

With Q calculated it can be compared to tabulated limit values. If the Q value calculated is smaller than the tabulated Q value then the suspected outlier is accepted with a confidence defined within the limit value.

If the value is larger than the outlier is excluded, any such outliers will be recorded in the discussion section all results could be accepted with 99% confidence. The maximum, a power conversion (PC) of 9.02% (Q= 0.11) and a maximum power of 103.5μW this cell shows huge potential for further applications. The average power conversion for these six cells is 4.8%. Graph 6. 1 shows the efficacies recorded for each run.
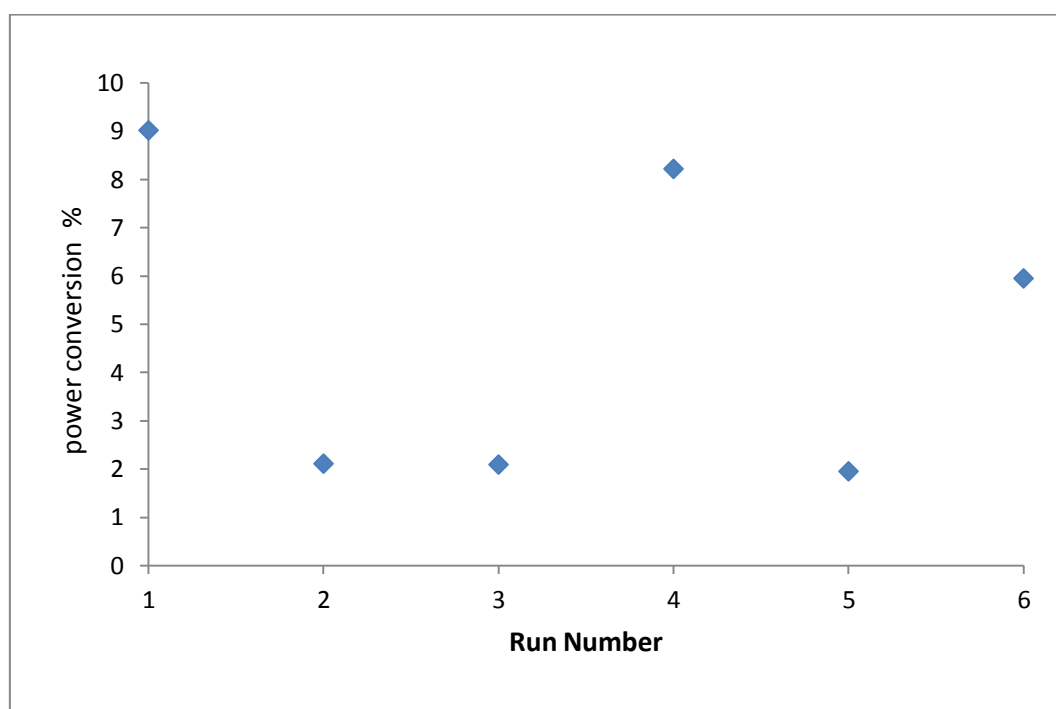
Graph 6.1: Power efficiencies of the 100mM NMP | 1mM $ZnCl_2$ in KCl Cell.

It should be noted that the unrepeatability of these results may prove problematic and so further study on optimal conditions for this cell should be conducted. The area of the zinc electrode seems to also have severe impacts on the ability for these cells to produce power consistently. Attempt should therefore be made to ensure that any further experiments try to keep the submerged electrode at the same depth. The voltage current graph produced for this reaction can be seen in Graph 6. 2:
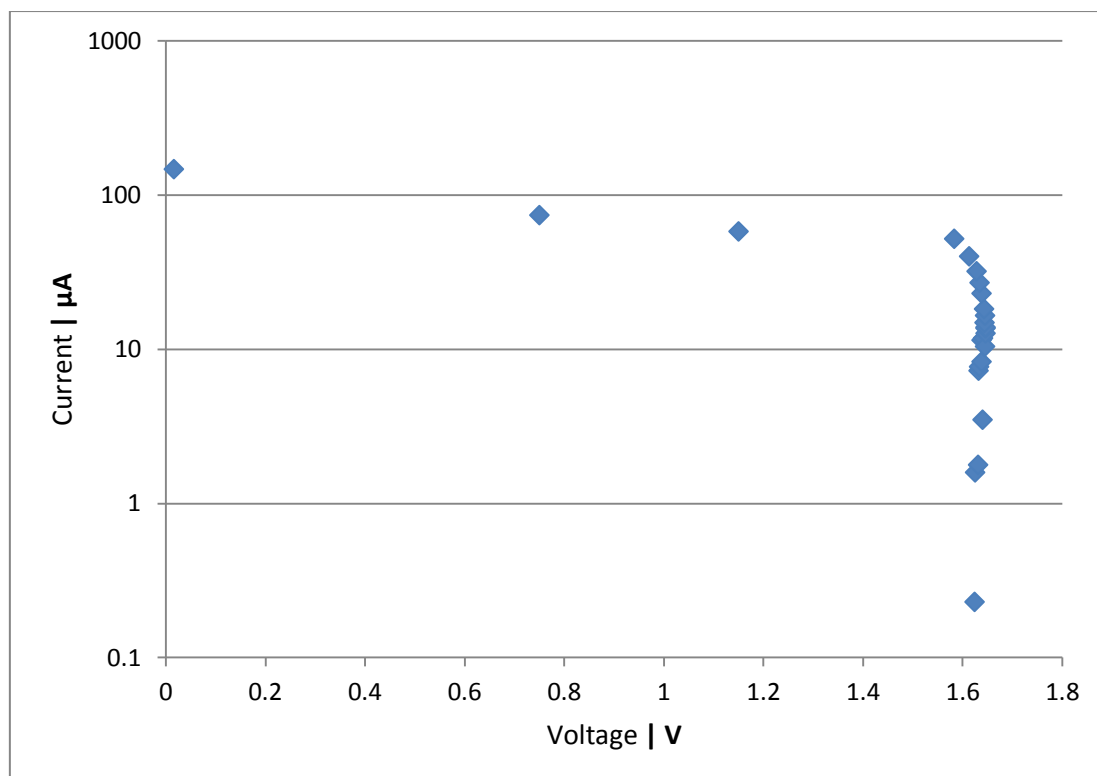
Graph 6. 2: The voltage-current plot collected during the experiment carried out

It can be seen that is very close to an ideal situation as shown in figure 6.2 with a fill factor of 15.9%.

- **The effect of electrolyte on PC**

The experiment was then conducted with $ZnSO_4$ rather that $ZnCl_2$.

Schematic Cell (B): *ITO/100Mm NMP & TBAP in 50:50 CHCl₃ CH₃CN/1mM*

__ZnSO₄__ in aq. KCl/Zn

This was to see if the effect of the metal species affected the overall cell power production. It can be seen that although this cell offers power conversions above 1% the poor unrepeatability and low power outputs made this cell unsuitable for further study.

100mM NMP/ 1mM $ZnSo_4.7H_2O$	
Max Power	44.08 µW
Fill Factor	11.25 %
Elect. Area	0.785398 Cm²
Max P Dens	56.13 µW/Cm²
Light Intensity	$1.74E^{+03}$ µW/Cm²
Power Conversion **(PC)**	3.21 %

Table 6.2: shows the highest PC that can get from cell (B).

- **The effect of solvent on PC**

The effect of solvent change was then studied. The effect of altering the ratio of chloroform and acetoilenitrile was looked at on the following system:

ITO\100Mm NMP & TBAP \10 mM $ZnCl_2$ in aq. KCl \Zn

%CH$_3$CN:CHCl$_3$	CH$_3$CN						CHCl$_3$				
	100	90:10	80:20	70:30	60:40	50:50	40:60	30:70	20:80	10:90	100
PCE %	n/a	1.83	5.62	3.09	2.63	1.85	3	4.04	3.32	1.09	1.89
P$_{max}$ μW	n/a	25.52	78.52	43.22	50.62	31.38	28.76	52.05	43.30	20.03	33.39

Table 6.3: PCE% when the concentration between CH$_3$CN: CHCl$_3$ are in the ratio.

This system was used above the more efficient system shown above as the power efficiencies produced were more constant and reproducible.
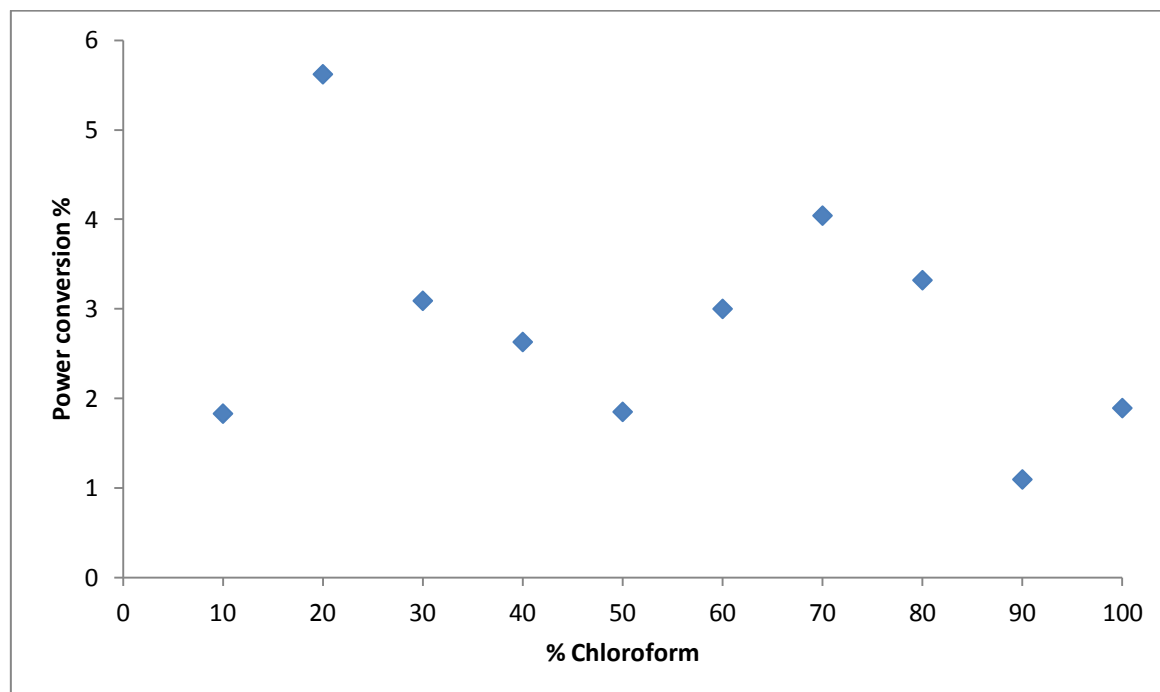
Graph6.3: The % power conversion of cells produced in the previous experiment
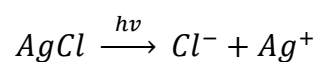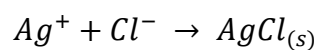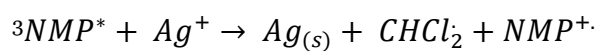
The trend seen above seems to show that power is produced even with low levels of chloroform. The peak values seem to lie at the extremes of the ratios. The cell produced with no chloroform in would cause the solid dissolved within it to precipitate out upon excitation with UV light. This effect may be due to the change in solubility of NMP and its excited triplet state however further study would be needed to demonstrate this.

This shows however that power can be produced even in a relatively low concentration of chloroform. This leads to the possibility that waste chlorinated water could be used in such devises. Further study would be needed however the hope that polluted river water or industrial waste water could be used to produce power in the future. If this is the case a large negative environmental factor, that of chlorinated waste, could be utilised and so reduce the impact such waste would have on the environment.

It could also mean that within areas of high pollution, say near industrial area within developing countries, these cells could be produced in a ad-hoc fashion from local water supplies making this technique available to the very poorest in the developed world.

- **The effect of electrode on PC**

The cells were then created using $AgNO_3$ and a silver electrode however very little power conversion was seen as well as low maximum power. The cell also forms a precipitate at the interface under high resistances. Further study of the system deduced that the following reactions must be occurring within the cell: [42]

$$^3NMP^* + CH_3Cl \rightarrow NMP^{+\cdot} + CHCl_2^- + Cl^-$$

$$^3NMP^* + Ag^+ \rightarrow Ag_{(s)} + CHCl_2^- + NMP^{+\cdot}$$

$$Ag^+ + Cl^- \rightarrow AgCl_{(s)}$$

$$AgCl \xrightarrow{hv} Cl^- + Ag^+$$

Some of the equations thought to occur with the silver cell proposed. This shows how several insoluble species would be produced upon irradiating this cell in UV light. To investigate this precipitate a TEM was conducted on a sample of the solid produced.
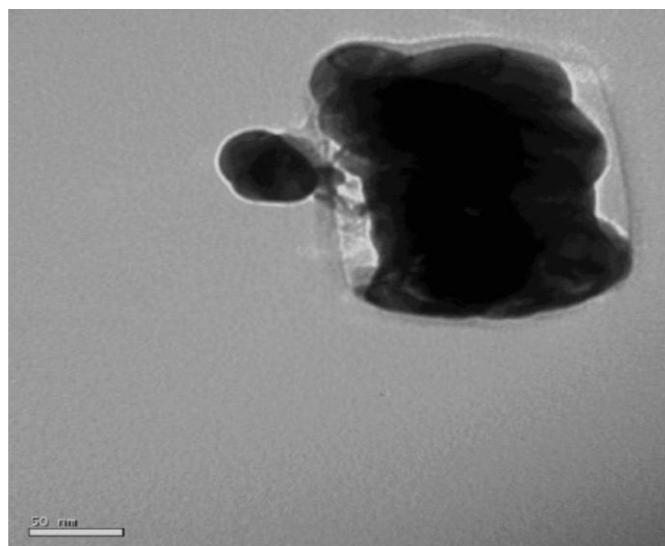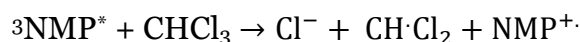

Figure 6.5: TEM image collected for silver partial seen when the system precipitated.

This image shows how the silver nanopartical can be seen surrounded by a layer of liquid. It is expected that this is the silver and chloride ions in solutions around a silver chloride nanopartical. With the above observations a reaction mechanism for the other cells containing NMP can be postulated.

- **Possible reaction mechanism**

Using the analogues reaction outlined in the introduction section of this document by Girault a reaction mechanism can be postulated.[43]

In the organic phase:

$$\text{NMP} \xrightarrow{hv} {}^1\text{NMP}^* \xrightarrow{Fast} {}^3\text{NMP}^*$$

$$^3\text{NMP}^* + \text{CHCl}_3 \rightarrow \text{Cl}^- + \text{CH}^\cdot\text{Cl}_2 + \text{NMP}^{+\cdot}$$

Where $^1\text{NMP}^*$ is the excited singlet state and $^3\text{NMP}^*$ is the excited triplet state.

At the light electrode:

$$\text{NMP}^{+\cdot} + \text{e}^- \rightarrow \text{NMP}$$

At Dark Electrode:

$$\frac{1}{2}\text{Zn} - \text{e}^- \rightarrow \frac{1}{2}\text{Zn}^{2+}$$
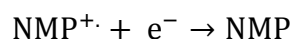
This shows how NMP can be used as the light harvester and the zinc electrode is sacrificial. The excited singlet state is the most likely to be produced on direct excitation however it will quickly relax into the less excited triplet state.

- **The effect of light harvesting agent on PC**

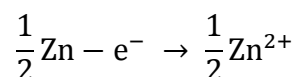The active, light harvesting, agent of the cell was then changed to see if further deviations on the system could be produced. The use of TBA, a large and conjugated species, was hoped to invoke much larger power efficiencies and absorb more of the UV light thus driving power production. As you can see above none of the cells produced a large enough max power or a significantly large power conversation to warrant further study.

100mM TBA/ 10mM $ZnCl_2$	
Max Power	14.18 µW
Fill Factor	45.54 %
Elect. Area	0.785398 Cm^2
Max P Dens	18.03 µW/Cm^2
Light Intensity	$2.94\times10^{+03}$ µW/Cm^2
Power Conversion**(PC)**	0.61 %

Table 6.4: shows the highest PC that can get from TBA as active agent.

The TBA system was also far less ideal that the previous example.
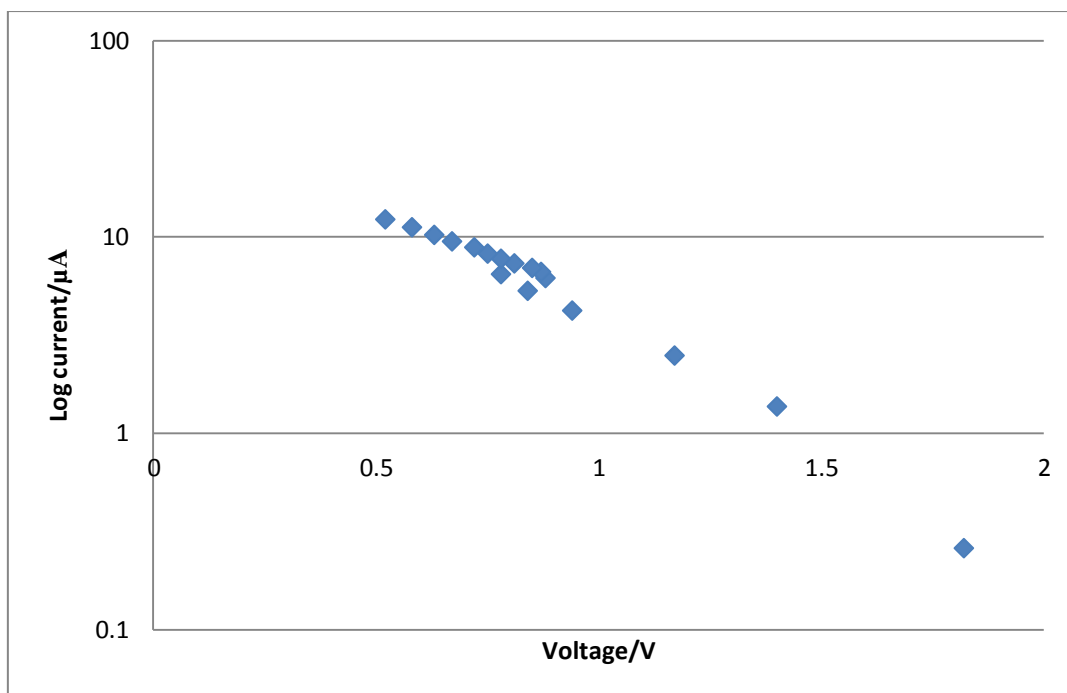
Graph 6.4: voltage-Current graph of ZnCl$_2$ 100mM TBA 10mM

Graph 6.4 shows the voltage current graph for previous experiment which recorded in a table 6.4 above as can be seen the systems behaves far from ideally. To discover why this was the case a UV experiment was conducted upon the TBA sample.
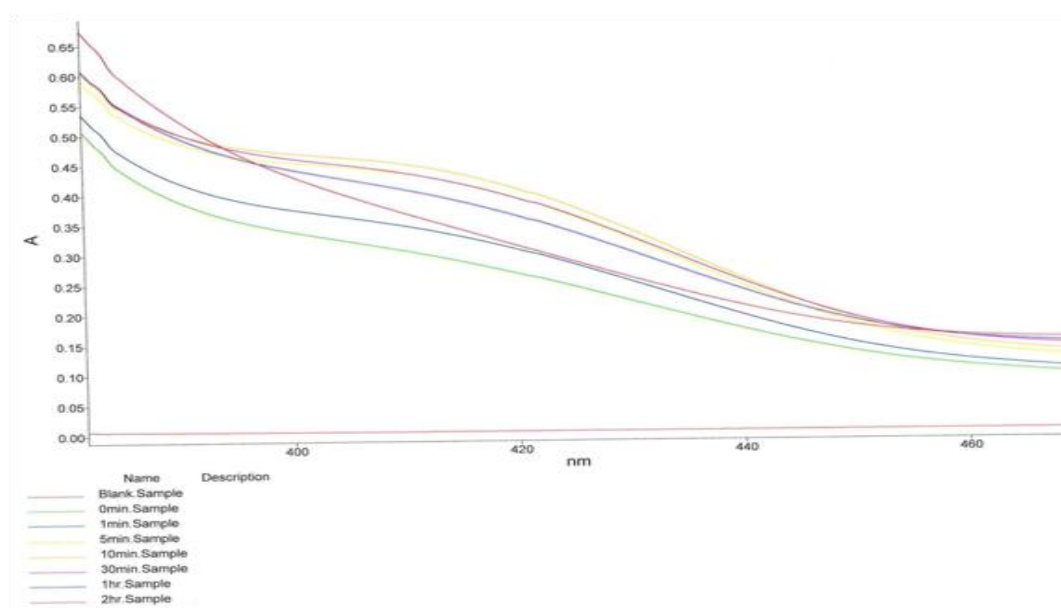
Figure 6.6: UV experiment shows the UV spectra that were collected over a period of excitation.

The spectra show how the sample did absorb the UV light in the wavelength band that the irradiation source for the cell experiment was emitting. It can be concluded that another factor rather than lack of absorption was to blame for the poor power such as solubility issues or a prolific back reaction.

The excitation of the TBA molecule should be thought of as the same as the NMP molecule; [44]

$$\text{TBA} \xrightarrow{hv} {}^{1}\text{TBA}^{*} \xrightarrow{Fast} {}^{3}\text{TBA}^{*}$$

The excited triplet state is then used the same way as the excited NMP molecule in the reaction scheme shown above.

- **The effect of changing a chlorinated organics**

The use of DCP (2, 4 Dichlorophenol) as a replacement to chloroform was suggested as it would fit the model in the above reaction if the systems using DCP were less efficient that the one utilizing chloroform.

It was expected to be less efficient[45, 46] as the dissociation reaction is step wise rather than concerted this means it will take longer for the reaction to occur and the possibility of a back reaction to occur is also present.

ITO\ NMP, DCP \ ZnCl$_2$ in aq. KCl \Zn

Despite the systems being almost identical to the above NMP cells huge differences in power efficiencies were seen. The experiment conducted with 1mM NMP and 1mM ZnCl$_2$ it is seen that a efficiency of 0.3% was produced.

1mM NMP/ 1mM ZnCl$_2$	
Max Power	2.93 µW
Fill Factor	7.64 %
Elect. Area	0.785398 Cm^2
Max P Dens	3.73 µW/Cm^2
Light Intensity	$2.94 \times 10^{+03}$ µW/Cm^2
Power Conversion**(PC)**	0.31 %

Table 6.5: shows the highest PC that can get from DCP as organochloride (artificial pulsation).

This is a factor 10 higher than any two-phase cell systems produced with DCP.

	Concentration of DCP			
	0mM DCP	1mM DCP	10mM DCP	100mM DCP
PCE in Run1	0.008%	0.004	0.007	0.021
PCE in Run2	0.0063%	0.0048	0.0058	0.023
PCE in Run3	-	0.0053	0.0092	0.021

Table 6.6 shows power conversion efficiency % in two phase system containing DCP.

The table 6.6 shows the data collected. It should be noted that one of the 100mM values was excluded after a Dixon Q test with a 99% confidence. The control runs, that contained no DCP, were of poor efficiency however improvements are seen when DCP is added above 10mM. Further study on systems containing concentrations in excess of 100mM should be conducted to see if the trend continues.

• **One phase system containing DCP and CPZ**

Table 6.7 shows the efficiencies of a single phase photogalvanic cell; in this system chlorpromazine (CPZ) was used instead of NMP as the solubility in water of NMP is

very low in aqueous solutions. [47] Chlorpromazine is very close to the structure of NMP and so a substitution was made.

ITO\ CPZ, DCP \ ZnCl$_2$ in aq.KCl\Zn

	Concentration of DCP			
	0mM DCP	1mM DCP	5mM DCP	10mM DCP
PCE in Run1	0.01%	0.017	0.013	0.05
PCE in Run2	0.022	0.018	0.015	0.058
PCE in Run3	0.024	0.02	0.13	0.077

Table 6.7: shows power conversion efficiency % in one phase system containing DCP

It can be seen that low efficacies of this system was also observed however adding DCP above 5mM would appear to have a positive effect on the cells power production and below that concentration very little, if no, change is observed.
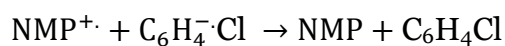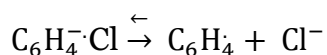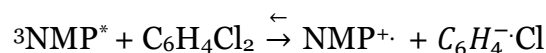
It can be seen from these experiments that DCP may give a positive effect to the ability for a NMP photogalvanic cell to produce power. Further study using this

chemical should be attempted. It should however be considered that DCP is highly poisonous unlike the other chemicals used within this type of cell.

Although the concentrations are very low it should not be underestimated the danger of using this chlorinated pollutant. Therefore any power production boosts should be viewed with the knowledge that they would have to be weighed against the environmental and health impacts associated with this chemical.

- **Mechanism for the cells containing DCP**

The DCP containing cells above can be considered the same as the other proposed mechanism[48] however the dissociation of DCP is step wise rather than concerted:

$$\text{NMP} \xrightarrow{hv} {}^{1}\text{NMP}^{*} \xrightarrow{Fast} {}^{3}\text{NMP}^{*}$$

$$^{3}\text{NMP}^{*} + \text{C}_6\text{H}_4\text{Cl}_2 \xrightarrow{\leftarrow} \text{NMP}^{+\cdot} + C_6H_4^{-}\cdot\text{Cl}$$

$$\text{C}_6\text{H}_4^{-}\cdot\text{Cl} \xrightarrow{\leftarrow} \text{C}_6\text{H}_4 + \text{Cl}^{-}$$

$$\text{NMP}^{+\cdot} + \text{C}_6\text{H}_4^{-}\cdot\text{Cl} \rightarrow \text{NMP} + \text{C}_6\text{H}_4\text{Cl}$$

6.7 Conclusion

This work has demonstrated that a photogalvanic cell can be constructed that can have high conversion rates, $\approx$ 9 %. Although the reaction mechanisms given cannot be fully verified it does seem to fit the empirical evidence. Namely that the stepwise reaction is far less efficient than the concerted, faster reaction.

The ability for power to be produced even when very little chloroform is present is a property that makes this type of cell of interest. As stated above the ability to run of waster industrial flow is highly possible, the high concentration of zinc in waste water is also a major factor which may make cells made primarily of waste waster a reality.

The poor efficiency of TBA still requires some explanation. This may be due to the size of the molecule and so the ability to move around the system that limits its efficacies. The back reaction may also prove to be prolific. It may be advantages to try this cell with a surfactant molecule present and above the Critical Micelle Concentration (CMC). This would reduce the rate of the back reaction if it is under diffusion control. Further cells containing different metal ions were discarded due to poor efficacies. These include silver and $ZnSO_4$. Although these devise may prove efficient after further work the time constraints of this project impeded further study.

The silver cell did however aid the production of a mechanism for the energy production seen the cells. This cell may also prove useful in the production of silver nanoparticals as electrochemical method for synthesis.

Further studies should focus on improving the NMP cell and should be aimed in two main areas. Firstly instead of artificial pollutants and used here waste water samples should be used. This may include river water from the local vicinity or targeted sampling in places were high pollution is known to occur. The second direction of further study should focus on the effect other variables have on this system, as mention in the introduction, temperature, pH and surfactant effects should all be looked at to see if the high power conversion can be increased.

References for Chapter 6

1. R. Parsons, in A. J. Bard, R. Parsons, J. Jordan (eds.), Standard Potentials in Aqueous Solution, IUPAC, Marcel Dekker, Inc., New York, 1985, p.13.

2. M. D. Archer, *J. Appl. Electrochem.*, 1975, **5**, 17.

3. C.-T. Lin, N. Sutin, *J. Phys. Chem.*, 1976, **80**, 97

4. W. J. Albery, M. D. Archer, *Electrochim. Acta*, 1976, **21**, 1155.

5. W. J. Albery, M. D. Archer, *J. Electrochem. Soc.*, 1977, **124**, 688.

6. W. J. Albery, M. D. Archer, *Nature*, 1977, **270**, 399

7. W. J. Albery, M. D. Archer, *J. Electroanal. Chem.*, 1978, **86**, 1.

8. W. J. Albery, M. D. Archer, *J. Electroanal. Chem.*, 1978, **86**, 19.

9. W. J. Albery, A. W. Foulds, *J. Photochem.*, 1979, **10**, 41.

10. M. D. Archer, M. I. C. Ferreira, in J. Connoly (ed.), *Photochemical Conversion and Storage of Solar Energy*, 1980, Academic Press, San Diego, p.201.

11. M. D. Archer, *Specialist Periodical Reports in Photochemistry*, 1995, volume 6, The Chemical Society, London, p.739.

12. W. D. K. Clark, J. A. Eckert, *Solar Energy*, 1975, **17**, 147.

13. D. E. Hall, J. A. Eckert, N. N. Lichtin, P. D. Wildes, *J. Electrochem. Soc.*, 1976, **123**, 1705.

14. P. D. Wildes, N. N. Lichtin, *J. Am. Chem. Soc.*, 1978, **100**, 6568.

15. J. C. M. Brokken-Zijp, M. S. de Groot, *Chem. Phys. Letts.*, 1980, **76**, 1.

16. J. C. M. Brokken-Zijp, M. S. de Groot, P. A. J. M. Hendriks, *Chem. Phys. Letts.*, 1981, **81**, 129.

17. T. J. Meyer, *Prog. Inorg. Chem.*, 1983, **30**, 389; (b) R. Foster, *Organic Charge-Transfer Complexes*, Academic Press, New York, 1973.

18. M. Tsionsky, A. J. Bard, M. V. Mirkin, *J. Phys. Chem.*, 1996, **100**, 17881.

19. M. Tsionsky, A. J. Bard, M. V. Mirkin, *J. Am. Chem. Soc.*, 1997, **119**, 10785.

20. A. L. Barker, P. R. Unwin, S. Amemiya, J. Zhou, A. J. Bard, *J. Phys. Chem. B*, 1999, **103**, 7260.

21. F. Li, A. L. Whitworth, P. R. Unwin, *J. Electroanal. Chem.*, 2007, **602**, 70.

22. K. Becquerel, *C. R. Acad. Sci.,* 1839, 9, 14.

23. E. Rabinowitch, *J.Chem.Phys.*, 1940, 8, 551-559.

24. R.C. Srivastava, R. Srinivasan, P.R. Marwadi, S.B. Bhise, S.S. *Mathur, Current Science*, 1982, 51, 1015-1017.

25. W. J. Albery, *Accounts of Chemical Research*, 1982, 15, 142-148.

26. C. Creutz, N. Sutin, J. *Am. Chem. Soc.,* 1976, 98, 6384-6385.

27. W. J. Albery, P. N. Bartlett, J. P. Davies, A. W. Foulds, *Faraday Discussions*, 1980, 70, 341-357.

28. S. Lee, A. Mills, *J.Fluorescence*, 2003, 13, 375-377.

29. C. Lal, *J. Power Sources*, 2007, 164, 926-930.

30. E. Rabinowitch, *J. Chem.Phys.,* 1940, 8, 560-566.

31. K.M. Gangotri, V. Ibdora, *Solar Energy*, 2010, 84, 271-276.

32. K.K. Rohatgi-Mukherjee, M. Bagchi, B.B. Bhowmik, *Electrochimica Acta*, 1983, 28, 293-300.

33. S. Dube, S.L. Sharma, S.C. Ameta, *Energy Convers. Mgmt*, 1997, 38, 101-106.

34. R.C. Meena, G. Singh, N. Tyagi, M. Kumari, *J. Chem. Sci.*, 2004, 116, 179-184.

35. E. Groenen, M.S. De Groot, R. De Ruiter, N. De Wit, *J.of Phys. Chem.,* 1984, 88, 1449-1454.

36. A. Mackay, N.S. Dixit, *J.Phys. Chem.,* 1982, 88, 4593-4598.

37. K.M. Gangotri, P. Gangotri, *Arab. J. Sci. Engi.,* 2010, 35, 19-28.

38. Y. Chen, C. Jiang, H. Ma, J. Yu, Y. Liu, *Appl. Phys. Lett.,* 2011, 98, 232116.

39. J.D. Wadhawan, J.E. Halls, *Energy Environ. Sci.,* 2012, 5, 6541-6551.

40. A.A. Kamshilin, A.I. Grachev, S.S. Golik, R.V. Romashko, Y.N. Kulchin, *Appl Phys B*, 2012, 106, 899-903.

41. Y.H. Chem, X.Y. Peng, Q. Zhang, B. Shen, J.R. Shi, C.M. Yin, X.W. He, F.J. Xu, X.Q. Wang, N. Tang, C.Y. Jiand, Y.H. Chen, *Phy. Rev. B*, 2011, 84, 075341.

42. C.W. Wayne, R.P. Wayne, Photochemistry, 1996, New York: Oxford University Press.

43. M.D. Archer, *J. Appl. Electrochem.,* 1975, 5, 17-38.

44. W. Bott, *Curr. Sep.*, 1998, 17, 87-91.

45. R.G. Comptom, G.H.W. Sanders, *Electrode Potentials*, 1996, New York: Oxford University Press.

46. R.A. Marcus, *J. Phys. Chem.,* 1963, 67, 853-857.

47. J.N. Robinson, D.J. Cole-Hamilton, *Chem. Soc. Rev.*, 1991, 20, 49-94.

48. H.H. Girault, D.J. Ferm n, H.D. Duong, Z. Ding, P.F. Brevet, *Electrochem. Commun.*, 1999, 1, 29-32.

Chapter 7- Wastewater as a Photoelectrochemical Fuel Source:

Light-to-Electrical Energy Conversion with Organochloride Remediation

---

7.1   Aim and Scope

Polluted water such as industrial effluent, minewater or landfill leachate is highly diversified and complex in its composition, but generally contains a variety of environmentally toxic chlorinated organic (such as 2, 4-dichlorophenol, DCP) and toxic heavy metals ions (such as Zn^{2+}).[1, 2] Of these, the organochlorine derivatives, with their high phytotoxicity and zootoxicity are considered as "priority pollutants",[3] with concentrations on the order of ca 3 mM.[4]

These two types of pollutant are difficult to detoxify simultaneously through electrochemical routes, since metal ion removal requires its reduction, and dehalogenation of organic halides necessitates reductive conditions, so that carbon-halogen bond rupture occurs either in concert with electron transfer, or from an intermediate state following electron transfer.[5]

Accordingly, remediation strategies of these two types of species generally involve the electrolytic removal of the toxic heavy metal ions,[4] with after dehalogenation of the organohalide, either through the use of microbes,[6] or through photolysis.[7] Such attractive environmental clean-up processes however, only consume energy;[8] there is no route by which energy may be generated during the detoxification process.

Thus, in an attempt to encourage these processes to become more sustainable. In this work, we employ an artificial polluted water system to illustrate, in a proof-of-principle, that light energy may be capitalised to remediate DCP, exploiting the presence of Zn^{2+} whilst concurrently generating electricity within a photogalvanic (PG) cell.

7.2   Experimental

• All chemical reagents were purchased from Sigma-Aldrich or Acros in the purest commercially-available grade, and used as received.

• Water, with a resistivity of not less than 18 MΩ cm, was taken from an Elgastat system (Vivendi, Bucks., UK).

• Zn (dark electrodes) (Alfa Aesar) were cleaned and polished using wetted carboundum paper (P1200 grade, Presi, France) and stored under degassed, distilled water prior to their deployment.

• ITO (illuminated electrodes) were rinsed with both ethanol and water, and dried immediately prior to deployment.

• Cells were constructed by pouring the electrolyte into a cavity of known dimensions (4.0 x 3.5 x 0.4 cm for experiments in homogeneous solutions, or 2.0 x 2.0 x 0.3 cm for experiments involving immobilised reagents) that had been prepared by gluing a Teflon separator onto the zinc (dark) electrode, and then fixing

the ITO (illuminated) electrode in place using a low melting depilatory wax. It was found necessary to overfill the cavity slightly prior to placing the ITO electrode.

- Electrical connection to both electrodes was achieved through the use of copper tape with conductive adhesive underside. Electrochemical experiments were undertaken at 20 ± 2 °C (for cells involving only homogeneous solutions).

- Open circuit voltages were recorded using a potentiostat/galvanostat (μAutolab Type III, Eco Chemie); current-voltage characteristics of the device under illumination were recorded manually.

- Readings were taken after 3 s of illumination. The light intensity was monitored in each experiment using a radiometer calibrated at 365 nm (UVP).

7.3   Results and Discussion

Photogalvanic devices function through a light-induced change in the concentration *ratio* of the oxidised and reduced forms of a species in one half of a galvanic cell (battery), [9] whilst such systems are rarely greater than 0.5% efficient in light-to-electrical power conversion.

We have demonstrated[10] that the use of both a sacrificial anode and a structured, nano-restricted liquid medium can assist in improving the conversion efficiency to ~2%. To illustrate this, noting that chlorpromazine (CPZ) is thought to form
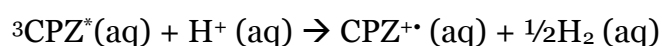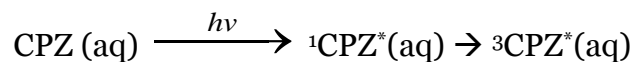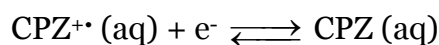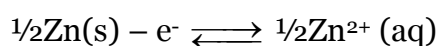
staircase-like stack micelles in aqueous solution, [11] we studied the following cell, using argon.

Zn | Zn²⁺ (aq, c=3.1 mM), CPZ (aq, c=1.8 mM), pH 5.8 | ITO (Cell A)

where ITO represents a transparent tin-oxide-doped-indium-oxide electrode. Illumination of the latter with violet light (λ=365 nm, of intensity, I_o=172 µW cm⁻²) gave rise to increases in the cell voltage of the illuminated electrode *versus* the dark electrode (sacrificial zinc anode) at open circuit (Figure 7.1).
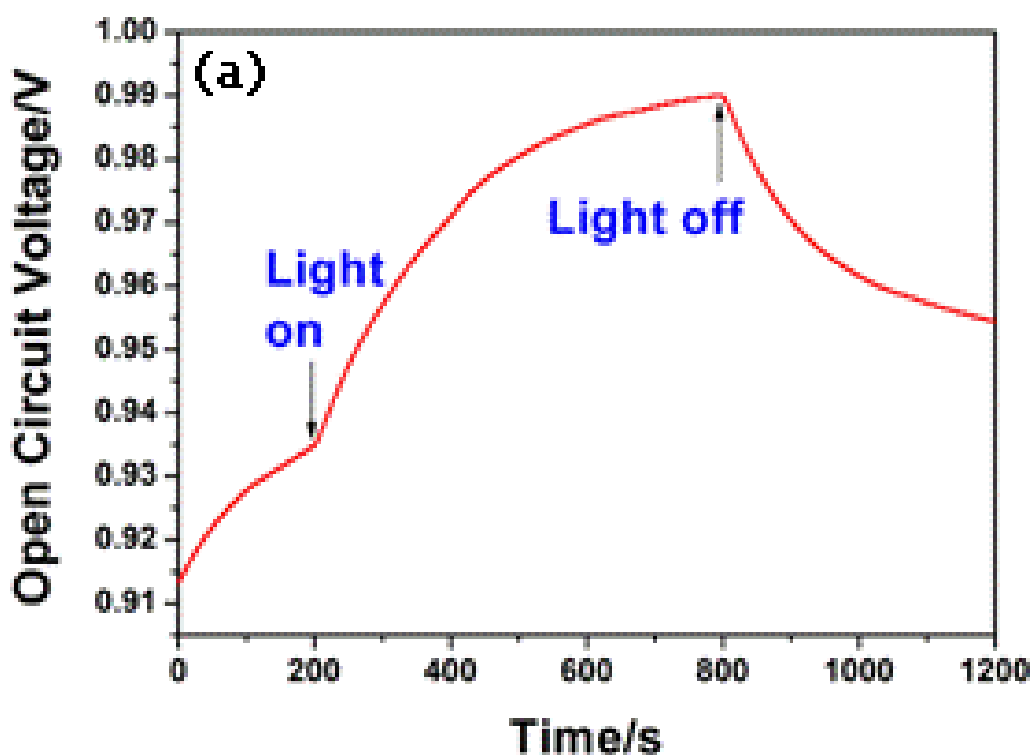
Figure 7.1: Variation of the open circuit voltage of Cell A in the presence of chopped light.

Possible reaction mechanism

In solution:

$$\text{CPZ (aq)} \xrightarrow{h\nu} {}^{1}\text{CPZ}^{*}\text{(aq)} \rightarrow {}^{3}\text{CPZ}^{*}\text{(aq)}$$

$${}^{3}\text{CPZ}^{*}\text{(aq)} + \text{H}^{+}\text{(aq)} \rightarrow \text{CPZ}^{+\bullet}\text{(aq)} + \tfrac{1}{2}\text{H}_{2}\text{(aq)}$$

At the light electrode:

$$\text{CPZ}^{+\bullet}\text{(aq)} + \text{e}^{-} \rightleftharpoons \text{CPZ (aq)}$$

At the dark electrode:

$$\tfrac{1}{2}\text{Zn(s)} - \text{e}^{-} \rightleftharpoons \tfrac{1}{2}\text{Zn}^{2+}\text{(aq)}$$

Photocurrent-photovoltage characteristics for this cell, recorded at steady-state under a variable load, are reported in Figure 7.2, from which it is seen that a maximum power (P_m) conversion efficiency (η) defined as:

$$\eta = \frac{P_m}{I_0 S} \times 100$$

Where S is the area of the parallel-plate electrodes, of 1.3% is obtained, with a fill factor (F) defined as:

$$FF = \frac{P_m}{V_{oc}\, j_{sc}\, S} \times 100$$

In which V_{oc} is the open circuit voltage and j_{sc} is the current density at short circuit of 7.2%, suggesting a low quality light-to-electrical energy conversion device.
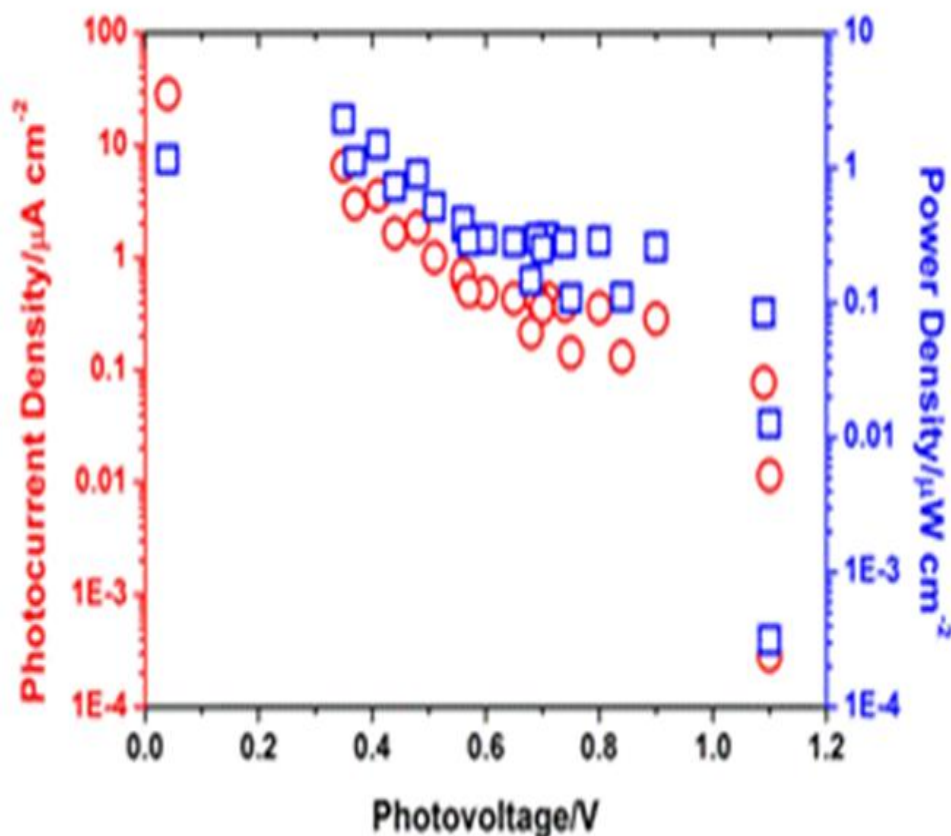
Figure 7.2: illuminated current-voltage characteristics of Cell A (red circles correspond to current density; blue squares represent power density).

Noting that *N*-substituted phenothiazines in the triplet excited state are powerful reducing agents, capable of reducing organochlorides,[11] to adapt this engineered approach for light-induced reduction of DCP in *mimetic* polluted waters, *without* first having to add in a soluble photoactive catalyst.

The ITO electrode was modified with an *N*-substituted phenothiazine, first through covalent attachment of *p*-nitrobenzene, followed by its reduction to the primary amine in acid, [12] with subsequent reaction with phenothiazine-10-carbonyl chloride under Schotten-Baumann conditions (Scheme 1).
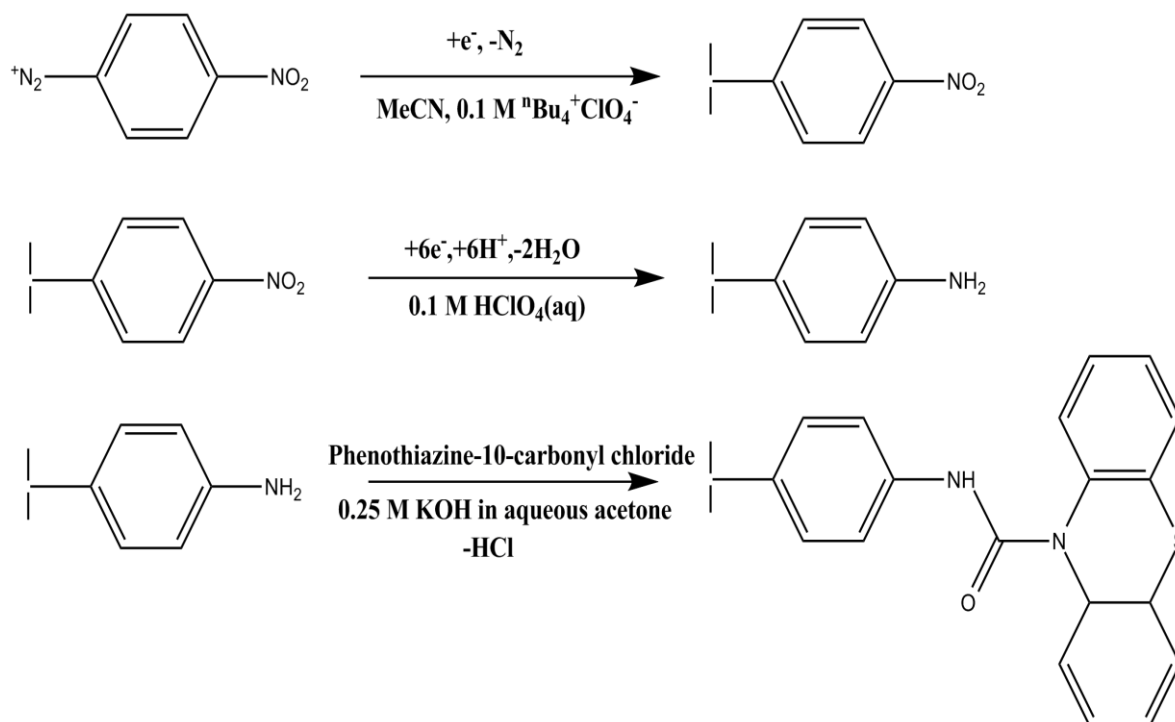

Scheme 1: Preparation of the PZ | ITO electrode.

The immobilised phenothiazine (PZ | ITO) was interrogated voltammetrically in aqueous 0.1 M KCl (pH 6.7). The solution was not buffered, owing to the known interaction of buffer anions with *N*-substituted phenothiazine radical cations:[13] McCreery *et al.*[13b,c] have noted that between pH 2 and 7, the cation radical of chlorpromazine[13b] and related derivatives[13c] undergo hydrolysis with direct nucleophilic attack by a buffer anion (*inter alia* citrate, succinate, maleate, phosphate, acetate, glycine) to form the neutral parent and the sulfoxide, in a non-

disproportionation scheme that is second-order in the cation radical, first-order in buffer anion, and inverse first-order in proton concentrations.

Voltammetric oxidation of the immobilised phenothiazine afforded two one-electron waves, as anticipated, with the first being electrochemically-reversible ($E_p{}^{Ox}$ = +0.38 V *vs*. SCE, $E_p{}^{Red}$ = +0.30 V *vs*. SCE, recorded at 0.1 V s^{-1}), and the second unstable owing to follow-on chemistry.[13]
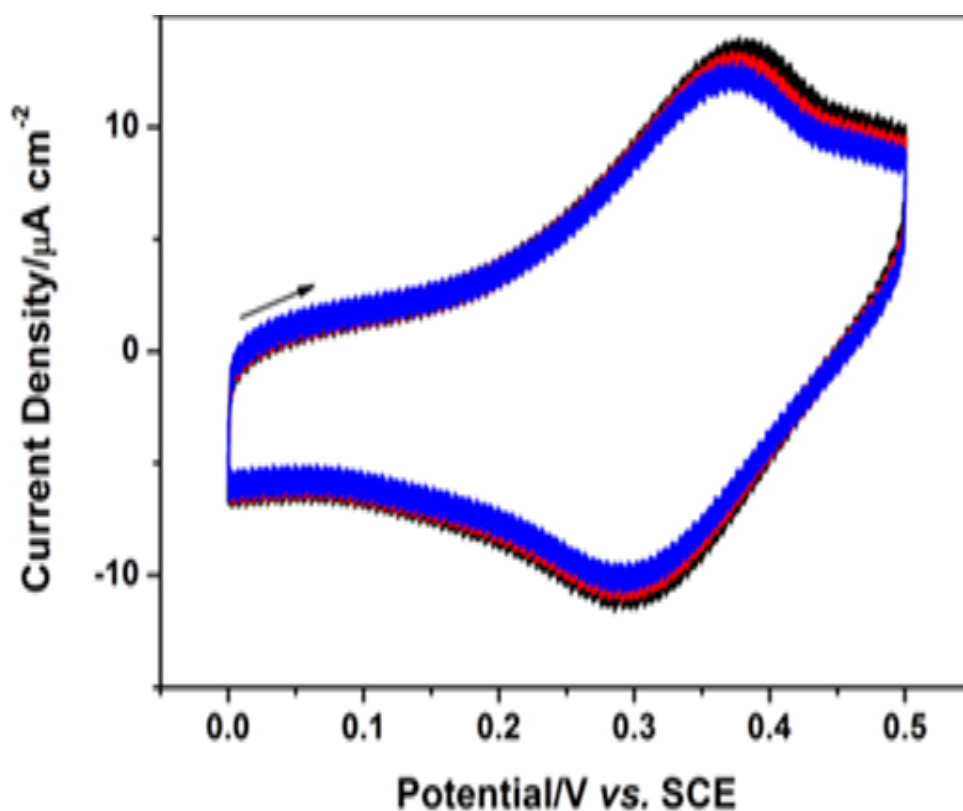
Figure 7.3: Cyclic voltammograms (three scans, 0.1 V s^{-1}) for the oxidation of PZ | ITO in 0.1 M aqueous KCl. The arrow indicates the direction of the initial sweep. SCE=saturated calomel electrode.

Limiting the voltammetry to the formation of the cation radical, integration of the current-potential curves suggests a surface coverage of 3.2×10^{-10} mol cm^{-2}, consistent with the presence of a monolayer of PZ | ITO. Accordingly, the modified electrode was employed within two types of PG cell, with experiments undertaken at 14 ± 2 ^oC, so as to mimic freshwater temperature.[14] Note, all solutions contained 0.1 M potassium chloride as electrolyte, and were purposely not degassed so as to ensure conformity of our model system with real ones.

First, control experiments were undertaken in the cell:

Zn | Zn^{2+} (aq,c=11.0 mM),alginic acid(aq,saturated),pH 2.4 | PZ | ITO

(Cell B)

Where alginic acid derived from brown algae (pK$_a$ reported[15,16] as being between 1.5 and 3.5) was used to :

(1) Foul the solution with biological-type material, in order to mimic a real sample,[14]

(2) Buffer the aqueous phase close to the pK$_a$ of the exicited state of DCP.

 The latter was estimated as being 2.3 at 25 ^oC, through a Förster cycle (noting that the pK$_a$ of ground state DCP is[17] 7.9) under the assumption that the vibrational spacings of the excited state and conjugate pair are commensurate, and that the energy distribution between the vibrational levels are identical, so that absorption

maxima in the UV (λ_{max}=284 nm for DCP in aqueous solution[18] and 307 nm for the phenoxide in aqueous alkali[19]) can be used to determine the relative positions of the energy levels.

The open circuit voltage of the cell changed only by a few millivolts in the presence of chopped light at 365 nm; no changes were observed when an unmodified ITO electrode was employed in the above cell.
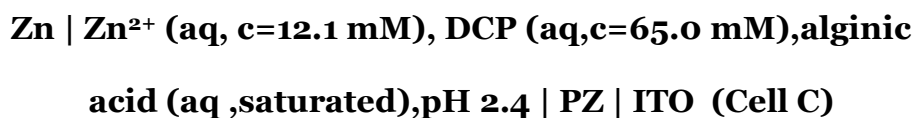
Photocurrent-photovoltage characteristics under load are given in Figure 7.4 ; these data suggest that the maximum power conversion efficiency is η=1.4% (FF=4.4%), with the slightly higher efficiency compared with the case of CPZ likely resulting from the spatial separation of the immobilised photoactive material in the oxidised form from the aqueous solution, and the higher proton concentration in the solution.

Note that in these experiments, maximum power conversion occurs close to the short-circuiting of the cell.
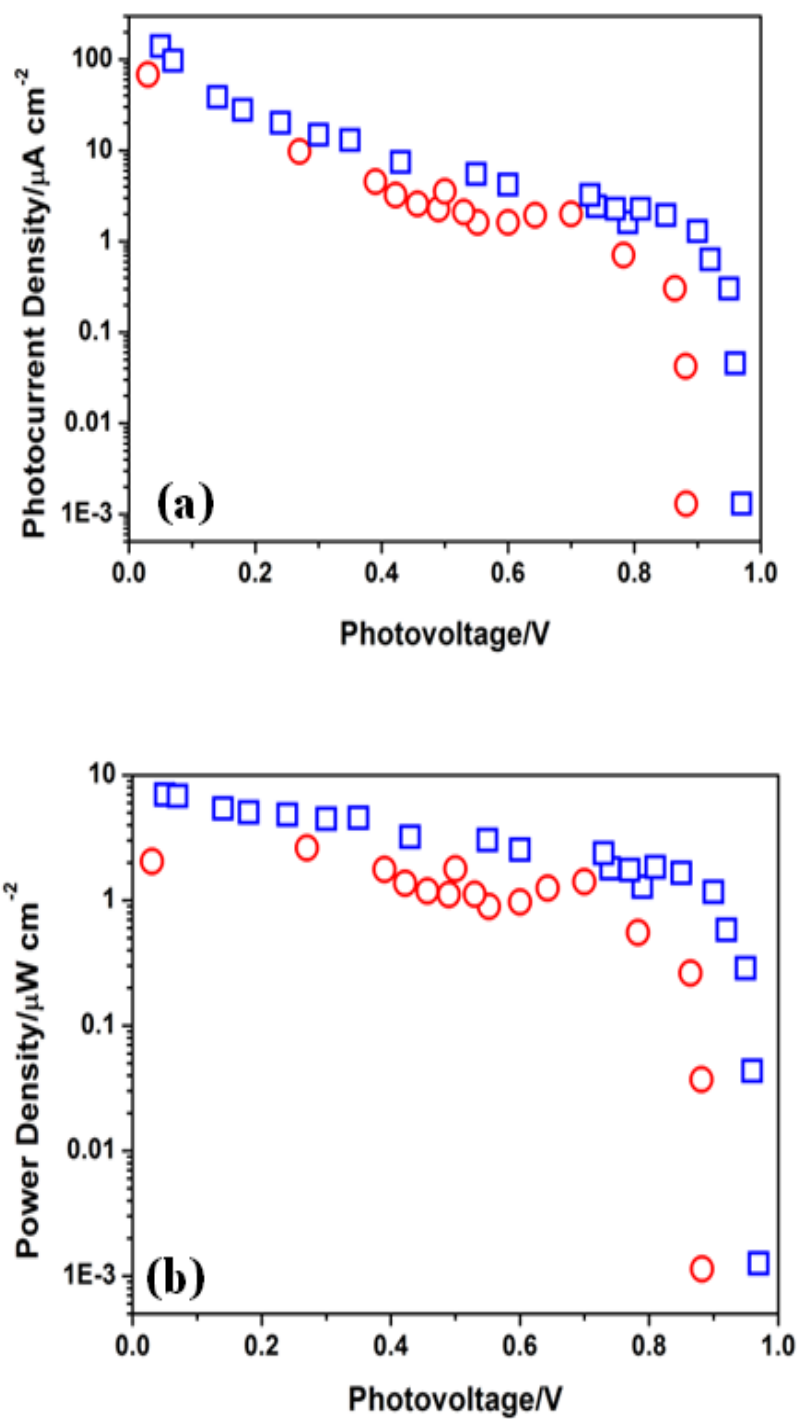
Figure 7.4: Photocurrent-photovoltage (a) and power-photovoltage (b) characteristics of Cells B (red circles) and C (blue squares). λ=365 nm; I_o=188 μW cm^{-2} (cell B) or 184 μW cm^{-2} (cell C).

Next, experiments were undertaken in the cell:

Zn | Zn²⁺ (aq, c=12.1 mM), DCP (aq,c=65.0 mM),alginic

acid (aq ,saturated),pH 2.4 | PZ | ITO (Cell C)

where the concentration of DCP was intentionally made higher than the aqueous oxygen concentration, and kept to a massive excess compared with real levels (~3 mM), since the cell is static, and not flowing. This time, greater changes (~10 mV) in open circuit voltage were observed upon illumination with 365 nm light, which translated to maximum power conversion of η=3.9% (FF=7.4%), again occurring close to the cell at short circuit (Figure 7.3). Again, no changes in open circuit voltage were observed in control experiments using an unmodified ITO electrode.

The larger changes in photovoltage and the greater current densities observed for this cell compared with that in the absence of DCP are attributed to the reductive dechlorination of DCP by photo-excited ^{3}PZ* | ITO, since DCP has a higher concentration than both protons and O_2 within this cell.

In general, chlorophenol reductions occur through a stepwise dissociative electron transfer pathway, involving C-Cl bond rupture during the transfer of up to two-electrons per molecule, [19] in a manner similar to the dechlorination of chloronitrobenzenes, [20] with the production of chloride ions.[7, 19] We note that the efficiency of the photocatalytic process could be artificially lower in the cell examined owing to the blocking of UV light by the very high concentration of 24DCP used (65.0 mM).

7.4   Conclusions

This work has demonstrated that photogalvanic cells, operating under violet light, can be used to generate electrical energy through the photoelectrochemical reduction of 24DCP in the presence of Zn^{2+}. We estimate that the electrical energy consumed by powering the light source (~80 J) is six orders of magnitude larger than the electrical energy produced by the system (~70 µJ), indicating that there is much work required to make this system truly sustainable.

Nevertheless, whilst the exact operating mechanism has not been established, it is noteworthy that if the photomineralisation process were to occur through a concerted (rather than stepwise) dissociative electron transfer process,[5] there is no possibility for recombinative relaxation occurring, translating into higher light-to-electrical power conversion efficiencies that those reported in this work.

Moreover, the use of flowing rather than static systems may allow for more efficient separation of immobilised cation radical and the reduced chlorinated organic through convective-diffusion compared with diffusion-only (where deactivation in the case of the stepwise dissociation depends on the rate of surface transport cf. C-Cl bond cleavage kinetics). Although this system can remediate the chlorophenol, it does so at the expense of increasing the concentration of zinc ions; efficient electricity generation in this step may, attractively, be capitalised to reduce those metal ions in a sustainable second step, provided the light-induced reaction is able to function using lower energy photons – less than 5% of sunlight contains a violet light component.

References for Chapter 7

1. G. Varank, A. Demir, S. Top, E. Sekman, E. Akkaya, K. Yetilmezsoy, M. S. Bilgili, *Sci. Tot. Environ,* 409 (2011**)** 3183.

2. T. Pandiyan, O.M. Rivas, J.O. Martínez, G.B. Amezcua, M.A.Martínez-Carrillo, *J. Photochem. Photobiol. A*, 146 (2002**)** 149.

3. *Water Resources, England and Wales – The Surface Waters (Danger Substances)*, Statutory Instruments 1998/289, 1998.

4. A.J. Chaudhary, S.M. Grimes, *Chemosphere*, 72 (2008) 1636.

5. C. Costentin, M. Robert, J.-M. Savéant, *Chem. Phys.*, 324 (2006) 40.

6. J.F. Ferguson, J.M.H. Pietari, *Environ. Poll.*, 107 (2000) 209.

7. T.J. Kemp, P.R. Unwin, L. Vincze, *J. Chem. Soc., Faraday Trans.*, 91 (1995) 3893.

8. F.C. Walsh, *Pure Appl. Chem.*, 73 (2001) 1819.

9. W.J. Albery, M.D. Archer, *Nature*, 270 (1977) 399.

10. J.E. Halls, J.D. Wadhawan, *Energy Environ. Sci.* 5 (2012) 6541.

11. P.K. Dea, H. Keyzer in F. Gutmann, H. Keyzer (eds.), *Modern Bioelectrochemistry*, Plenum Press, New York, 1986, p.481.

12. Y. Dou, S.J. Haswell, J. Greenman, J. Wadhawan, *Electroanalysis*, 24 (2012) 264.

13. (a) G. Dryhurst, K.M. Kadish, F. Scheller, R. Renneberg, *Biological Electrochemistry*, volume 1, Academic Press, New York, 1982, p.180; (b) H.Y. Cheng, P.H. Sackett, R.L. McCreery, *J. Am. Chem. Soc.*, 100 (1978) 962; (c) H.Y. Cheng, P.H. Sackett, R.L. McCreery, *J. Med. Chem.* 21 (1978) 948.

14. M. Rogerson, H.M. Pedley, J.D. Wadhawan, R. Middleton, *Geochim. Cosmochim. Acta*, 72 (2008) 4976.

15. J. Pavez, J.F. Silva, F. Melo, *J. Cryst. Growth*, 282 (2005) 438.

16. T.D. Perry IV, R.T. Cygan, R. Mitchell, *Geochim.*, 70 (2006) 3508.

17. G. Kortüm, W. Vogel, K. Andrussow, *Dissociation Constants of Organic Acids in Aqueous Solution*, Butterworths, London, 1961.

18. Q. Lu, J. Yu, J. Gao, *J. Hazard. Mater. B*, 136 (2006) 526.

19. T.J. Davies, J.D. Wadhawan, R.G. Compton, *Photochem. Photobiol. Sci.*, 1 (2002) 902.

20. G. Macfie, J. Wadhawan, R.G. Compton, *J. Electroanal. Chem.*, 510 (2001) 120.

Chapter 8 – Conclusion

To sum up, the range of electrochemical studies presented has shown that the electrochemical chemistry is a useful tool in environmental applications, allowing mechanistic studies, bond cleavage and bond forming dynamics together with mass transport theory to be investigated.

The lyotropic liquid crystals provide an attractive and synthetically-inexpensive, three-dimensional nanostructured framework for electron transport processes. These have been seen to be remarkably affected by the type of ionic electrolyte doping and the hydrophobicity of the redox solute, as well as orientation of the liquid nanosystem, allowing for the development of unusual routes for material transport over distance; a unique route is through the partitioning of species across pseudophases with cross-pseudophase electron transfer.

The study on the electron transfer of ^{t}BuFc, concentration-dependent diffusion coefficients, in the I_1 phase of LLCs occur as a result of the partitioning of the oxidised form (^{t}BuFc) between surfactant and aqueous subphases. It important noting that the very high viscosity of the I_1 phase allows charge diffusion to occur *faster* than in polymeric systems.

However, the occurrence of diffusion of analytes within a micellar framework compared with transport of micelle-containing analytes can be modulated by a number of factors including: the type of ionic doping as well as analyte hydrophobicity and the type of nanostructure formed rather than the particular

orientation of the structure, with the H_1 phase acting as a medium that may offer a lower degree of Ohmic loss.

The final study has demonstrated that photogalvanic cells, operating under violet light, can be used to generate electrical energy through the photoelectrochemical reduction of 2, 4 dichlorophenol in the presence of Zn^{2+}. We estimate that the electrical energy consumed by powering the light source (~80 J) is six orders of magnitude larger than the electrical energy produced by the system (~70 µJ), indicating that there is much work required to make this system truly sustainable.

Overall, this work has shown that the electro-analytical methods can be applied to generate working galvanic cells that can be used in portable devices with the intention to converting the cell into an operable photogalvanic cell in the future. The battery will consist of using lyotropic liquid crystals as a medium for the electrochemical process to occur, where the redox species is contained within the micelles of the liquid crystal and the electron transfer between the micelles, the lamella and hexagonal phase will each be used to determine whether a certain phase induces a better potential difference.

Chapter 9 – Appendix

9.1   Publications

- Chapter four: Concentration-Dependent Diffusion Coefficients of *tert*-Butylferrocene within I_1 phase liquid crystals has been published in Electrochemistry Communications **(2012,DOI:10.1016/j.elecom.2012.01.013)**

Concentration-dependent diffusion coefficients of *tert*–butylferrocene within dodecyltrimethylammonium chloride/brine liquid crystals

Jonathan E. Halls [a,*], Amal A. Altalhi [a], Fabiane C. de Abreu [a,b], Marília O.F. Goulart [b], Jay D. Wadhawan [a,**]

[a] Department of Chemistry, Hull University, Cottingham Road, Hull HU6 7RX, United Kingdom
[b] Universidade Federal de Alagoas, Instituto de Quimica e Biotecnologia, Tabuleiro do Martins, 57072-970–Maceío, Alagoas, Brazil

ABSTRACT

The title lyotropic liquid crystal is examined as a framework to investigate long-range charge transfer, using *tert*-butylferrocene ([t]BuFc) as model hydrophobic system. It is found that the apparent one-dimensional diffusion coefficient depends on the [t]BuFc loading. It is suggested that an efficient relay mechanism for electron transfer is through the partitioning of the oxidised form between the two subphases, with inter-pseudophase reaction.

- Chapter five: Voltammetry within Structured Liquid Nanosystems: Towards the Design of a Flexible, Three-Dimensional Framework for Artificial Photosystems has been published in electrochemica Acta

(2012,DOI:10.1016/j.electacta.2012.03.52)

Voltammetry within structured liquid nanosystems: Towards the design of a flexible, three-dimensional framework for artificial photosystems

Jonathan E. Halls [1], Kevin J. Wright, Jonathan E. Pickersgill, Jamie P. Smith, Amal A. Altalhi, Richard W. Bourne, Padina Alaei, Thippeswamy Ramakrishnappa, Stephen M. Kelly, Jay D. Wadhawan [*]

Department of Chemistry, The University of Hull, Cottingham Road, Kingston-upon-Hull HU6 7RX, United Kingdom

ABSTRACT

Normal lyotropic liquid crystals (in the lamellar or hexagonal phases) are investigated as a route to afford a structured, three-dimensional, quasi-biphasic framework within which electron transfer cascades may be initiated voltammetrically. For model systems, we show that these can take place through reagent partitioning between the hydrophobic and hydrophilic subphases, and illustrate how the structure and its orientation, the nature of the ionic doping of the framework, and the hydrophobicity of the redox

- Chapter seven: Wastewater as a Photoelectrochemical Fuel Source: Light-to-Electrical Energy Conversion with Organochloride Remediation has been published in Electrochemistry Communications

(2012,DOI:10.1016/j.elecom.2012.04.024)

Wastewater as a photoelectrochemical fuel source: Light–to–electrical energy conversion with organochloride remediation

Jonathan E. Halls [*,1], Timothy Johnson, Amal A. Altalhi, Jay D. Wadhawan [*]

Department of Chemistry, The University of Hull, Cottingham Road, Kingston-upon-Hull HU6 7RX, United Kingdom

A R T I C L E   I N F O

A B S T R A C T

A photogalvanic cell that employs 2,4-dichlorophenol as a fuel source, an *N*-substituted phenothiazine as light harvester, and sacrificial zinc anode is presented, and shown to afford a *ca.* 4% light-to-electrical power conversion efficiency in violet light.

9.2   Conferences

- Oral presentation about Concentration-dependent diffusion coefficients of tert-butylferrocene within dodecyltrimethylammonium chloride/brine liquid crystals

In June 24, 2011, **Kingston-upon-Hull. The Robin Hood Interdisciplinary Network in. Electrochemistry (RHINE) meeting.**

NEWSLETTER

info Echem

Serving Electrochemical Science, Technology and Engineering within the catchment of
The Royal Society of Chemistry
and
The Society of Chemical Industry

SCI   Where science meets business
an environment to advance knowledge exchange

RSC | Advancing the Chemical Sciences

- Oral presentation about Concentration-dependent diffusion coefficients of tert-butylferrocene within dodecyltrimethylammonium chloride/brine liquid crystals

In June 18, 2012, **Great Western Electrochemistry Meeting-Bath.**

Frank Marken
Professor
Telephone 01225 383694
Mobile 07977 298205
Facsimile 01225 386231
Email FMarken@bath.ac.uk

UNIVERSITY OF
BATH
Department of Chemistry
Bath BA2 7AY · United Kingdom

20th June 2012

ISE Satellite Regional Symposium
Great Western Electrochemistry Meeting
University of Bath, Monday 18th June 2012

This is to certify that

Amal Altalhi
Department of Chemistry
University of Hull

Attended the above meeting and presented

" Concentration-Dependence of Diffusion Coefficients in the I1 phase"

Event Organiser
(F. Marken)

- Oral presentation about (Wastewater as a Photoelectrochemical Fuel Source Light-to-Electrical Energy Conversion with Organochloride Remediation)

In Oct 14, 2012, **the 6th Saudi Scientific International Conference-London.**

SiC
Saudi Scientific International Conference
المؤتمر العلمي السعودي الدولي
Investing in knowledge

CERTIFICATE OF AWARD

This is to certify that AMAL AHMAD ALTALHI has been awarded the best paper titled **Wastewater as a Photoelectrochemical Fuel Source:Light-to-Electrical Energy Conversion with Organochloride Remediation** at the 6th Saudi Scientific international conference held on 11th – 14th of Oct 2012 at the Brunel University Sponsored by King Fahd University of Petroleum & Minerals

- Poster presentation about Concentration-dependent diffusion coefficients of TMPD within the L_α phase LLCs

In June 2nd, 2012**, the 7th meeting of Electrochemistry North-West-Manchester.**

9.3   Awards

The best paper in titled Wastewater as a Photoelectrochemical Fuel Source Light-to-Electrical Energy Conversion with Organochloride Remediation was achieved in **the 6th Saudi Scientific International Conference-Brunel University-London**